DYNAMICS IN FIRE-INDUCED CEILING-JET

Khadouma Nechab

Final Report of the Thesis Presented to the

School of Technology and Management

Polytechnic Institute of Bragança

To the Fulfilment of the Requirements for the Master of Science Degree in

Industrial Engineering

(Mechanical Engineering branch)

July 2017

This page was intentionally left in blank

DYNAMICS IN FIRE-INDUCED CEILING-JET

Khadouma Nechab

Final Report of the Thesis Presented to the

School of Technology and Management

Polytechnic Institute of Bragança

To the fulfilment of the Requirements for the Master of Science Degree in

Industrial Engineering

(Mechanical Engineering branch)

Supervisor at IPB: Prof. Dr. Paulo Alexandre Gonçalves Piloto

Supervisor at UHBC: Prof. Dr. Abdallah Benarous

July 2017

This page was intentionally left in blank

ACKNOWLEDGMENT

My thanks go to all the members of the jury, to accept to participate, to contribute to improve this reflection and to stimulate that to come. I thank them for the support and attention they have given us throughout the duration of the thesis.

I would like to express my gratitude to my supervisor at IPB, Portugal, Dr. Paulo Alexandre Gonçalves Piloto. I thank him for having supervised, helped and advised me during the thesis. He was always available whenever i ran into a trouble spot or had a question about my research or writing. He consistently supervised this thesis to be my own work, but steered me in the right direction whenever he thought I needed it.

I would also like to thank to my supervisor at the University Hassiba Benbouali of Chlef (UHBC), Algeria, Dr. Abdallah Benarous for his support. I appreciated the constant help, advices, and support while conducting my thesis.

I would like to express my sincere appreciation to all the professors, researchers and others who, through their words, writings, advice and criticism, have guided my thoughts and have agreed to meet and answer my questions during my research.

I thank my dear parents, who have always been there for me, "You sacrificed everything for your children sparing neither health nor effort. You have given me a magnificent model of toil and perseverance. I am indebted to an education of which I am proud. "

I thank my brothers and sister for their unconditional support and encouragement.

I thank all my friends whom I love so much for their sincere friendship and trust and to whom I owe my gratitude and my attachment especially to H Ghania and Z soumia and M Fayssal and K Seddik and A Soufyane, Z abdelkader for help me.

To all these people, I offer my thanks, respect and gratitude.

This page was intentionally left in blank

ABSTRACT (EN)

The aim of this thesis is to test the ability of some correlative models to recover both dynamic and thermal characteristics of a fire induced ceiling-jet flow. The flow occurs when the fire plume impinges the ceiling and develops in the radial direction of the fire axis. These correlative models were also compared with a two-zone model (CFAST) and with an advanced calculation method (Computational Fluid Dynamics) for the calculation of the temperature and velocity near the ceiling. These calculations were developed inside an open car park, using different fire events (localized fires).

Both temperature and velocity predictions are decisive for sprinklers positioning, fire alarms positions, detectors positions and activation times and back-layering predictions. Simple graphs were depicted for the time of the fire event and another ones were depicted for the maximum value expected during the fire event.

Some correlative models agree well with the results obtained with CFAST. The CFD results over predicted the dynamics of the fire events.

Key words: Fire, Correlative models, CFAST, ANSYS FLUENT, Localized fires; Plume and Ceiling jet fires, fire scenario, two zone models.

This page was intentionally left in blank

ABSTRACT (PT)

O objetivo desta tese é testar a capacidade de alguns modelos correlativos para descrever as características dinâmicas e térmicas de um fluxo de jato de teto induzido por um incêndio. O fluxo ocorre quando a chama de incêndio atinge o teto e se desenvolve na direção radial em relação ao eixo do fogo. Estes modelos correlativos também foram comparados com um modelo de duas zonas (CFAST) e com um método de cálculo avançado (Computational Fluid Dynamics) para o cálculo da temperatura e da velocidade perto do teto. Estes resultados foram determinados dentro de um parque de estacionamento aberto, usando diferentes eventos de incêndio (incêndios localizados).

As previsões de temperatura e velocidade são decisivas para o posicionamento dos sprinklers, posições de alarmes de incêndio, posições de detetores e tempos de ativação e previsões de camadas com refluxos. São apresentados gráficos para representação destas quantidades durante o tempo do evento de incêndio e outros gráficos são apresentados para o valor máximo esperado durante o evento de incêndio.

Alguns modelos correlativos concordam bem com os resultados obtidos com o CFAST. Os resultados do CFD sobre avaliam a dinâmica dos eventos de incêndio.

Palavras-chave: Fire, modelos correlativos, CFAST, ANSYS FLUENT, Incêndios localizados; incêndio com pluma e a jato, cenário de incêndio, modelos de duas zonas.

This page was intentionally left in blank

INDEX

ACKNOWLEDGMENT i

ABSTRACT (EN) iii

ABSTRACT (PT) v

INDEX vii

INDEX OF FIGURES xii

INDEX OF TABLES xiv

NOTATION xv

1- INTRODUCTION 1

1.1- State of the art 1

1.2- Plume and Ceiling jet fires 5

1.2.1- Ceiling jet fire 5

1.2.2- Plume fire 7

1.2.3- Fire spread 12

1.3- Plan of thesis 13

2- FIRE SCENARIO 14

2.1- Localized fires 15

2.1.1- Small fires 15

2.1.2- Large fires impacting on the ceiling 17

2.2- Definition of fire (HRR) fire event 17

2.2.1- Factors controlling energy release rates in enclosure fires 19

2.2.2- Energy release rates based on free burn measurements 20

2.3- Definition of fire compartment 21

2.3.1- Phases of fires in compartment 21

2.3.2- Characteristics of the fire compartment 22

2.4- Definition of different fire events 23

2.5- Fire detection 23
3- HEAT TRANSFER 25
3.1- Conduction 25
3.2- Convection 26
3.3- Radiation 26
4- CORRELATIVE MODELS 28
4.1- Definition of correlative models 28
4.2- Alpert correlations 29
4.2.1- Maximum Velocity and Temperature during the fire event 30
4.2.2- Maximum Temperature and Velocity for different ratio r/H 32
4.3- Cooper correlations 33
4.3.1- Maximum Velocity and Temperature during the fire event 33
4.3.2- Maximum Temperature and Velocity for different ratio r/H 35
4.4- Heskestad and Delichatsios correlations 36
4.4.1- Maximum Velocity and Temperature during the fire event 37
4.4.2- Maximum Temperature and Velocity for different ratio r/H 38
4.5- Comparison of results 39
4.5.1- Maximum temperature comparison for class 1 39
4.5.2- Maximum temperature comparison for class 2 40
4.5.3- Maximum temperature comparison for class 3 40
4.5.4- Maximum temperature comparison for class 4,5 41
4.5.5- Maximum velocity comparison for class 1 41
4.5.6- Maximum velocity comparison for class 2 42
4.5.7- Maximum velocity comparison for class 3 43
4.5.8- Maximum velocity comparison for class 4,5 43
5- CFAST model 45
5.1- Presentation of CFAST 46

5.2- The model 46
5.2.1- Simulation environment 46
5.2.2- Thermal properties 46
5.2.3- Compartments 47
5.2.4- Wall vents 48
5.2.5- Fires 48
5.2.6- Defining targets 48
5.2.7- Defining the fire detectors 48
5.2.8- Output results 49
5.3- Comparison of results 52
5.3.1- Maximum temperature comparison for all car classes 53
5.3.2- Maximum velocity comparison for all car classes 53
6- FLUENT model 55
6.1- Presentation of FLUENT 55
6.2- Equations to be solved 56
6.2.1- Continuity equation 56
6.2.2- Navier-stokes equation 56
6.2.3- Energy equation 57
6.2.4- Other equations 57
6.3- The model 58
6.3.1- Material models 59
6.3.2- Boundary conditions 60
6.4- Comparison of results 61
6.4.1- Temperature results from ANSYS fluent simulation 61
6.4.2- Velocity results from ANSYS fluent simulation 62
6.4.3- Maximum temperature comparison for all car classes 63
6.4.4- Maximum velocity comparison for all car classes 64

7- Conclusions 68
References 69
Annex 1: Results from correlative models 74
1- Alpert's results 74
2- Cooper's results 74
3- Heskestad and Delichatsios's results 74
4- Maximum temperature comparison between correlative models 75
5- Maximum temperature comparison between correlative models 76
Annex 2: Results from CFAST simulation 78
1- Positions of targets and heat alarm entering in CFAST simulation 78
2- Maximum temperature from CFAST numerical simulation 78
3- Maximum velocity from CFAST numerical simulation 78
4- Maximum temperature comparison between the correlations and CFAST 79
5- Maximum velocity comparison between the correlations and CFAST 80
Annex 3: Results from ANSYS fluent simulation 82
1- Material models 82
2- Boundary condition 82

This page was intentionally left in blank

INDEX OF FIGURES

Figure 1.fire plume and ceiling jet [15]..... 5
Figure 2.The three zones of the axisymmetric buoyant plume [5]..... 7
Figure 3.Schematic of plume and ceiling jet flow for an unconfined ceiling I: Plume Region; II: Turning Region; III: Ceiling Jet Region [27]..... 8
Figure 4.Modeled fires anchored on the burner setup corresponding to ˙Qc = (a) 1500, (b) 4500, and (c) 7500kW, illustrated with the instantaneous isocountour of stoichiometric mixture fraction. 11
Figure 5. Fire Scenarios [42]..... 15
Figure 6. Schematic diagram for small localised fires [47]. 16
Figure 7. Energy release rate measured when burning 1.2 m by 1.2 m wood pallets, stacked to different heights [48]..... 18
Figure 8.HRR of different car classes. 19
Figure 9.Localized fire of our compartment. 23
Figure 10.Ceiling jet flow beneath an unconfined ceiling [54]..... 28
Figure 11.The geometry of the compartment..... 29
Figure 12.Temperature near the ceiling from Alpert correlations. 31
Figure 13.Velocity near the ceiling from Alpert correlations. 31
Figure 14.Tmax of all car classes calculated by Alpert correlations. 32
Figure 15.Vmax of all car classes calculated by Alpert correlations. 32
Figure 16.Temperature near the ceiling from Cooper correlations. 34
Figure 17.Velocity near the ceiling from Cooper correlations..... 34
Figure 18.Tmax of all car classes calculated by Cooper correlations 35
Figure 19.Vmax of all car classes calculated by Cooper correlations 35
Figure 20.Temperature near the ceiling from Heskestad and Delichatsios correlations..... 37
Figure 21.Velocity near the ceiling from Heskestad and Delichatsios correlations. 38
Figure 22.Tmax of car classes from Heskestad and Delichatsios correlations 38
Figure 23.Vmax of car classes from Heskestad and Delichatsios correlations..... 39
Figure 24.Comparison of the value of T_{max} from the correlative models for class 1..... 40
Figure 25.Comparison of the value of T_{max} from the correlative models for class 2..... 40
Figure 26.Comparison of the value of T_{max} from the correlative models for class 3..... 41
Figure 27.Comparison of the value of T_{max} from the correlative models for class 4,5..... 41
Figure 28.Comparison of the value of V_{max} from the correlative models for class 1 42

Figure 29.Comparison of the value of V_{max} from the correlative models for class 2 42
Figure 30.Comparison of the value of V_{mac} from the correlative models for class 3..... 43
Figure 31.Comparison of the value of V_{max} from the correlative models for class 4,5 44
Figure 32.compartment in a two-zone model [43]. 45
Figure 33. Specific heat of concrete (left) and Thermal conductivity of concrete (right) [55].47
Figure 34. The geometry of our fire compartment. 48
Figure 35. Grid size of the compartment. 49
Figure 36.Results of temperature from CFAST simulation. 50
Figure 37.Results of velocity from CFAST simulation. 50
Figure 38.Results of T_{max} from CFAST simulation. 51
Figure 39.CFAST simulation for T_{max}. 51
Figure 40.Results of V_{max} from CFAST simulation. 52
Figure 41.CFAST simulation for V_{max}. 52
Figure 42.Comparison of Tmax for all car classes. 53
Figure 43.Comparison of Vmax for all car classes. 54
Figure 44.the Mesh of the model. 59
Figure 45.Properties of the air. 59
Figure 46.Boundary condition of the compartment. 60
Figure 47. Results of Tg from CFAST of all car classes. 61
Figure 48. Results of Vg from CFAST of all car classes. 61
Figure 49.Results of temperature from ANSYS fluent simulation of all car classes. 62
Figure 50.Results of velocity from ANSYS fluent simulation of all car classes. 63
Figure 51.Results of Tmax from ANSYS fluent simulation of all car classes. 64
Figure 52.Results of Vmax from ANSYS fluent simulation of all car classes. 65
Figure 53.Model and the grid size. 65
Figure 54.Results of Temperature when t=1500 s for all car classes. 66
Figure 55.Results of velocity when t=1500 s for all car classes. 67

INDEX OF TABLES

Table 1.Rough Measure of Energy Released or Generated from Various Sources [48]. 17
Table 2.HRR of different car classes. 19
Table 3.Thermal properties of Concrete and Steel. 22
Table 4.Tmax and Vmax getting form Alpert's correlations. 74
Table 5.Tmax and Vmax getting form Cooper's correlations. 74
Table 6. Tmax and Vmax getting form Heskestad and Delichatsios correlations. 75
Table 7.Comparison between correlative models for Tmax of class 1. 75
Table 8.Comparison between correlative models for Tmax of class 2. 75
Table 9.Comparison between correlative models for Tmax of class 3. 75
Table 10.Comparison between correlative models for Tmax of class 4,5. 76
Table 11.Comparison between correlative models for Vmax of class 1. 76
Table 12.Comparison between correlative models for Vmax of class 2. 76
Table 13.Comparison between correlative models for Vmax of class 3. 76
Table 14.- Comparison between correlative models for Vmax of class 4,5 77
Table 15.Data of the six targets in the compartment. 78
Table 16.Data of the six heat alarms in compartment. 78
Table 17.results of CFAST simulation for maximum temperature. 78
Table 18.results of CFAST simulation for maximum temperature. 79
Table 19.Comparison of Tmax between correlative models and CFAST for class 1. 79
Table 20.Comparison of Tmax between correlative models and CFAST for class 2. 79
Table 21.Comparison of Tmax between correlative models and CFAST for class 3. 79
Table 22.Comparison of Tmax between correlative models and CFAST for class 4,5. 80
Table 23.Comparison of Vmax between correlative models and CFAST for class 1. 80
Table 24.Comparison of Vmax between correlative models and CFAST for class 2. 80
Table 25.Comparison of Vmax between correlative models and CFAST for class 3. 80
Table 26.Comparison of Vmax between correlative models and CFAST for class 4,5. 81
Table 27.Properties of concrete based on data points. 82
Table 28..Data of the target 7 in the compartment. 82
Table 29.Data of the heat alarm7 in the compartment. 82
Table 30.Maximum velocity and temperature from ANSYS fluent. 85

NOTATION

NOMENCLATURE

Latin lower-case letters

$\dot{m}_p$	Plume mass flow rate [kg/s]
r	Radial distance from the fire [m]
t	Time [min]

Latin upper-case letters

C_p	Specific heat at constant pressure [kJ/ (kg K)]
D	Diameter of fire source [m]
E	Energy of combustion [MJ]
H	Distance between the fire and the ceiling [m]
H_f	Vertical distance between the floor and the ceiling [m]
H_s	Distance between the fire source of the car and the floor [m]
$K_{xx,yy,zz}$	Thermal conductivity in x,y,z directions
L_f	Flame height [m]
L_h	Horizontal flame length [m]
Q_V	Volumetric heat source
$\dot{Q}$	Total heat release rate (HRR) [kW]
$\dot{Q}_c$	Convective part of the rate of heat release [kW], $\dot{Q}_c = 0{,}8\dot{Q}$ by default
T_{max}	Maximum temperature [°C]
T_∞	Ambient temperature [°C]
V	Velocity vector
V_{max}	Maximum velocity [m/s]
$V_{x;y;z}$	Velocity in x, y, z directions
Z	Height along the flame axis [m]
Z_0	Virtual origin or height of virtual source above burning item [m]
Z'	Vertical position of the virtual heat source [m]

Greek letters

α	Convection [-]
α_c	Coefficient of heat transfer by convection [W/m2 K]
ε	Emissivity [-]
σ	Stephan Boltzmann constant =5.67×10^{-8} [w/m^2k^4]
δ	Thickness of ceiling jet [m]
λ	Thermal conductivity [kW/ (m °C)]
ρ	Density [kg/m^3]
ρ_∞	Ambient air density[kg/m^3]
∇	Del operator [-]

1- INTRODUCTION

One of the most important problems in fire protection is the rapid detection of fire in a room while the fire is sufficiently small to be easily controlled. Controllable fires generally exist for more than half a minute after ignition when flames are confined by inert barrier for air gaps to a distinct portion of the total available fuel.

Much of the work that is collected below deals with means to predict the temperature and velocities in the ceiling jet flow both above and remote from the fire source. In facilities with very high ceilings, the detectors could be closer to the ceiling than 1% of the ceiling-to-fire-source distance and will fall in the ceiling jet thermal and viscous boundary layers.

The velocity and temperature of the hot gases due the fire in compartment are two major dynamic characteristics that must be take in consideration in events of fire. The main goal of this work is to develop numerical simulations using two different software, which are CFAST (Consolidated Model of Fire and Smoke Transport), a calculation method based on the two zone models and CFD (Computational Fluid Dynamics), a finite volume based method. Also, simple calculation methods, based on the correlative models devoted to fire plumes and ceiling jets were used to compare results of temperature and velocity near the ceiling. The flow produced by the fire is considered unconfined with respect to the localized fire.

Five car classes were used to define different fire scenarios in open car parking that are to be analysed.

1.1- State of the art

In 1972, Alpert [1] presented Data on near maximum gas velocity and excess temperature in the ceiling jet induced by large scale fires that were used to obtain well-known ceiling jet formulas. These formulas have been re-examined in light of knowledge on the virtual plume origin and the convective component of the fire heat release rate. According to this research, fire detectors should be located in a vertical distance below the ceiling of no more than 6 % of the ceiling height.

In 1979 Gunnar Heskestad and Michael A. Delichatsios [2] did three wood-crib fires tests of different fire-growth rates that were combined with three different ceiling heights under large flat ceilings for a total of nine setup configurations. The experimental fires were power-law fires growing with the second power of time. These relations may be used to predict temperature and velocity histories for arbitrary combinations of ceiling clearance and fire-

growth rate. The local gas velocity in the hottest layer under flat ceilings can be related directly to the local temperature rise and ceiling clearance, regardless of time from ignition, fire-growth rate and, possibly, fire-growth behaviour.

In 1986 L. Y. Cooper and A. Woodhouse [3] studied the convective heat transfer from buoyant plume-driven ceiling jets to unconfined ceilings. The heat transfer was estimated using a formula for the temperature distribution below an adiabatic ceiling T_{ad} (one obtained from experimental data in the range $0 < r/H < 0.7$ (r is the radial distance from the plume and H is the plume source-to-ceiling distance)). The new results were used to modify equations. The unconfined ceiling equations were used to estimate heat transfer to the confined ceilings of real compartment fire scenarios.

In 1987 L. Y. Cooper and D. W. Stroup [4] developed procedure to measure the thermal response of unconfined compartment, using an algorithm for convective heat transfer to the ceiling material from the fire-plume-driven ceiling jet. The results give an indication of the influence of convective heat transfer on peak ceiling thermal response, losses from fire plume gases, and radial variations and peak values of ceiling-to-floor irradiation during fires. The algorithm developed was used to predict the response of a variety of realistic ceiling constructions to different fire scenarios. In general, the results of the calculations presented were plausible, and they provide useful insight into the response of real ceilings to hazardous fires.

In 1989 Gunnar Heskestad & Michael A. Delichatsios [5] did a brief note to update correlations established previously by the authors for the ceiling flow generated by fires growing with the second power of time, based on knowledge of the actual heat of combustion of wood. The correlations were generalized to include combustibles with a significantly different convective fraction of total heat release rate than wood. An existing set of ceiling flow correlations for fires growing with the second power of time has been updated to reflect improved knowledge of the heat of combustion of wood. An additional set has been established based on convective heat release rate, useful for combustibles with different convective heat fractions than wood.

In 1992 Stephen M. Olenick and Douglas J. Carpenter [6] presented the categories chosen for computer fire models, including zone models, field models, detector response, fire endurance, egress, and miscellaneous. The miscellaneous category included models that have characteristics covering several of the categories, making it difficult to be placed in a single category, or models that have unique capabilities which do not allow them to be categorized anywhere else. The miscellaneous models are increasing in numbers due to a greater, more

accessible database of fire data. Computer fire modelling is moving in a trend to provide predictions that are more accurate, as well as predictions about fire phenomenon that previously no computer fire model addressed.

In 1993 Leonard Y. Cooper [7] developed a research about the effect of the heat transfer on the location of the fire within a rectangular parallelepiped compartment. The model considered uniform ceiling temperatures, presenting an estimation of the convective heat transfer, due to ceiling-jet driven flows, to both the upper and lower parts of the walls. The model also presented the velocity and temperature distributions in the ceiling jet. The model equations were used to develop an algorithm and associated modular computer subroutine to carry out the indicated heat transfer calculations. The algorithm and subroutine are suitable for use in two-layer zone-type compartment fire model computer codes. CEILHT has been tested for a variety of instantaneous fire environments involving a 10 MW fire in an 8x8x4 m high enclosure.

In 2005, W. G. Weng and Y. Hasemi [8] presented a model to calculate the thermal response of an unconfined non-burning ceiling from an impinging buoyant diffusion flame. The model uses an algorithm that considers heat transfer into the ceiling. Also takes in to account the heat transfer due to radiation from the fire source to the ceiling surface, and from the ceiling surface to other materials. The predicted heat fluxes were compared with the existing experimental data, helping to validate the model.

In 2010 João Carlos Viegas [9] did a sensitivity analysis to study the interaction between the fire ceiling jet and the flow driven by jet fans, using CFD simulations, considering important parameters as position and intensity of fire source, transversal distance between jet fans, restriction of exhaust flow rate and dimension of car park exhaust opening. An analytical model for the flow field near the ceiling is developed and compared with CFD simulations.

In 2010 Yasushi Oka, Osamu Imazeki and Osami Sugawa [10] developed an experimental study to clarify the effect of inclination angle of the smooth ceiling on the decrease in temperature along the steepest run in the upward direction, horizontal distribution of temperature in the span wise direction and the back-layering distance (velocity reversal distance) in the down direction. Two kinds of formulae that enhanced up to the sloped ceiling angle of 40º were developed considering whether the flame reaches the sloped ceiling or not. The temperature spread in span-wise direction is assumed to be approximated by the Gaussian distribution and the dependence of spread width of the temperature on the inclination angle of sloped ceiling was clarified experimentally and the empirical formula was developed.

In 2011 Ronald L. Alpert [11] revisited data on near-maximum gas velocity and excess temperature in the ceiling jet induced by large-scale fires that were used to obtain well-known ceiling-jet formulas published in 1972 have been re-examined in light of knowledge on the virtual plume origin and the convective component of the fire heat release rate. The new data correlations developed from this re-examination are compared with the original correlations that were based on actual ceiling height above the top fuel surface and actual fire heat release rate, instead of being based on ceiling height above the virtual origin and on the convective heat release rate. Such algebraic formulas are useful for predicting detection/activation times of ceiling mounted devices, e.g., fire sprinklers. To determine what mass flux of agent droplets from these activated sprinklers arrives at the fire source, it is shown that CFD coupled with droplet trajectory calculations have been used beginning in the mid-1980's to quantify the interaction between the fire induced plume/ceiling jet flow and droplet sprays.

In 2012 Yasushi Oka and Masaki Ando [12] developed a series of pool fire tests, using a flat unconfined ceiling and changing the ceiling inclination angle up to 40º. Two different fire heat release rates were used to simulate the effect of touching and not touching the ceiling, using steady-state conditions. The maximum temperature and its position were determined. The maximum velocity and its position were obtained by the particle image velocimetry method. These results were compared with the velocities obtained using a bi-directional flow probe. Empirical formulae for the temperature rise and velocity versus the radial distance from the plume impingement point along the steepest run in the upward direction were developed considering the effect of the inclination angle.

In 2013 Nils Johansson, Jonathan Wahlqvist and Patrick van Hees [13] did an evaluation of previously derived correlations for ceiling jet excess temperatures and velocities, after the development of 90 simulation in FDS. Authors also demonstrate how computer simulations could be used as a complement to actual fire experiments in fire science research. The evaluation indicates that the existing correlations will give a good estimate of the average temperature in a ceiling jet. However, it seems that the correlations will not give a good estimate of the maximum excess temperature or velocity. A new correlation to estimate the maximum temperature was developed.

In 2016 Tiannian Zhou, Yaping He, Xiao Lin, Xuehui Wanga and Jian Wanga [14] did a sequence of tests and simulations with different fire locations using a full-scale tunnel to investigate the constraint effect of sidewall on the maximum smoke temperature distribution under a tunnel ceiling. Numerical simulations were also conducted to extend the fire scenarios with a wider range of fire locations. The numerical simulations in the current study over

predicted the ceiling jet temperature rise at the impingement point when the fire is located closely to the tunnel wall, but underestimated the normalized longitudinal distribution at a given location. The wall constraint effect on the normalized impingement ceiling jet temperature rise seemed independent of the heat release rate of the fire.

These experimental and mathematical modelling studies have provided the necessary understanding to predict some of the general transport behaviour in fires based on empirical correlations. The results of these investigations have advanced the understanding of fire phenomena and improved the design of fire protections systems. However, detailed measurements in well-controlled experiments are required for model development. In particular, characterizations of the velocity field in fire plume configurations are notably absent.

1.2- Plume and Ceiling jet fires

1.2.1- Ceiling jet fire

The ceiling jet is created when there is an impingement between a buoyant plume and flat unobstructed ceiling where the hot gases spreads radically under the ceiling, see Figure 1. Ceiling jet fire can also be defined as the rapid flow of gas in a surface layer below the ceiling surface that is driven by the buoyancy of hot combustion products.

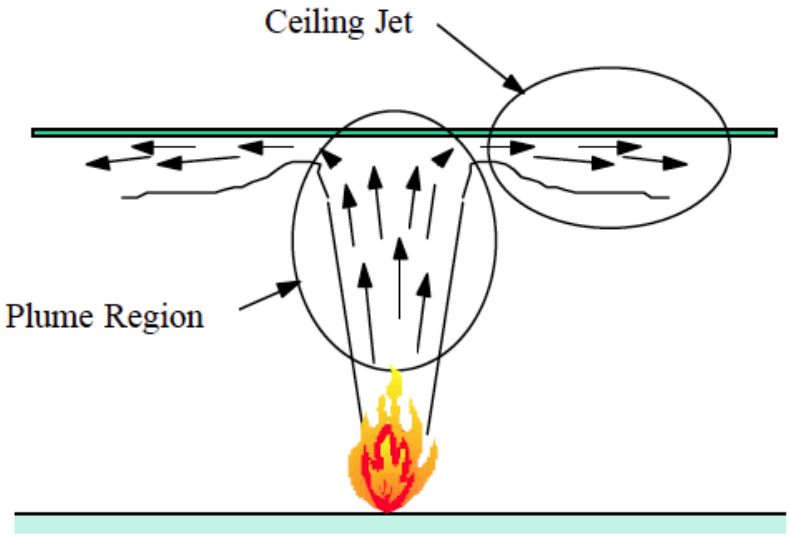

Figure 1.fire plume and ceiling jet [15].

1.2.1.1- Ceiling jet velocity

The ceiling jets in ordinary building enclosure fires have been investigated by Alpert [16] and Heskestad et al. [17]. However, the ceiling jets in tunnel fires, especially in longitudinally ventilated tunnel fires, is completely different with those in room fires. Hinkley [18] proposed an equation to estimate the gas velocity for small corridor fires, however, it is based on a simple assumption of constant Richardson number which is not suitable for the momentum dominant ceiling jet flows in tunnel fires. Li et al. [19] analysed the ceiling jet flows for small corridor fires. However, no entrainment was considered for the ceiling jets and the Reynolds' analogy was misused since in reality the convective heat flux rather than total heat flux should be used in the analogy.

1.2.1.2- Ceiling jet flow rate

Li et al. [20] proposed an equation to estimate the smoke flow rate at a certain height in a small fire under ventilation. This should be equivalent to the initial ceiling jet flow rate. However, the equation was only validated using the temperature data. Data of the initial ceiling gas flow rate are needed to validate this equation. Further, this equation could not be suitable for the strong flame plume.

1.2.1.3- Ceiling jet temperature

Li et al. [20, 21] have theoretically and experimentally investigated the maximum ceiling gas temperature and its corresponding position in tunnel fires and robust equations have been proposed for both low ventilation and high ventilation. However, how the flame temperature varies with distance in the vicinity of the fire has not yet been fully explored. Ingason and Li [22] found that while correlating all the temperature distribution curve, there is a "virtual origin" along the ceiling. The horizontal distance at the ceiling between the fire source and virtual origin needs to be clearly determined.

1.2.1.4- Ceiling jet radiation

Ingason et al. [23] investigated the radiation from the ceiling flame to the tunnel structure in the Runehemar tunnel fire tests. Ingason and Li [24] also found that there is a strong correlation between the ceiling gas temperature and the heat flux at the floor level in the far-field of the fire. However, the radiation directly from the flame to the objects at floor level or at a certain height in the vicinity of the fire needs to be thoroughly investigated, since the fire spread to the neighboring objects or vehicles mainly results from this radiation.

1.2.2- Plume fire

The fire plume is usually divided into three regions: ‘persistent flame’ zone at the flame base, ‘intermittent flame’ zone following, and ‘buoyant plume’ in the highest region see Figure 2. The persistent zone has chemical reactions and air entrainment taking place and thus is the most interesting regarding flame establishment, stabilization, and mass formation. In this first zone, where the chemical reactions and heat release occur, the flame appears nearly laminar with a light blue colour. The heat release induces a large increase in the gas velocity and temperature in this region. The characteristics of flame in this zone is generated by the following basic mechanism as heat transfer, radiative and convective. In the intermittent zone, the flame turns into yellow colour with the temperature maximum shifting toward the burner axis. Air entrainment in these two zones pushes the flame inward, forming a characteristic ‘neck’ at the top of which intermittent, large eddy structures are formed, see Figure 3. In the plume zone, velocities and temperatures decrease with height [25].

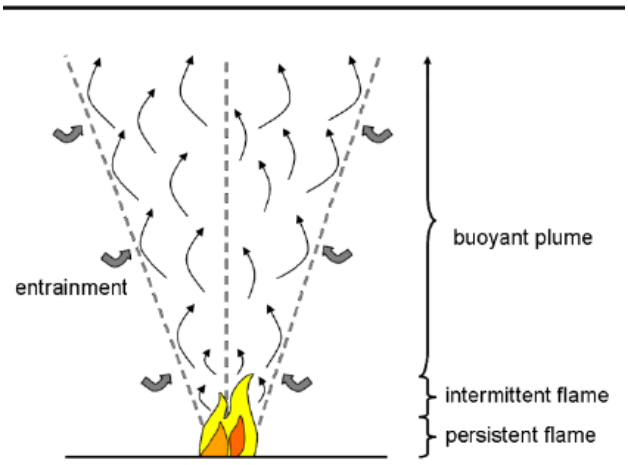

Figure 2.The three zones of the axisymmetric buoyant plume [5].

The unconfined point-source plume configuration has been used by previous researchers to establish plume theory. This theory provides solutions for the temperature profile, velocity profile and entrainment for thermal plumes at various elevations above the source [15] . Based on point source theory, the behaviour of the fire plume is independent of the details of the heat source including the fuel source and source geometry. The turbulent flow above a point source of heat is analysed in terms of the total mass, momentum and energy integrated across the plume cross section assuming that the entrainment velocity is proportional to the centreline plume velocity. Assuming the average temperature and velocity across the plume have Gaussian profiles, Zukosiki et al. [26] provides a theoretical solution for the plume momentum and energy equations by using an integral method.

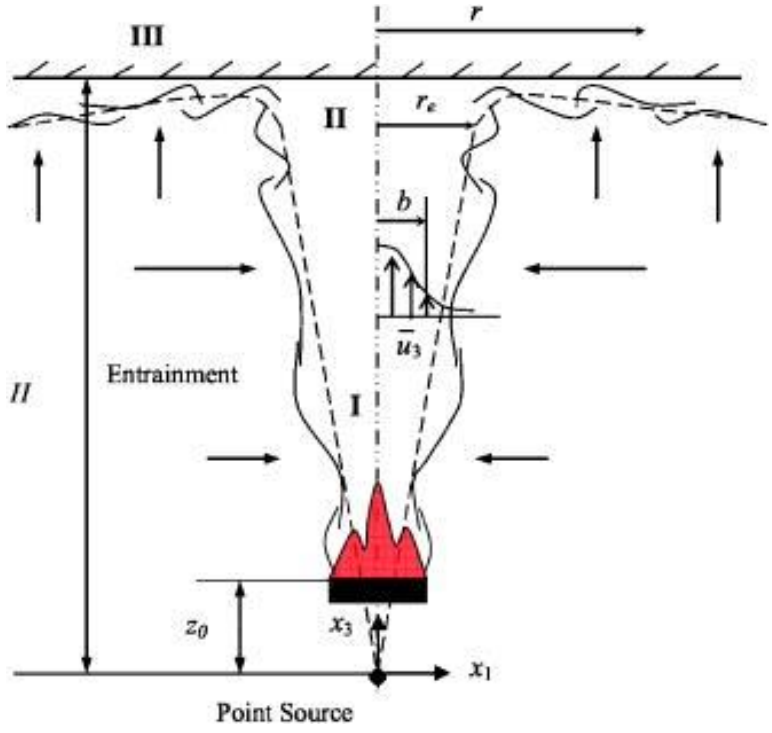

Figure 3.Schematic of plume and ceiling jet flow for an unconfined ceiling I: Plume Region; II: Turning Region; III: Ceiling Jet Region [27].

The virtual origin Zo [m] of the axis is given by Eq 1:

$$Z_0 = -1.02D + 0.00524Q^{2/5} \qquad \text{Eq 1}$$

Once the plume impinges on a ceiling, it turns to form a radially expanding ceiling jet. The flow behaviour becomes more complicated compared with the fire plume. Due to the

viscous interactions with ceiling, there is a competition between turbulent mixing and stable stratification along the ceiling. A number of theoretical and experimental fire studies were performed in the impinging plume configuration. Most notably, Alpert [27] performed an analytical and experimental study developing the theory and associated scaling laws for fire induced ceiling jets. His analysis successfully predicted the maximum temperature distributions in the ceiling jets and is widely used in hazard analysis. Based on his analysis, he provided relationships for dimensionless ceiling layer thickness, velocity, and temperature, which compares favourably with measurements. In fact, his analysis revealed that these flow quantities are relatively insensitive to geometric scale. Alpert suggested that credible small-scale fire experiments could be conducted at ceiling heights down to 0.6 m.

Motevalli and Marks [28] conducted small-scale experiments of ceiling jet heat transfer, which generally compared favourably with other ceiling jet data and analysis for $x_1/H < 2$. The velocity and temperature measurements were obtained for unconfined ceiling jets under ceiling transient and steady-state conditions. Small fires of 0.5 kW to 2.0 kW were produced with a premixed methane-air burner. These measurements represented one of the most detailed studies of unconfined ceiling jets and were in general agreement with large scale data. Noticeable discrepancies were encountered when comparing measured momentum and thermal thickness between investigations. These discrepancies were attributed to coarse measurements and simplifying assumptions by other investigators concerning the equivalency of the momentum and thermal thicknesses in other analyses. However, no convective heat transfer rate to the ceiling was studied in that investigation.

Convective heat transfer from the ceiling jet layer to the ceiling surface has been studied by Veldman et al. [29]. They conducted experiments to investigate the axisymmetric heat transfer from small scale fires (1.17 kW and 1.53 kW) under the impinging plume condition. An empirical correlation involving the source strength, Q, and ceiling height, H, was found to correlate measurements of the adiabatic wall temperature and its radial variation in the range from $0 \leq x_1/H \leq 0.7$. A similar correlation for estimating the ceiling heat transfer coefficient was confirmed by the experimental results. However, their study was limited by the absence of velocity measurements in both plume and ceiling jet configurations. You and Faeth [30] also conducted a study on heat transfer from an impinging fire plume to a horizontal ceiling. Their measurements were compared with predictions of both differential and integral models where $x_1/H < 1.7$. The integral model provided a reasonable prediction of flow properties and ceiling heat fluxes. According to their results the estimation of flow characteristics was greatly

influenced by entrainment. Ceiling friction has only had a secondary effect on the flow structure predictions.

Cooper [31, 32, 33] developed a heat transfer analysis by using an adiabatic ceiling surface temperature, T_{ad}, as the reference temperature in Newton's law of cooling. The adiabatic surface temperature, T_{ad}, depends on the fire configuration, but is independent of the ceiling surface temperature. This adiabatic surface temperature describes the gas temperature decay along the ceiling due to entrainment.

Cooper provided correlations for T_{ad} distributions along the ceiling by analysing previous researcher's experimental data [29, 34]. Correlations of the heat transfer coefficient, h, in the turning region and the ceiling jet region of the plume are also provided. Convective heat transfer from the ceiling jet to the ceiling surface has been estimated using correlations of T_{ad} and h in the range of $0 \leq x_1/H \leq 2.2$.

Goldstein et al. [35] also investigated the convective heat transfer of a heated circular air jet impinging on a flat surface using T_{ad} as a reference temperature. The concept of effectiveness has been adopted to express the adiabatic surface temperature in dimensionless form. The heat transfer coefficient was also found to be independent of the relative magnitude of the jet temperature and the ambient temperature, if the adiabatic wall temperature is used as a reference temperature in the definition of the heat transfer coefficient. In the current research, the concept of effectiveness is applied with modification to the analysis of the convective heat transfer rate from the ceiling jet to the ceiling.

1.2.2.1- Fire Plume Characterization

The primary purpose of designing the simulated fires was to reproduce temperatures and velocities representative of rack-storage fire plume distributions. Figure 4 shows instantaneous snapshots of the three modelled fires corresponding to $\dot{Q}_c$=1500, 4500 and 7500kW. Flame heights of 2.91, 5.15 and 6.70 m were predicted for each $\dot{Q}_c$, respectively. These compared favourably with flame heights estimated from experiments. The air inlet located below the central burner provided additional airflows to the burner generated plumes so that rack-storage fire plume velocities could be achieved. In the experimental setup, the inlet air velocities varied between 8 and 9.3 m/s, corresponding to 1500 and 7500kW plumes, respectively. However, for the simulations, velocities at the inlet were varied between 10 and 20 m/s. This is because the

experimental burner setup involves spray flames that produce jet flames of high momentum. Higher velocities are required in the simulations applying buoyant diffusion flames of propane, which do not provide sufficient momentum to the resulting plumes as compared to the spray flames. Similar to previous studies [36], by adjusting the air inlet velocities a reasonably accurate match with experimental results was obtained. As a reference case, results from the simulation of the $\dot{Q}_c$=1500kW plume with the volumetric fire source. The volumetric plume source, not surprisingly, produces good comparisons and the computed temperature distribution matches the experimental data and its slope compares well with the correlation between 2.5 and 6 m; velocities are slightly over-predicted compared to the correlation values, however they fall within the experimental uncertainty. Figure 4 also shows the predicted centreline excess temperature and velocity using the burner setup, compared against experimental data and correlations [37] for Q_c=1500kW. Here, it should be mentioned that plume centreline temperatures from the thermocouples were corrected for radiation loss by equating convective heat transfer (calculated with the application of a Nusselt number correlation) from the hot gases to the thermocouple bead to the radiation loss from the bead to the ambient. An optimum condition with inlet air velocity of 10 m/s was determined with emphasis given to the temperature profile as relative thermal index (RTI) is strongly affected by temperature variation as compared to velocity on which there is a square root dependence.

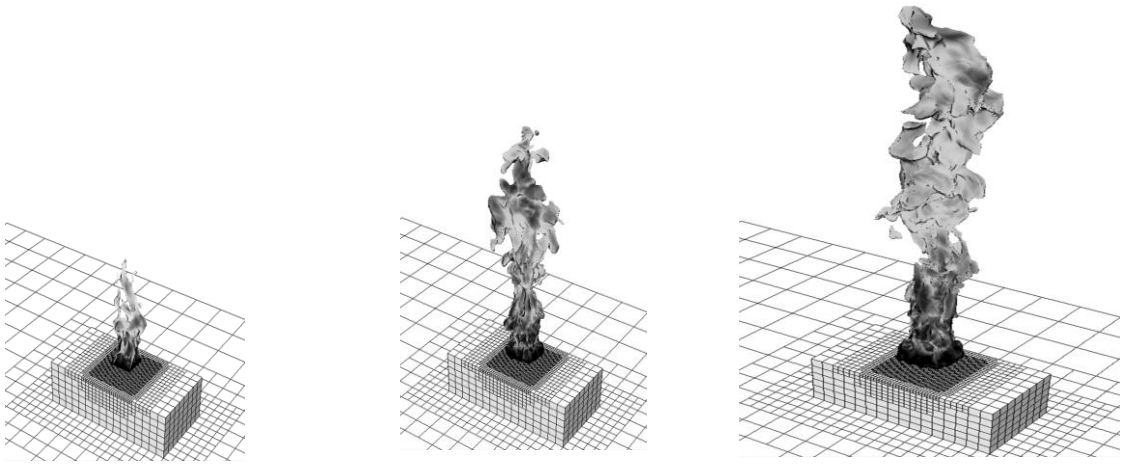

Figure 4.Modeled fires anchored on the burner setup corresponding to $\dot{Q}c$ = (a) 1500, (b) 4500, and (c) 7500kW, illustrated with the instantaneous isocountour of stoichiometric mixture fraction.

1.2.2.2- Flame length

Limited research has been carried out on the flame length in a large tunnel fire. Rew and Deaves [38] presented a flame length model for tunnel fires, which included heat release rate and longitudinal velocity. However, neither tunnel width nor tunnel height was considered. Their research was based on the investigation of the Channel Tunnel Fire in 1996 and test data from the HGV-EUREKA 499 fire test [39] and the Memorial Tests [39]. The equation is a conservative fit to a limited data obtained from the HGV-EUREKA 499 test. The weakness of the proposed equation is that no geometrical parameter has been taken into account, which makes it impossible to predict the flame length for other tunnels with different geometries. Lönnermark and Ingason [40] investigated the flame lengths from the Runehamar tests and used Alpert's equation [16] for ceiling jet temperatures to estimate the form of equation for flame length, and determined the uncertain coefficients by regression analysis. However, the tunnel ceiling is confined and thus the equation proposed by Alpert [16] may not be appropriate for large tunnel fires. Ingason and Li [22] presented a dimensionless equation to estimate the flame lengths under high ventilation. However, the flame lengths under low ventilation have not yet been investigated. Moreover, a theory needs to be proposed to clarify the correlation between ceiling flame combustion and flame length.

1.2.3- Fire spread

Limited research has been carried out on the fire spread in a tunnel fire. Newman and Tewarson [41] argued that in duct flow the material at a location will ignite when the average temperature of the tunnel flow at this position has obtained a critical value. Lönnermark and Ingason [40] tested and investigated the fire spread in full-scale tunnel fires and the results show that an average temperature of approximately 500 ºC seems to give the best correlation with fire spread. However, the data are rather limited. All the above work is based on the assumption of one-dimensional flow, however generally there is a strong stratification in the vicinity of the fire where the fire spread potentially occurs. Furthermore, the assumption of one-dimensional flow is completely invalid under low ventilation. Ingason and Li [24] found that fire spread to a neighboring wood crib occurs when the ceiling gas temperature above the wood crib rises to about 600 ºC. However, the materials are also a key parameter in fire spread and different materials perform differently while exposed to the same flame radiation. Therefore, the mechanism needs to be known more clearly and also more tests data with different materials are required.

1.3- Plan of thesis

In chapter 1, the definition of jet fire is explained; the state of the art is presented and the plan of the thesis is summarised.

In chapter 2, the definition of fire scenarios using a localized fire for the event of a car fire is presented. Different car classes burning events are presented with the results of the Heat Release rate (HRR).

Chapter 3 provides a general definition of heat transfer with discussion of the different modes of heat transfer which are included in the fire events.

Chapter 4 presents different correlative models (Alpert, Cooper, Heskestad and Delichatsios) to estimate the maximum temperature and velocity near the ceiling. The results are compared for different fire events and one fire compartment.

Chapter 5 is dedicated to the numerical simulation using CFAST software. A brief definition of CFAST will be presented followed by a discussion of the results about the maximum temperature and velocity obtained near the ceiling, between this simulation and results from the correlative models.

Chapter 6 is dedicated to the field analysis using computational fluid dynamics, where different fire events are going to be simulated, based on specific solution for equations.

Chapter 7 presents the conclusions and the future research about fire induced ceiling jets.

2- FIRE SCENARIO

The fire scenario (position of the vehicles) should represent the most unfavourable situation for the elements (or substructure). The vehicles' type mostly used in fire scenarios are cars, classified according their calorific potential or combustion energy (E). Five different car classes were defined: class 1-E=6000 MJ (ex. Peugeot 106); class 2-E=7500 MJ (ex. Peugeot 306); class 3-E=9500 MJ (ex. Peugeot 406), and classes 4 and 5-E=12 000 MJ (ex. Peugeot 605 or 806) [42].

According to statistical studies of actual fires in car parks, 90% of the vehicles involved in a fire are classified as class 1, 2 or 3. The INERIS-*Institut National de l'Environnement Industriel et des Risques*, considers that fire scenarios with cars of class 3 should be used to evaluate the structural stability of the car park under fire, and the fire resistance of the structure should be ensured during the entire fire scenario, or at least, if allowed by National requirements, up to a certain resistance time R of the elements defined as for the ISO curve. In addition, a scenario including a commercial vehicle (van containing 250 kg of highly flammable material: E=19 500 MJ) corresponds to an extreme situation and should only be used to check the global behaviour of the structure, assuming local collapse, without progressive collapse [42].

Five fire scenarios recommended or already used for the study of fires in car parks are presented and described. ECCS indicates that one or two vehicles in fire correspond to the most critical scenario in an open car park. One car burning at mid-span under the beam (corresponding to the maximum bending moment position) is defined as scenario 1. The scenario 2 involves two burning cars, one on each side of the column; this fire event was considered being the most dangerous for the columns. INERIS defines three additional fire scenarios: i) scenario 1 of ECCS, but with a commercial vehicle under the beam, ii) scenario 3 - involving seven class 3-cars, with possibility of a commercial vehicle in places 0 or 1a (Figure 5), iii) scenario 4 - involving four class 3-cars parked face to face, with possibly a commercial vehicle in places 0, 1a, 1b or 2 [42].

According to INERIS, and for all scenarios, the fire spread time from a vehicle to another is 12 minutes; the initial document by ECCS recommended a time delay equal to 15 minutes. The evolution of the composition of vehicles may also explain the decrease in the time delay. Another scenario already considered by CTICM is scenario 5: three class 3-cars, parked side by side. According to the same statistical source, a scenario of 3 class 3-cars (scenario 5) involved in a fire is an envelope scenario of around 98.7% of all possible scenarios [42].

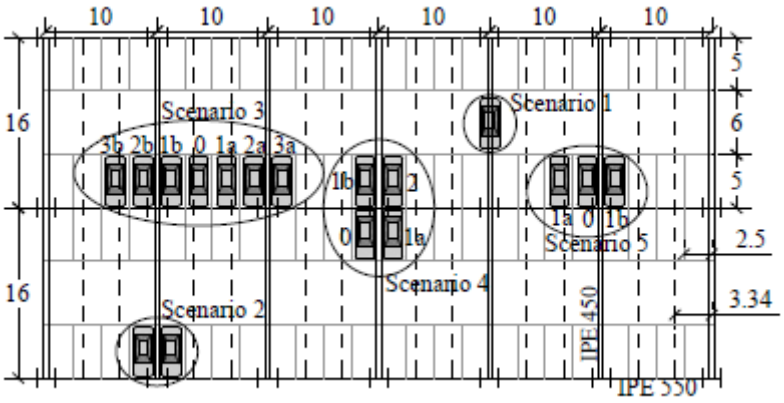

Figure 5. Fire Scenarios [42].

2.1- Localized fires

Depending on the height of the fire flame, relative to the ceiling of the compartment, a localised fire can be defined as either a small fire (or open-air fire) or a large fire impacting on the ceiling. For a small fire, a design formula is given to calculate the temperature in the flame along the vertical axis. For a bigger fire, some simple steps have been developed to calculate the heat flux received by the surfaces exposed to the fire at the ceiling level. The limitations of this approach include: (i) the diameter (D) of fire: $D \leq 10$ m, and (ii) the heat release rate (Q) of the fire: $Q \leq 50$ MW [43].

In a localized fire, there is an accumulation of combustion products in a layer beneath the ceiling (upper layer), with a horizontal interface between this hot layer and the lower layer where the temperature of the gases remains much colder. This situation is well represented by a two-zone model, useful for all pre-flashover conditions. Besides calculating the evolution of gas temperature, these models are used in order to know the smoke propagation in buildings and to estimate the life safety as a function of smoke layer height, toxic gases concentration, radiative flux and optical density. The thermal action on horizontal elements located above the fire also depends on their distance from the fire. It can be assessed by specific models for the evaluation of the local effect on adjacent elements, such as Heskestad's or Hasemi's method [43].

2.1.1- Small fires

In a localised fire, as shown in Figure 6, the highest temperature is at the axis of the vertical flame, decreasing towards the edge of the flame. The flame axis temperature changes with height. It is roughly constant in the continuous flame region and represents the mean flame temperature. The temperature decreases sharply above the flames as an increasing amount of fresh air enters into the fire compartment [44]. EN 1991-1-2 [45] provides a design formula to calculate the temperature in the plume of a small localised fire, based on the fire model developed by Heskestad [46]. It can be applied to open-air fires as well. Considering a localised fire as shown in Figure 6, the flame height L_f of the fire is provided by:

$$L_f = -1.02D + 0.0148Q^{2/5} \qquad \text{Eq 2}$$

Where D is the diameter of the fire (m); Q is the heat release rate of the fire (W).

This model allows determining the temperatures along the vertical axis of the flame. However, in a real structural scenario, a column and respective flame are likely to be positioned side by side. Therefore, the temperature estimated by the first model is unlikely to be the boundary temperature of a column subjected to a localised fire. In order to use this fire model, a configuration factor is needed to estimate the radiative heat flux from the flame to the steel column. Moreover, an estimation of gas temperatures in the vicinity of the column is a prerequisite to assessing the convective heat flux. For these reasons, the heat flux from a localised fire to a steel column cannot be estimated using Eurocode procedures [47].

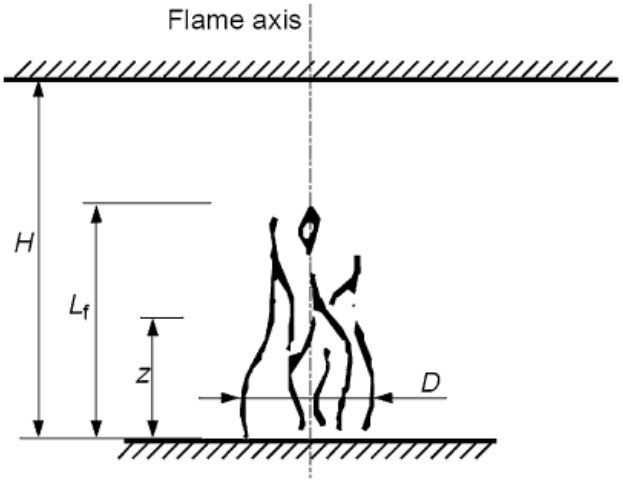

Figure 6. Schematic diagram for small localised fires [47].

2.1.2- Large fires impacting on the ceiling

When a localised fire becomes large enough, with $L_f \geq H$, the fire's flames will impact on the ceiling of the compartment. The ceiling surface will cause the flame to turn and move horizontally beneath the ceiling. EN 1991-1-2 [45] presents a design formulation to calculate temperatures in a ceiling slab and in the beams, that may support the slab. This model is based on the experimental works performed by Hasemi to calculate the location of the virtual heat source. Figure 7 shows a schematic diagram of a localised fire impacting on the ceiling with the ceiling jet flowing beneath [47].

2.2- Definition of fire (HRR) fire event

Energy release rate (often termed heat release rate or HRR) is measured in W, kW, or MW. Table 1 gives some characteristic values of energy released by various burning fuel packages and heat output from different sources.

Table 1.Rough Measure of Energy Released or Generated from Various Sources [48].

Heat source	Power
A burning cigarette	5 W
A typical light bulb	60 W
A human being at normal exertion.	100 W
A burning wastepaper basket.	100 kW
A burning $1m^2$ pool of gasoline.	2.5 MW
Burning wood pallets, stacked to the height of 3 m.	7 MW
Burning polystyrene jars, in cartons, 2 m, 4.9 m high.	30–40 MW
Output from a typical reactor at a Nuclear Power Plant.	500–1000 MW

Fire development is generally characterized in terms of energy release rate vs. time. Once the energy release rate vs. time is determined for a certain scenario, it is termed the design fire load. Table 1 indicates that for many design purposes, the design fire energy output could be in the range 100 kW to 50 MW.

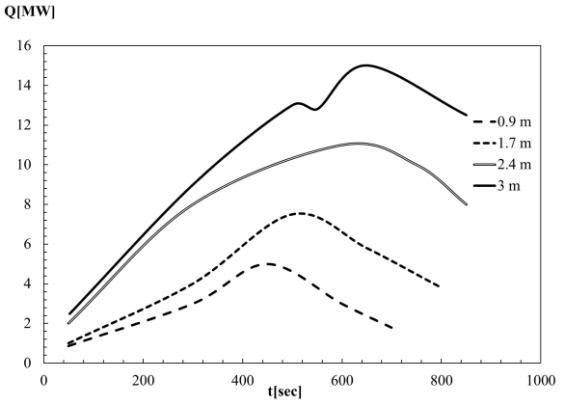

Figure 7. Energy release rate measured when burning 1.2 m by 1.2 m wood pallets, stacked to different heights [48]

The rise of the rate of heat release to the maximum value (see Figure 7, Figure 8) may be given by the Eq 3 or by other specific equation, where the HRR represents the Heat Release Rate of the fire during the growth phase [MW], t represents the time [s] and t_a represents time constant.

$$HRR = \left(t / t_a\right)^2 \qquad \text{Eq 3}$$

There are basically two approaches available when determining the design fire for a given scenario. One is based on knowledge of the amount and type of combustible materials in the compartment of fire origin. The other is based on knowledge of the type of occupancy, where very little is known about the details of the fire load. In the first case, an object is assumed to ignite and start to burn. The resulting energy release rate vs. time can in many cases be estimated using data from previous experiments where energy release rate has been measured. However, in many design situations there is very little information available on the combustible content of the room of fire origin. In this case, knowledge of the type of occupancy, any available statistics, and engineering judgment must be used to arrive at a design fire load.

The Table 2 shows the value of the total heat release rate (HRR) in [kW] of car class 1, class 2, class3, classe4 and 5 getting from tests of burning car in specific time which is in minutes. This classification was made in 1996 by European manufacturers and divide them into five categories [48].

Table 2.HRR of different car classes.

Time Min	Time Sec	Class 1 HRR [kW]	Class 2 HRR [kW]	Class 3 HRR[kW]	Class 4 HRR[kW]	Class 5 HRR[kW]
0	0	0	0	0	0	0
4	240	884	1105	1400	1768	1768
16	960	884	1105	1400	1768	1768
24	1440	3474	4342	5500	6947	6947
25	1500	5242	6553	8300	10484	10484
27	1620	2842	3553	4500	5684	5684
38	2280	632	789	1000	1263	1263
70	4200	0	0	0	0	0

As can be seen from the results of cars burning tests, both car class 4 and 5 have the same values of HRR. The heat release rate curves of the different car classes for the new generations is depicted Figure 8 and shows a comparison between these curves. During any, time dependent fire, such as a class 3 vehicle, the energy release rate (HRR) increases from zero to a maximum value for time equal to 25 minutes and decreases to zero at the end of the event.

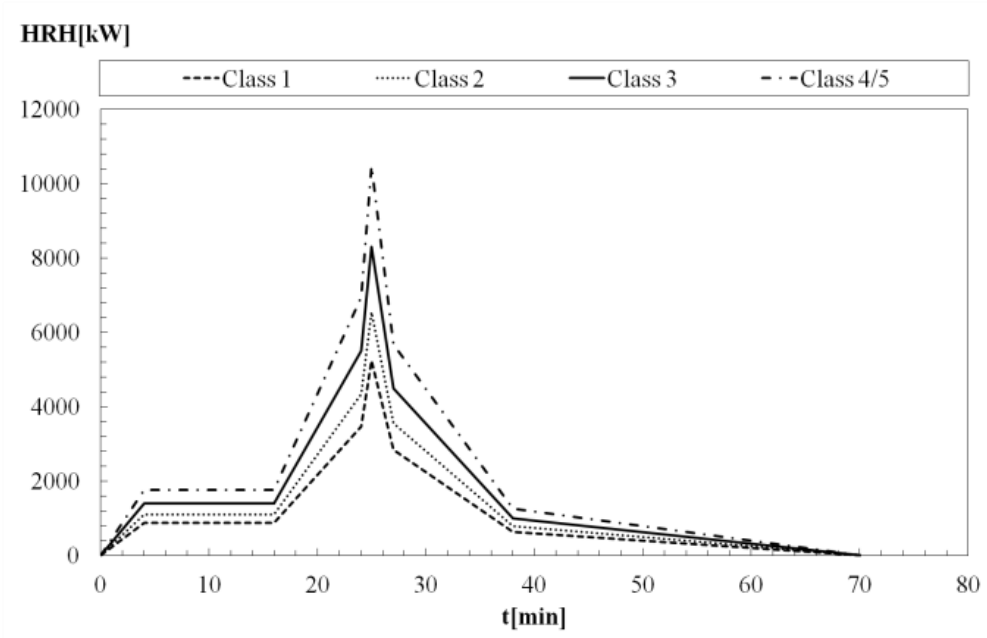

Figure 8.HRR of different car classes.

2.2.1- Factors controlling energy release rates in enclosure fires

The rate at which energy is released in a fire depends mainly on the type, quantity, and orientation of fuel and on the effects that an enclosure may have on the energy release rate.

The energy release rate will vary with time. Figure 7 shows a schematic graph of the energy release rate vs. time measured when wood pallet stacks of different heights burn. Such measurements are often termed “free burn” tests, indicating that the items are burning without any effects of the enclosure in which the fire takes place [48].

2.2.1.1- Enclosure effects

When an item burns inside an enclosure, two factors mainly influence the energy released and the burning rate. First, the hot gases will be collected at the ceiling level and heat the ceiling and the walls. These surfaces and the hot gas layer will radiate heat toward the fuel surface, thus enhancing the burning rate. Second, the enclosure vents (doors, windows, leakage areas) may restrict the availability of oxygen needed for combustion. This causes a decrease in the amount of fuel burnt, leading to a decrease in energy release rate and an increase in the concentration of unburnt gases.

If, however, the opening is relatively small, the limited availability of oxygen will cause incomplete combustion, resulting in a decrease in energy release rate, which in turn causes lower gas temperatures and less heat transfer to the fuel. The fuel will continue to release volatile gases at a similar or somewhat lower rate. Only a part of the gases combusts, releasing energy, and unburnt gases will be collected at ceiling level. The unburnt gases can release energy when flowing out through an opening and mixing with oxygen, causing flames to appear at the opening.

In summary, compartment heat transfer can increase the mass loss rate of the fuel, while compartment vitiation of the available air near the floor will decrease the mass loss rate [48].

2.2.2- Energy release rates based on free burn measurements

The only practical way to determine the burning rate or energy release rate of an item is by direct measurement. Such measurements are termed free burn measurements, meaning that the enclosure effects are minimized. The hot gases are vented away from the fuel and there is no limitation on air supply to the fuel. The results can then be used by engineers as guidelines when determining the design fire for a certain scenario. In the case of liquid fuels, such measurements have resulted in expressions that allow the energy release rate to be calculated if the liquid pool diameter is known. Below, we briefly discuss the most common measurement

techniques, discuss methods for calculating energy release rate from pool fires, and show experimentally determined energy release rate curves for various residential and industrial items [48].

2.3- Definition of fire compartment

Space within a building, extending over one or several floors, which is enclosed by separating elements such that fire spread beyond the compartment is prevented during the relevant fire exposure. Fire compartment is a volume within a building which is completely surrounded with fire-resistant construction elements, which can be integrated right into the structure of the building. Fire compartments are not absolutely fire proof. Fire can work its way into or out of a fire compartment if it is intense enough, poorly managed, or not addressed quickly enough. Existing buildings can be retrofitted to create fire compartments.

Movable barriers can be installed, or people can remodel parts of a building to create a fire compartment. Also known as a fire zone, a fire compartment can also sometimes address the potential of flood damage, as the same materials which keep fire out can sometimes keep water at bay as well. The fire compartments can consist of rooms or groups of rooms. When a fire starts inside a compartment, the sealed nature of the area can be partitioning the fire, preventing it from spreading to other areas. The fire compartment used in this study represents a fire in open car park, being the dimensions defined in the next sections [49].

2.3.1- Phases of fires in compartment

The fire in compartment is characterized by four principal phases. The first phase is the fire development which is the evolution of the size of the fire from a small incipient fire. If there is no action to stop the fire, it will have the maximum size. In this situation, the fire size will be controlled by the amount of existing fuel or by the amount of ventilation.

The second phase is the flashover which is usually obvious to the observer of fire growth. When an object begins to burn in a compartment, gives rise to the appearance of a fire plume of hot gases and smoke. By natural convection rises to the ceiling, where it begins to spread horizontally, forming a layer. An unconfined flame tends to follow the initial growth period, a law in which the heat release rate is proportional to the square of time. Thus, the layer next to the ceiling increases temperature and thickness because the plume continues to transport mass and energy from the burning material. The temperature increase of that layer makes the

emission of radiation, being primarily directed downward, higher and higher. This radiation focuses on the existing objects in the compartment is partially absorbed and increases the temperature of these objects, which continue to produce volatile combustibles. When the upper layer reaches of 600°C order, the incident radiation is sufficient to ignite these released volatile combustibles, bringing simultaneously all objects under fire. This incident radiation has an estimation value of 20 kW/m^2 at ground level [50].

The third phase corresponds to the full development of the fire, which is affected by: a) the size and shape of the enclosure, b) the amount, distribution and type of fuel in the enclosure, c) the amount, distribution and form of ventilation of the enclosure and d) the form and type of construction materials comprising the roof (or ceiling), walls and floor of the enclosure.

The fourth phase corresponds to the cool down of the fire, and depends on the fire brigade intervention or the limitation on fuel or oxygen.

2.3.2- Characteristics of the fire compartment

The compartment in this study is named open car parking and has the following geometry characteristics: 10m width, 10m depth, and height= 3m. It is characterized by the existence of concrete slabs. The compartment consists in two major walls, one ceiling and one floor. The heat flows through the ceiling, walls, and floor of a compartment. Two zones are expected to define the fire compartment, which are the lower layer zone and upper layer zone. The thermal properties of concrete and steel are presented in Table 3. Steel was considered to define the target material and concrete was considered to define the material of the slab. Two zones are expected to define the fire compartment, which are the lower layer zone and upper layer zone. The compartment has also two major wall vents (open lateral walls), with 0m for sill, 3m for soffit and 10m width [51], see Figure 9.

Table 3.Thermal properties of Concrete and Steel.

THERMAL PROPERTIES	CONCRETE	STEEL
Density	2200 kg/m^3	7850 kg/m^3
Thermal conductivity	0.002 kW/(m °C)	0.053 kW/(m ° C)
Specific heat	0.9 kJ/(kg °C)	0.425 kJ/(kg °C)
Emissivity	0.7	0.7

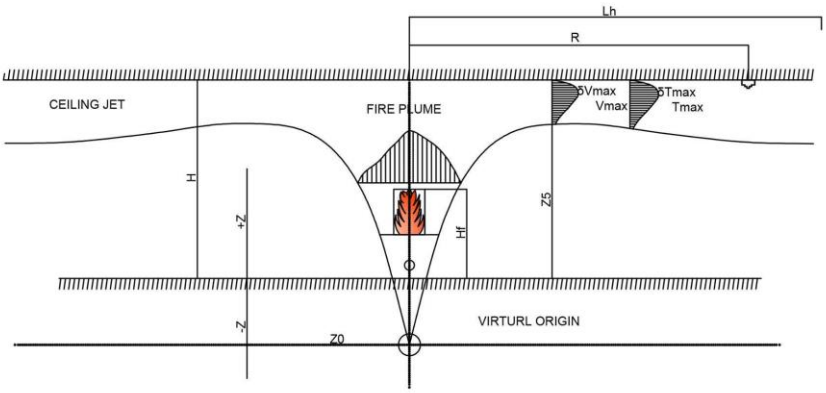

Figure 9.Localized fire of our compartment.

2.4- Definition of different fire events

A "fire event" shall be defined as an occurrence in which extinguishing media was used to suppress fire. This may mean a portable fire extinguisher, water from fire department efforts, the activation of a kitchen vent hood, a building's sprinkler system, or any other fire suppression system within a building. On the rare occasion when evidence of fire is present, and the fire has self-extinguished, this will also be identified as a fire event. In this study, the fire even of a burning car was considered.

Many tests were done in previous years to calculate the heat release rate from car fire events. The first tests carried out in opened conditions were developed by Mangs and Keski-Rahkonenin the 90’s [42].Ten tests of burning cars were done between 1995 and 1996, involving 15 cars old series (70ies/80ies) and a new generation series (90ies). For cars class 3, with the performance of one car in five tests and two cars in the other five tests. The graph of the comparison between the HRR of the two-generation showed that the energy released by a car made in 1995 was twice that of a 1980’s car. Some of the HRR results [49].

2.5- Fire detection

Reliable fire detection is an essential part of the fire protection program in nuclear power plants (NPPs), it relates to both fire control or extinguishment and safe evacuation of occupants. Most of the devices associated with fire detection and suppression are typically located near the ceiling surfaces. In the event of a fire, hot gases in the fire plume rise directly above the burning

fuel and impinge upon the ceiling. The ceiling surface causes the flow to turn and move horizontally beneath the ceiling to other areas of the building located at some distance from the fire. The response of detection devices (heat/smoke detectors) and sprinklers installed below the ceiling submerged in this hot flow of combustion products provides the basis for the building's active fire protection measures.

Smoke and heat detectors are best suited for fire detection in confined spaces, where rapid heat generation can be expected in the event of a fire. Smoke and heat detectors have been installed extensively in most nuclear power plants. Generally, such detectors are installed as part of a building-wide alarm system, which typically alarms in the main control room. The purpose of such systems is to provide early warning to building occupants, and rapid notification of the fire brigade. Some detection devices will also perform the function of automatically actuating suppression systems and interfacing with other building systems such as heating, ventilation, and air-conditioning (HVAC).

Detection is critical to fire safety in nuclear power plants since a potential fire hazard may involve safe plant shutdown. Consequently, safety-related systems must be protected before redundant safety related systems become damaged by the fire.

Throughout the nuclear industry, there has been considerable responsive action relative to the nuclear safety-related fire protection and incorporating sound fire protection principles in nuclear facility design. New standards, regulatory guides, and criteria have been published since the fire at the 1975, Browns Ferry Nuclear Power Plant. Recognizing the unique characteristics of fires in nuclear power plants, requirements have been established for locating smoke detectors. Particular emphasis has been given to establishing criteria for early warning detection of electrical cable fires [52].

3- HEAT TRANSFER

There are three mechanisms by which heat is transferred from one object to another: radiation, convection, and conduction. Classical textbooks on heat transfer provide innumerable hand-calculation expressions for calculating heat fluxes to and from solids, liquids, and gases, as well as expressions for estimating the resulting temperature profiles in a target. These analytical expressions are usually arrived at by setting up the energy balance, by assuming constant properties and homogeneity in the media involved, and by ignoring the heat transfer mechanisms that seem to be of least importance in each case. The radiative heat flux from flames, hot gases, and heated surfaces impinging on a solid surface can be estimated using classical heat transfer and view factors. The same applies for convective heat transfer to solids and conductive heat transfer through solids. The surface temperature of a solid subjected to a radiative, convective, or conductive heat flux can be calculated by hand assuming the solid is either semi-infinite or behaves as a thermally thin material. Numerous types of heat transfer problems can be solved in this way. Assuming that a secondary fuel package is subjected to a known heat flux and that it has a certain ignition temperature and constant thermal properties, then the time to ignition can be calculated. Similarly, if the activation temperature of a sprinkler bulb is known, the activation time can be estimated. Several other problems can be addressed in this way, including temperature profiles in building elements, flame spread over flat solids, heat detector activation, spread of fire from one building to another, etc. Analytical solutions to such problems can be found in standard textbooks on heat transfer [48].

3.1- Conduction

Conduction is at transfer through solids or stationery fluids. When someone touch a hot object, the heat that this person feel is transferred through the skin by conduction. Two mechanisms explain how heat is transferred by conduction: lattice vibration and particle collision. Conduction through solids occurs by a combination of the two mechanisms; heat is conducted through stationery fluids primarily by molecular collisions.

In solids, atoms are bound to each other by a series of bonds, analogous to springs. When there is a temperature difference in the solid, the hot side of the solid experiences more vigorous atomic movements. The vibrations are transmitted through the springs to the cooler side of the solid. Eventually, they reach an equilibrium, where all the atoms are vibrating with the same energy.

In fluids, conduction occurs through collisions between freely moving molecules. The mechanism is identical to the electron collisions in metals. The effectiveness by which heat is transferred through a material is measured by the thermal conductivity, k. A good conductor, such as copper, has a high conductivity; a poor conductor, or an insulator, has a low conductivity) [43].

3.2- Convection

Convection uses the motion of fluids to transfer heat. In a typical convective heat transfer, a hot surface heats the surrounding fluid, which is then carried away by fluid motion. The warm fluid is replaced by cooler fluid, which can draw more heat away from the surface. Since the heated fluid is constantly replaced by cooler fluid, the rate of heat transfer is enhanced.

Natural convection (or free convection) refers to a case where the fluid movement is created by the warm fluid itself. The density of fluid decrease as it is heated; thus, hot fluids are lighter than cool fluids. Warm fluid surrounding a hot object rises, and is replaced by cooler fluid. The result is a circulation of air above the warm surface

Forced convection uses external means of producing fluid movement. Forced convection is what makes a windy, winter day feel much colder than a calm day with same temperature. The heat loss from your body is increased due to the constant replenishment of cold air by the wind. Natural wind and fans are the two most common sources of forced convection [43].

3.3- Radiation

Radiative heat transfer does not require a medium to pass through; thus, it is the only form of heat transfer present in vacuum. It uses electromagnetic radiation (photons), which travels at the speed of light and is emitted by any matter with temperature above 0 Kelvin (-273 °C). Radiative heat transfer occurs when the emitted radiation strikes another body and is absorbed.

The electromagnetic spectrum classifies radiation according to wavelengths of the radiation. Main types of radiation are (from short to long wavelengths): gamma rays, x-rays, ultraviolet (UV), visible light, infrared (IR), microwaves, and radio waves. Radiation with shorter wavelengths are more energetic and contains more heat. X-rays, having wavelengths $\sim 10^{-9}$ m, are very energetic and can be harmful to humans, while visible light with wavelengths

$\sim 10^{-7}$ m contain less energy and therefore have little effect on life. A second characteristic, which will become important later is that radiation with longer wavelengths generally can penetrate through thicker solids. Visible light is blocked by a wall. However, radio waves, having wavelengths on the order of meters, can readily pass through concrete walls.

Anybody with temperature above 0 Kelvin emits radiation. The type of radiation emitted is determined largely by the temperature of the body. Most "hot" objects, from a cooking standpoint, emit infrared radiation. Hotter objects, such as the sun at 5800 K, emits more energetic radiation including visible and UV. The visible portion is evident from the bright glare of the sun; the UV radiation causes tans and burns [43].

4- CORRELATIVE MODELS

4.1- Definition of correlative models

Correlations to estimate temperatures and velocities in the hot gases beneath a ceiling in a fire, a so-called ceiling jet, have existed for at least four decades. These types of correlations are often used in fire safety engineering in order to get an estimate of sprinkler and/or heat detector activation in enclosure fires. Such correlations can also be used to estimate damage if a ceiling material will ignite or if structures will be affected. A ceiling jet is created when a buoyancy driven plume impinges on a flat un-obstructed ceiling and the hot gases spreads radially under the ceiling, see Figure 10. As the ceiling jet moves radially from the outward, air will be entrained and the temperature cools down due to entrainment of cold air and heat losses to the ceiling. If the ceiling jet is unconfined it will have a maximum thickness of about 5-13% of the total room height and the maximum temperature will be at a distance of 1% of the room height below the ceiling. The thickness of the ceiling jet has been defined as the distance to where the excess of gas temperature drops to 1/e of (1/2.72) the maximum excess temperature. In a normal compartment fire, this type of unconfined ceiling jet will only exist in the earliest stages of fire development before the hot gases will accumulate in the compartment. The correlations have also been implemented in computer software, like DETACT-QS and CFAST, and used as a part of the traveling fires concept. Presently, there is a range of ceiling jet correlations available for different applications, e.g. for transient fires and confined ceilings [53].

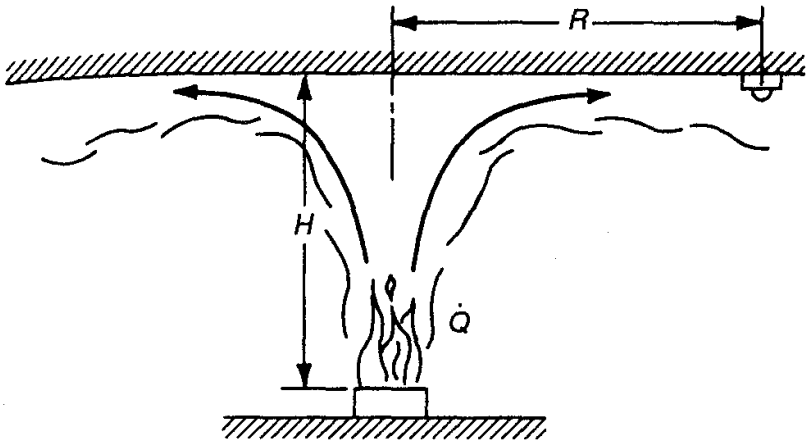

Figure 10.Ceiling jet flow beneath an unconfined ceiling [54].

The main parameters of the fire induce ceiling jet are represented. For this case, it is assumed that this fire is equivalent to a pool fire with a diameter D=2 m, an elevation surface Hs equivalent to 0.3 m above the ground and a remaining distance H up to the ceiling equals 2.7 m, see Figure 11.

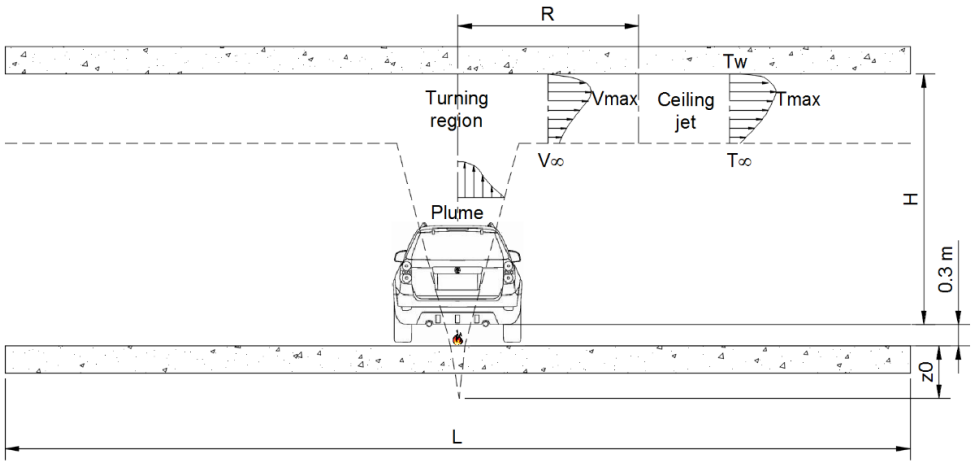

Figure 11.The geometry of the compartment.

4.2- Alpert correlations

Alpert assumed an axisymmetric fire induced flow beneath a flat, horizontal ceiling that was unobstructed by walls 1 and the ceiling jet was divided into two regions. Thus there are two sets of correlations, for the maximum excess temperature (t_{max}) and maximum velocity (u_{max}), presented. The first one is valid in the turning region where the plume impinges the ceiling ($r/H \leq 0.18$ for equation 3 and $r/H \leq 0.15$ for equation 5) and is independent of the radial distance of the plume. The second set of correlations is valid in the far field ($r/H > 0.18$ for equation 2 and $r/H > 0.15$ for equation 4) and is dependent on the radial distance from the plume centreline.

The correlations developed by Alpert for determining maximum ceiling jet temperatures and velocities in S.1. Units are:

r/H> 0,18

$$T_{max} = T_\infty + \frac{5{,}38 \times \left(\frac{Q}{r}\right)^{\frac{2}{3}}}{H} \qquad \text{Eq 4}$$

r/H≤0,18

$$T_{max} = T_\infty + \frac{16{,}9 \times \dot{Q}^{\frac{2}{3}}}{H^{\frac{5}{3}}} \qquad \text{Eq 5}$$

r/H> 0.15 $$V\max = 0{,}197 \times \frac{\dot{Q}^{1/3} H^{1/2}}{r^{5/6}}$$ Eq 6

r/H≤0,15 $$V\max = 0{,}96 \times (Q/H)^{1/3}$$ Eq 7

Where H is the ceiling height, r is the radial distance from the plume centreline and $\dot{Q}$ is the heat release rate of the fire. These original correlations where found with the help of qualitative curve fit of experimental data. A range of different types of fuels was used in the experiments but no regard was taken to the size of the convective part of the heat release rate, which later has been showed to control the properties of fire plumes. Alpert also conducted a numerical study of ceiling jets. It was, among other things, studied how heat transfer to the ceiling affects the ceiling jet and it was seen that there was no large effect on the ceiling jet temperature and thickness within a radial distance of less than 1 ceiling height (r/H<1). However, at distances of 3 to 5 ceiling heights, the effects were significant [53].

These correlations are divided into two zones, one part applies to the region of impingement where the upward flow of gas in the plume turns to flow out beneath the ceiling horizontally. The correlations are based on measurements collected during test burns of fuel arrays of wood and plastic pallets, cardboard boxes, plastic materials in cardboard boxes, and liquid fuels with energy release rates ranging from 668 kW to 98 MW under ceiling heights from 4.6 to 15.5 m.

4.2.1- Maximum Velocity and Temperature during the fire event

The results of the maximum velocity and temperature near the ceiling depends on the fire events. The following conditions were assumed in the compartment: T∞=20°C, H=2.7m, D=2m. The maximum velocity and temperature were calculated for six targets and sensors on the ceiling, corresponding to the radial position r/H=0, 0.37, 0.74, 1.11, 1.48 and 1.85, shown in Figure 12 and Figure 13.

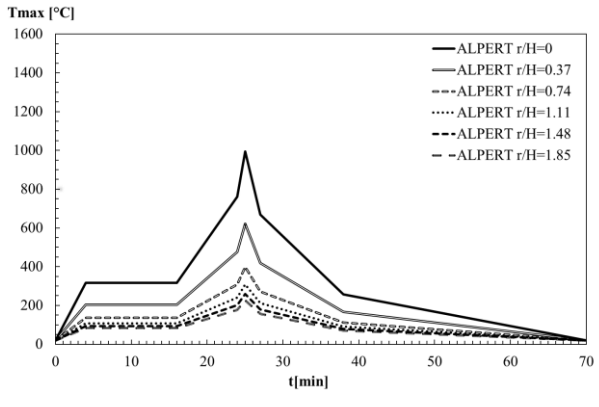

Class 1

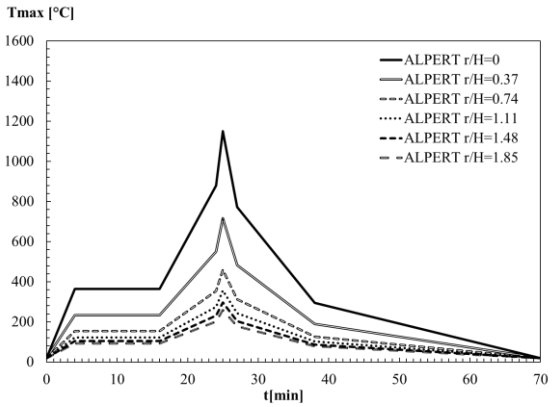

Class 2

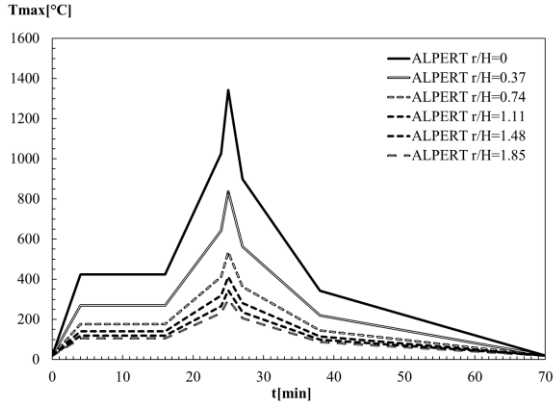

Class 3

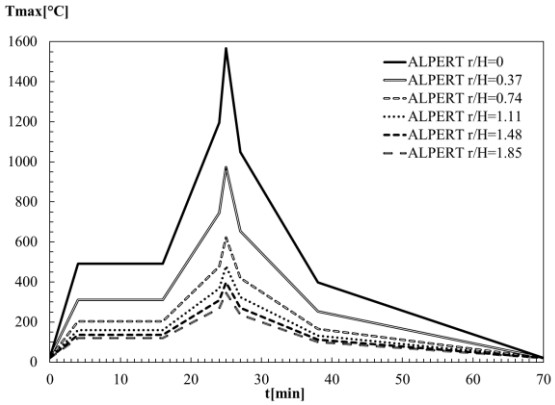

Class 4,5

Figure 12.Temperature near the ceiling from Alpert correlations.

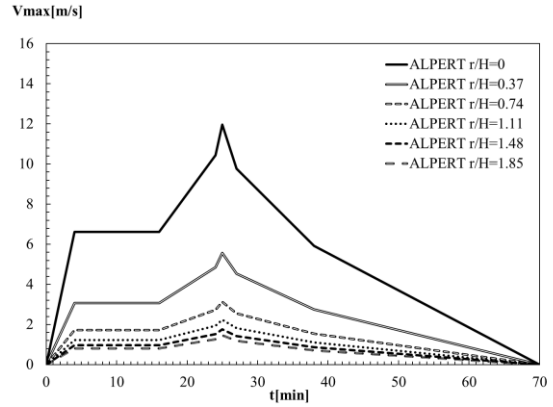

Class 1

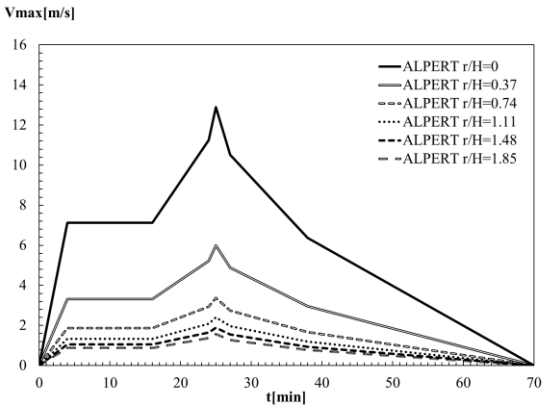

Class 2

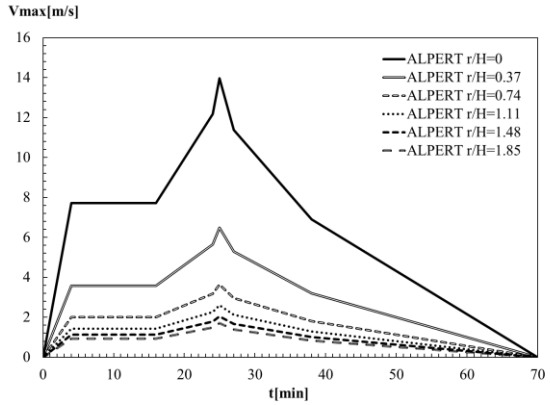

Class 3

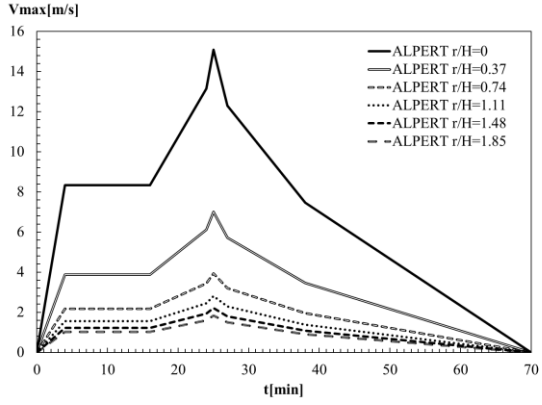

Class 4,5

Figure 13.Velocity near the ceiling from Alpert correlations.

4.2.2- Maximum Temperature and Velocity for different ratio r/H

From the results of the velocity and temperature in the hot zone layer, calculated by the correlations developed by Alpert, the maximum dynamic characteristics were extracted from the event for a time equal to 25 minutes (1500s). The maximum velocity and temperature curves are represented respectively in Figure 14 and Figure 15 against r / H in different positions for classes 1, 2, 3 and 4 5.

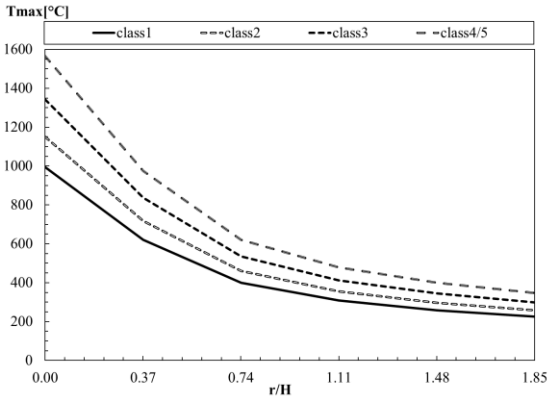

Figure 14.Tmax of all car classes calculated by Alpert correlations.

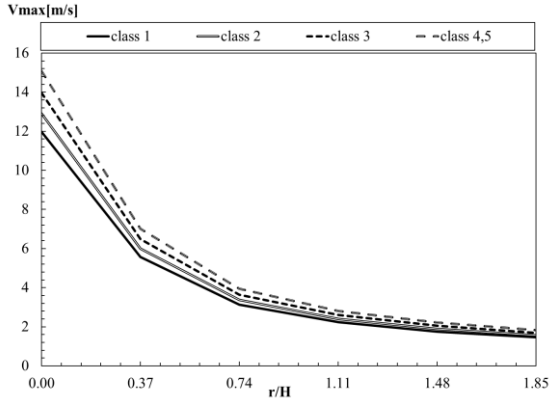

Figure 15.Vmax of all car classes calculated by Alpert correlations.

The maximum temperature and velocity decrease with the ratio r/H, as expected. These values also increase with with the energy of the fire events.

4.3- Cooper correlations

Cooper has also developed a method to estimate the plume properties and resulting ceiling jet characteristics. Cooper's equations account for the situation where only part of the plume is flowing into the upper layer and impinging on the ceiling [32].

The investigations of Cooper were done in detail about a ceiling jet in a region r/H > 0.2, measured horizontally from the centre axis of the plume to the wall. Correlations for velocity and temperature have been derived. Using steady-state and time varying heat release rates in full-scale multi-room fire scenarios to generate an experimental data base to use in mathematical fire simulation models. The tests focused on smoke filling and selected measurements of the increasing temperatures over time. Cooper developed correlations for the maximum temperature and velocity with limits, which are dependent on the ratio r/H, and defined in the following equations [33].

$0 \leq r/H \leq 0.75$ $$T\max = T\infty + 28{,}1EXP(-1{,}77 \times \frac{r}{H}) \times Q^{\frac{2}{3}} \times H^{-5/3}$$ Eq 8

$0.75 \leq r/H \leq 4.0$ $$T\max = T\infty + 5{,}77 \times (\frac{r}{H})^{-0{,}88} \times Q^{\frac{2}{3}} \times H^{\frac{-5}{3}}$$ Eq 9

$0.2 \leq r/H \leq 4.0$ $$V\max = 0{,}26 \times (\frac{r}{H})^{-1{,}1} \times Q^{1/3} \times H^{-1/3}$$ Eq 10

4.3.1- Maximum Velocity and Temperature during the fire event

The same calculation was done using Cooper correlative model, using the same time data, for the same dimensions of event, and the same positions for targets and sensors.

Figure 16 and Figure 17 present the results for the maximum velocity and the temperature values.

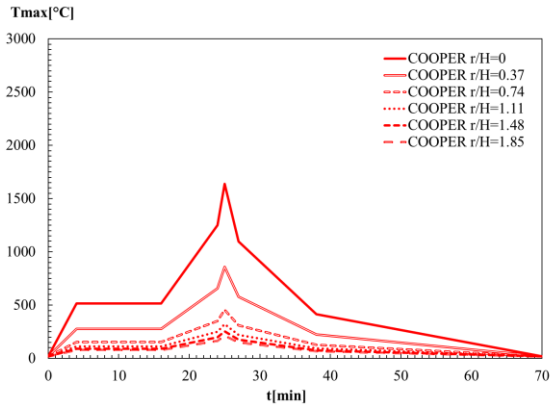

Class 1

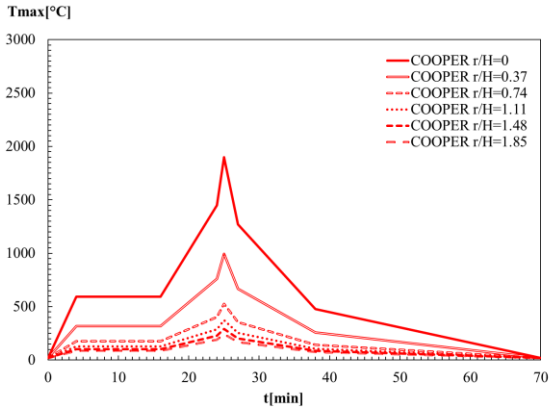

Class 2

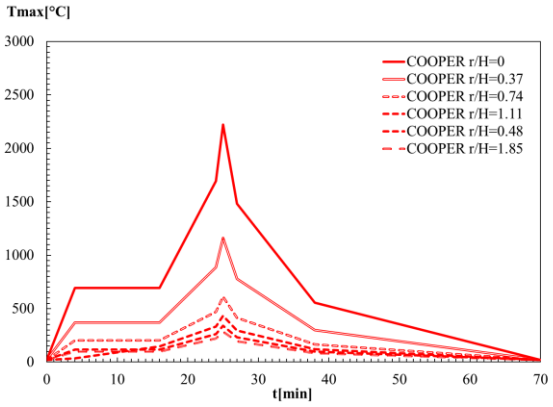

Class 3

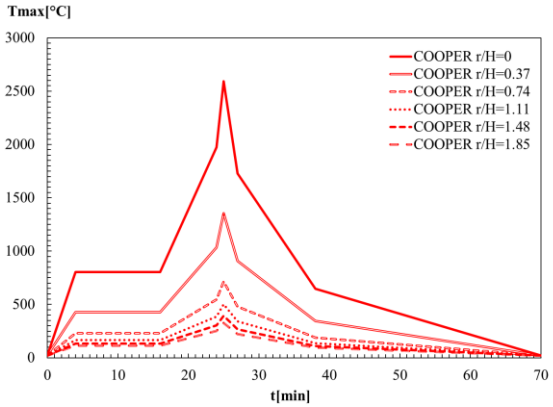

Class 4,5

Figure 16.Temperature near the ceiling from Cooper correlations.

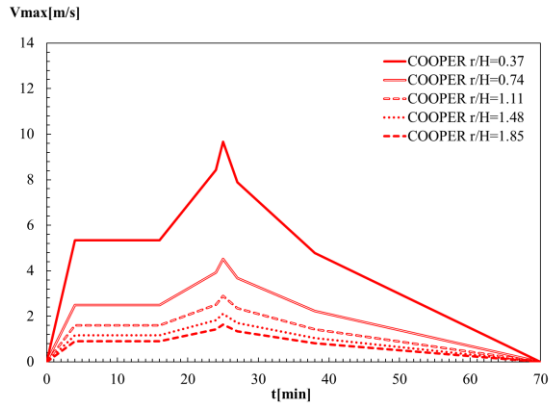

Class 1

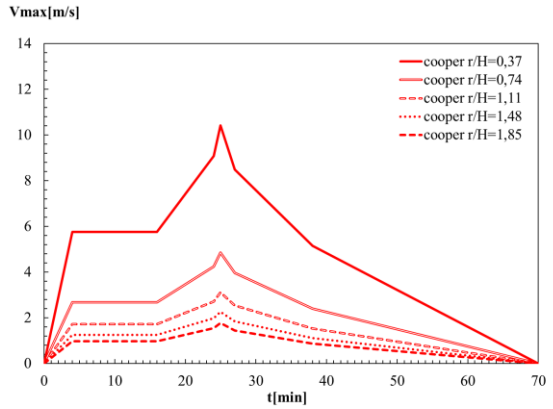

Class 2

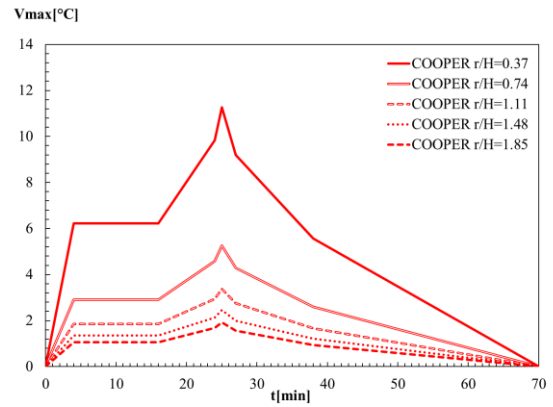

Class 3

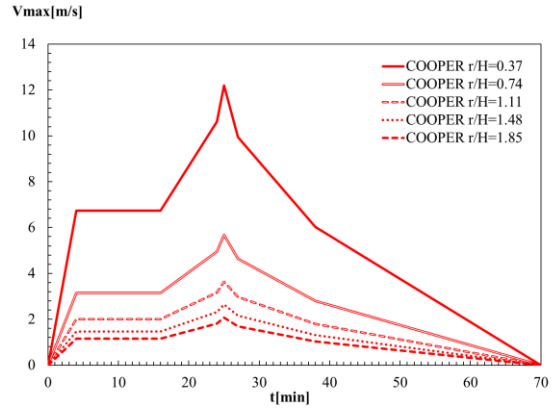

Class 4,5

Figure 17.Velocity near the ceiling from Cooper correlations.

4.3.2- Maximum Temperature and Velocity for different ratio r/H

The maximum value of the velocity and temperature of the gases near the ceiling are identified when the time is equal to 25 min. The variation of the maximum values is plotted against the ratio r/H, depending of the fire class in Figure 18 and Figure 19.

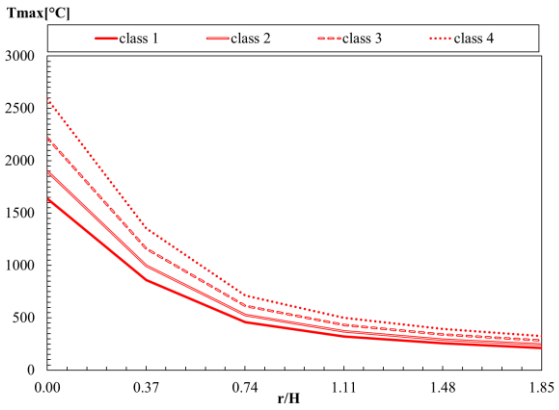

Figure 18.Tmax of all car classes calculated by Cooper correlations

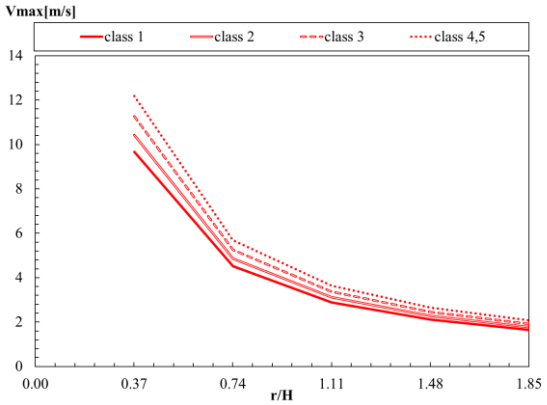

Figure 19.Vmax of all car classes calculated by Cooper correlations

These results are in agreement with the results obtained by Alpert correlative model

4.4- Heskestad and Delichatsios correlations

Heskestad and Delichatsios has presented the bulk of the theory regarding flows within a primary channel. His paper also presents correlations for the temperature and velocity of the ceiling jet within this channel. According to his work, the ceiling jet is initially axi-symmetric until it is intercepted by the beams. At this point a transition region begins until the flow converges to a two dimensional, channel flow. Upon intersection of the ceiling jet with the beams, a portion of the gases escape under the beam and into adjacent channels. The remainder of the gases flow within the channel in opposite directions. However, if the beams are sufficiently deep, large d/H, the leakage under the beams becomes small, and all of the fire gases are restricted to the primary channel. According to Delichatsios, this occurs at a beam depth to ceiling height ratio, d/H, of 0.2. The work developed by the authors has essentially confirmed this by showing that a d/H =0.15 produces an 80% reduction in flows under the beam at the closet radial location from the plume centreline. An asymptotic reduction toward a corridor flow occurs for d/H > 0.15 [5].

Temperature, gas velocity and optical density were measured at various locations along the ceiling. Cumulative weight loss of the fuel was also measured. In addition, several commercially available smoke and heat detectors were grouped together and located at several positions along the test ceiling. The response of these detectors was recorded.

A set of functional relationships for the temperature and velocity of ceiling jet gases has been proposed by Heskestad. The expressions relate fire size, fire growth rate, height above the fire, radial distance from the fire, gas temperature and gas velocity for the general class of fires called power-law fires.

For most ceiling jet models, it is necessary to know the height of the ceiling above the focal point of the fire plume. The focal point is also called the origin or virtual origin of the plume [17].

Plume	$T\max = 2{,}5\left(\frac{Q_c^{\frac{2}{5}}}{H - Z_0}\right)^{\frac{5}{3}}$	Eq 11
0 <r/H≤8	$T\max = T\infty + 2{,}75 \times (0{,}188 + 0{,}313 \times r/H)^{-4/3} \times Q^{2/3} \times H^{-5/3}$	Eq 12
Plume	$V\max = \left(\frac{Q_C}{H - Z_0}\right)^{1/3}$	Eq 13
0 <r/H≤8	$V\max = 0{,}197 \times (r/H)^{-0{,}63} \times (0{,}188 + 0{,}313 \times r/H)^{-2/3} \times Q^{1/3} \times H^{-1/3}$	Eq 14

Where (Q_c) is the convective energy release rate in [kW], H is the height in [m], (Q) is the total heat release rate HRR in [kW], (Z_0) is the virtual origin given in Eq 1.

4.4.1- Maximum Velocity and Temperature during the fire event

The results of the maximum velocity and temperature obtained from the simple correlative models of Heskestad and Delichatsios are shown in Figure 20 and Figure 21. The results are consistent with previous conclusions used for other correlative models.

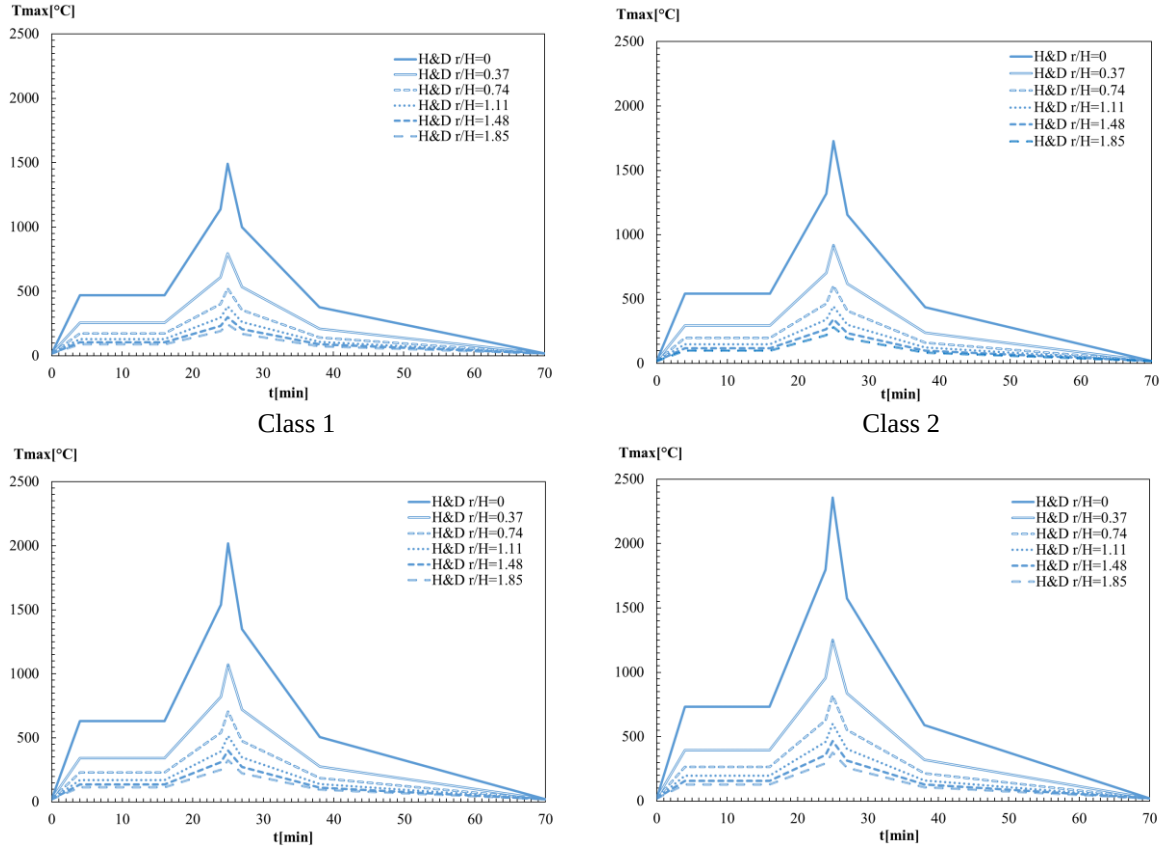

Figure 20.Temperature near the ceiling from Heskestad and Delichatsios correlations.

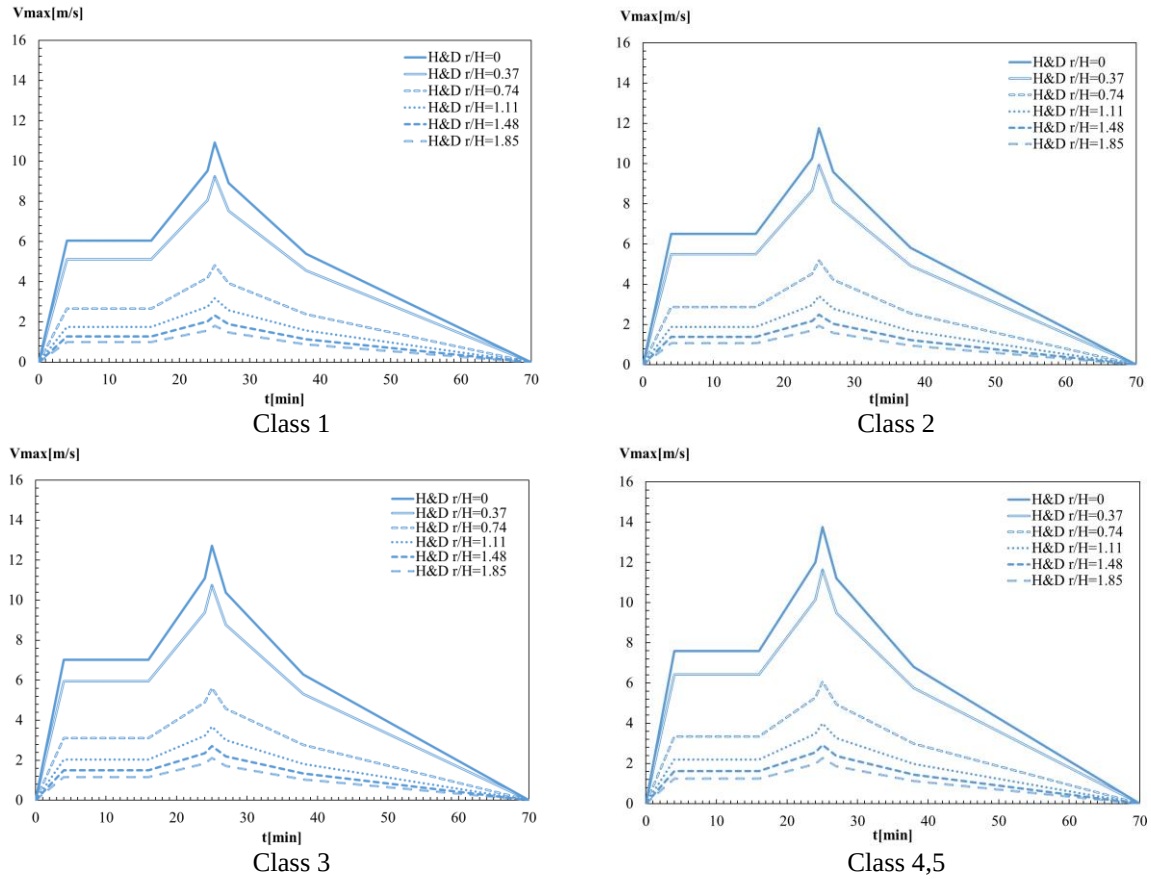

Figure 21.Velocity near the ceiling from Heskestad and Delichatsios correlations.

4.4.2- Maximum Temperature and Velocity for different ratio r/H

The maximum temperature and velocity values of the hot gases near the ceiling were calculated from the Heskestad and Delichatsios correlations, using the same time evant as the reference (t=25 minutes). Figure 22 and Figure 23 show the variation of each dynamic parameter.

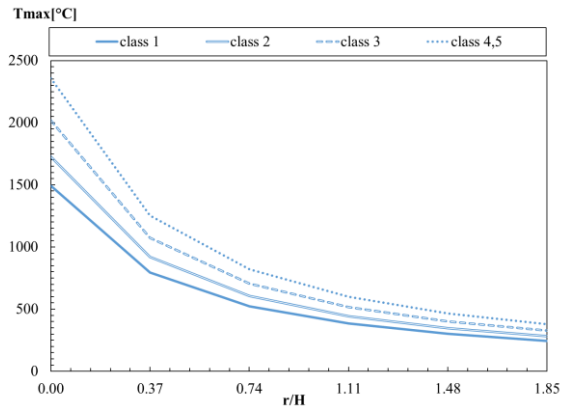

Figure 22.Tmax of car classes from Heskestad and Delichatsios correlations

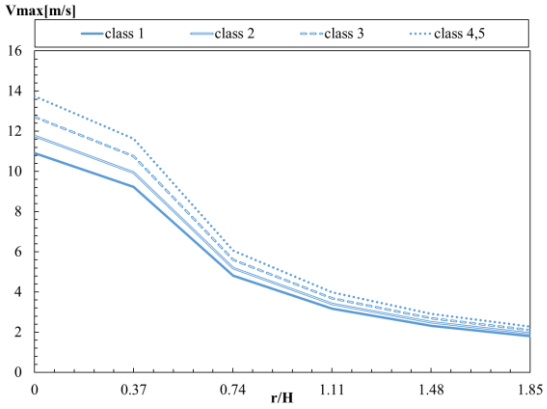

Figure 23.Vmax of car classes from Heskestad and Delichatsios correlations

4.5- Comparison of results

Temperature and speed are two major qualities that must be calculated in order to decide on any position of the sensor or activation system (sprinklers, heat alarm) during any time dependent fire. In all vehicle categories, the energy release rate (HRR) increases from zero to a maximum value and decreases to zero at the end of the fire. The correlated models (Alpert, Cooper, Heskestad and Delichatsios) were used to compare the speed and temperature near the ceiling for six target positions, corresponding to r/H=0, 0.37, 0.74, 1.11, 1.48 and 1.85.

4.5.1- Maximum temperature comparison for class 1

Figure 24 shows the comparison between different correlative models. The maximum temperature decreases with the increase of the ratio r/H, being the results obtained from Heskestad and Delichatios positioned between the other correlative models. After the ratio of r/H=0.74, this correlative model overestimates the maximum temperature compared to the Alpert and Cooper models. The Cooper model seems to correlate well with Alpert correlations for r/H greater than 1.1, with a difference between them below 5%. The results of the maximum temperature obtained from Heskestad and Delichatsios do not agree with Alpert. These results are approaching together when r/H is greater than 1.85. For this ratio, the relative difference is 8.8%. The Cooper model seems to underestimate the maximum temperature, compared to the results of Heskestad and Delichatsios for the r / H ratio greater than 0.5.

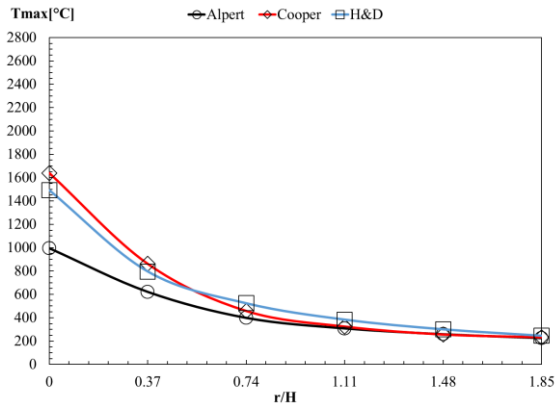

Figure 24.Comparison of the value of T_{max} from the correlative models for class 1

4.5.2- Maximum temperature comparison for class 2

Figure 25 represents the maximum temperature decreases with the increase of the ratio r/H, being the relative results obtained by all the correlative model in agreement with previous fire event class car. The maximum temperature increases with the class of the fire event.

Cooper model's correlate very well with Alpert model when the ratio of r/H is greater than 1.1, with relative deference between them below 5%. There is a good approximation between the Alpert and Cooper model when r/H>0.74 with relative difference smaller than 14.5%.

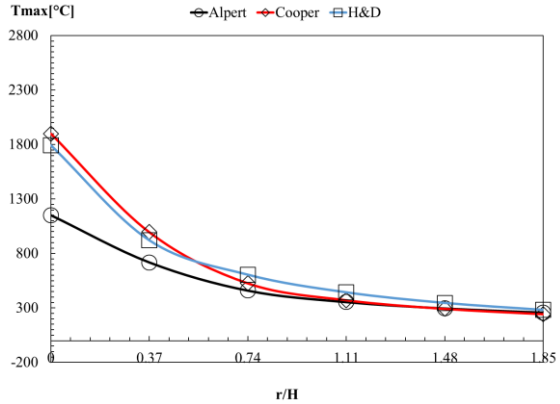

Figure 25.Comparison of the value of T_{max} from the correlative models for class 2

An approximation is noticed between the correlative models of Heskestad and Delichatsios, and Cooper at the region when the ratio r/H approaches 0.5.

4.5.3- Maximum temperature comparison for class 3

Figure 26 represents the evolution of the maximum temperature for a class 3 fire event. The maximum temperature decreases with the increase of the ratio r/H, being the relative results obtained by the entire correlative model in agreement with previous fire event class car. The maximum temperature increases with the class of the fire event.

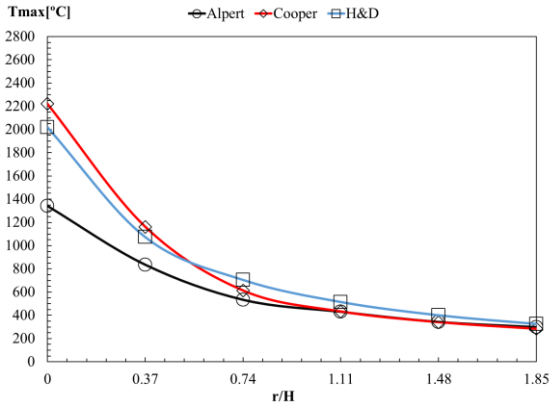

Figure 26.Comparison of the value of T_{max} from the correlative models for class 3

4.5.4- Maximum temperature comparison for class 4,5

Figure 27 shows the evolution of the maximum temperature for the firing event of Class 4 and Class 5. Higher values are expected because the HRR used for these fire events is higher. Once again, the maximum temperature decreases with the r / H ratio.

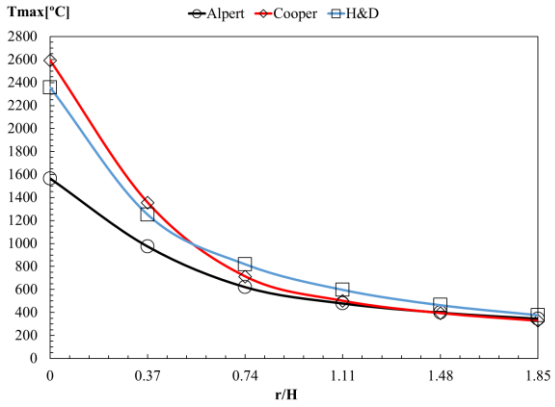

Figure 27.Comparison of the value of T_{max} from the correlative models for class 4,5

4.5.5- Maximum velocity comparison for class 1

Figure 28 shows the variation of the maximum velocity with respect to the ratio of the radial position r/H. The maximum velocity decreases with the radial position being the intermediate results with the Cooper correlative model.

Taking the Alpert model as a reference, the maximum speed near the ceiling decreases with the ratio between the radial position and the height of the ceiling. The correlative models of Heskestad and Delichatsios and Alpert are well suited for r / H equal to 0.0 with a relative difference between them equal to 0.5%. Cooper's correlative model for the plume is not presented.

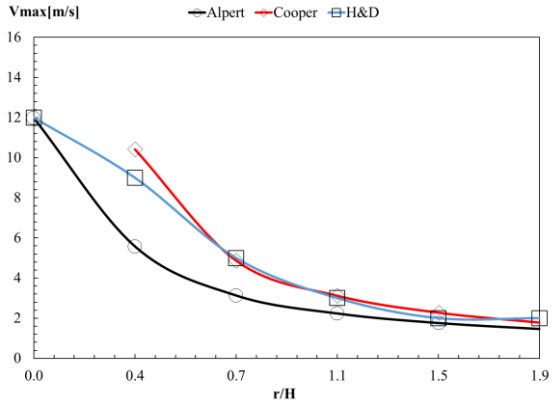

Figure 28.Comparison of the value of V_{max} from the correlative models for class 1

4.5.6- Maximum velocity comparison for class 2

Figure 29 represents the variation of the maximum velocity with respect to the ratio of the radial position r/H. The results show that there is a divergence between the results of Alpert and Heskestad and Delichatsios with 4.4% of relative difference between them in the plume zone.

There is a big difference between the two results (Alpert and Heskestad and Delichatsios) for ratios r/H greater than 0.37, with more than 60% of relative difference.

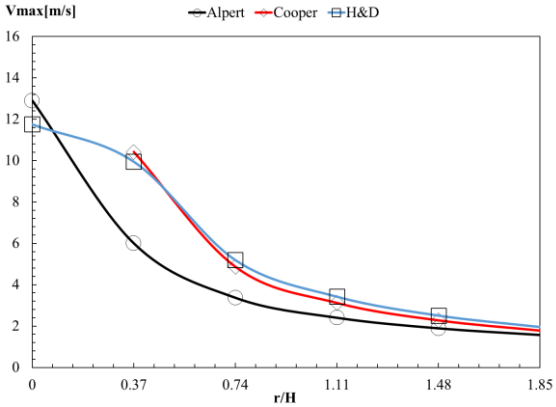

Figure 29.Comparison of the value of V_{max} from the correlative models for class 2

4.5.7- Maximum velocity comparison for class 3

The maximum velocity decreases with the ratio r/H and the results from Cooper model agree with Alpert model for the higher values of r/H. The relative difference between results from Heskestad and Delichatsios correlations and Alpert correlations reaches 9.9% for the ratio r/H=0.

Figure 30 represents the variation of the maximum velocity with respect to the ratio of the radial position r/H.

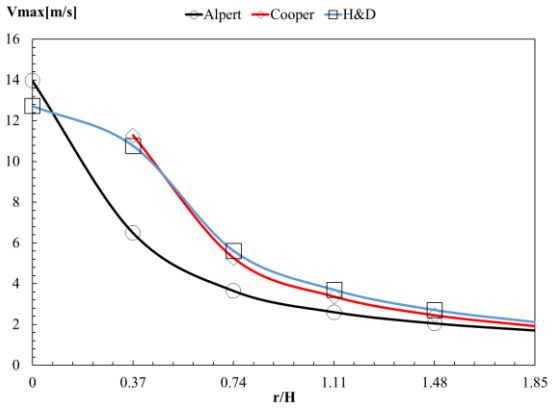

Figure 30.Comparison of the value of V_{mac} from the correlative models for class 3

4.5.8- Maximum velocity comparison for class 4,5

Figure 31 depicts the variation of the maximum velocity with respect to the ratio of the radial position r/H.

Similar conclusion regarding the correlative models can be made for this fire event. Higher difference was detected for the plume zone between the correlative model of Heskestad and Delichatsios and Alpert correlative model.

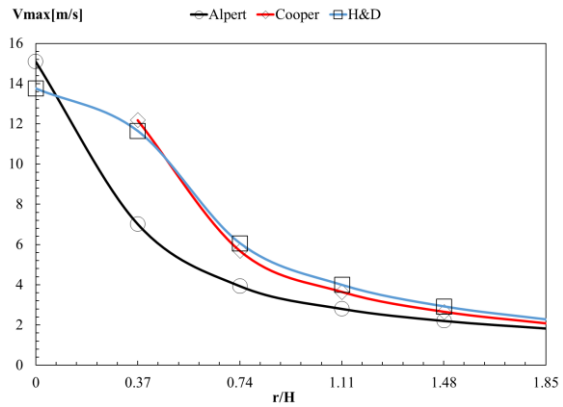

Figure 31.Comparison of the value of V_{max} from the correlative models for class 4,5

A table of comparison with the differences between the values of maximum temperature and velocity are presented in annex 1.

5- CFAST model

Zone model is the name given to numerical programs which calculate the development of the temperature of the gases as a function of time, integrating the ordinary differential equations which express the conservation of mass and the conservation of energy for each zone of the compartment. They are based on the fundamental hypothesis that the temperature is uniform in each zone. Zone models give not only the evolution of the temperature of the gases in the compartment, but also additional information such as the temperatures in the walls or the velocity of the gases through the openings.

The data which have to be provided to a zone model are: geometrical data, such as the dimensions of the compartment, the openings and the partitions; material properties of the walls; fire data, as HRR curve, pyrolysis rate, combustion heat of fuel.

As a result of the simulation, the gas temperature is given in each of the two layers, as well as information on wall temperatures and flux through the openings. An important result is the evolution, as a function of time, of the thickness of each layer. The thickness of the lower layer, which remains at rather cold temperature and contains no combustion products, is very important to assess the tenability of the compartment for the occupants. Figure 32 shows how a compartment is modelled by a two-zone model, with different terms of the energy and mass balance represented.

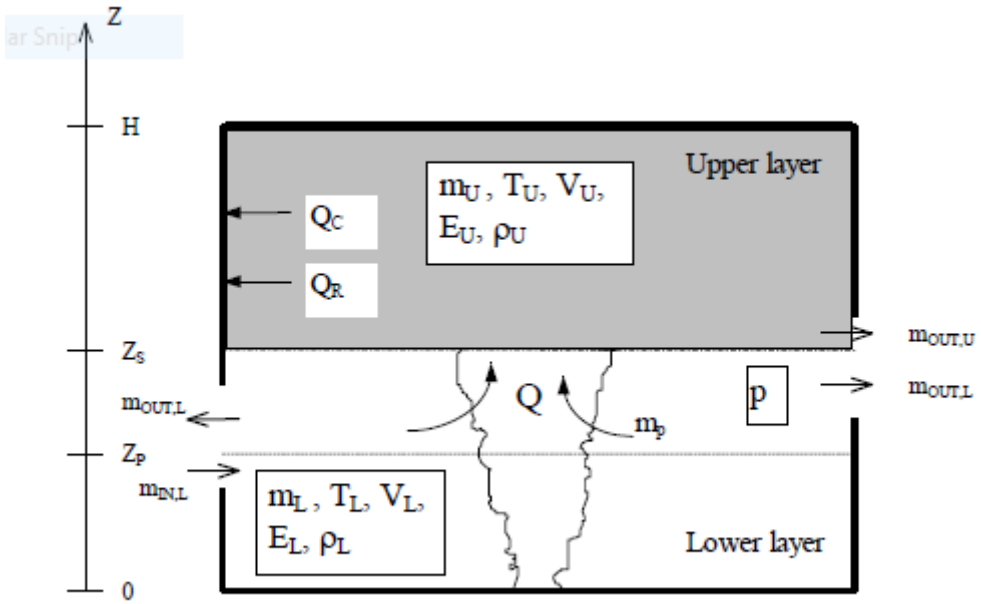

Figure 32.compartment in a two-zone model [43].

5.1- Presentation of CFAST

CFAST is a two-zone fire model that predicts the thermal environment caused by a fire within a compartmented structure. Each compartment is divided into an upper and lower gas layer (zone in the term zone fire model refers to the layers being modelled). The fire drives combustion products from the lower to the upper layer via the plume. The temperature within each layer is uniform, and its evolution in time is described by a set of ordinary differential equations derived from the fundamental laws of mass and energy conservation. The transport of smoke and heat from zone to zone is dictated by empirical correlations. Because the governing equations are relatively simple, CFAST simulations typically require a few tens of seconds of CPU time on typical personal computers.

CFAST can model a fire as a heat source or with a simple combustion model and was developed by the National Institute of Standards and Technology. CFAST is a two-zone fire model that can accommodate 30 compartments with multiple openings between compartments.

5.2- The model

The model analysed is the same as that used for the correlative models. Different fire events (car classes) have been defined to determine the temperature and velocity near the ceiling of a fire-induced ceiling jet. Different steps to perform this simulation are presented below with the specification of all data for each input parameter.

5.2.1- Simulation environment

The simulation times was set to 4200s, being the text output interval time defined to 50s, and spreadsheet output interval defined to 10s. The time defined for the smoke view output interval was set to 10s. The maximum time step was set to default.

The initial ambient temperature was defined to 20°C and the initial values for ambient atmospheric pressure inside and outside the compartment was defined to be 101325 Pa. The humidity inside the compartment was considered equal to 50%.

5.2.2- Thermal properties

Two materials were defined for the compartment, which are steel and concrete.

Steel material was used for the definition of the target and concrete for the definition of the slab and walls. The thermal properties for both of these two materials are presented above. In CFAST the specific heat of steel is assuming to be constant C_p but in reality, the specific heat depends on temperature.

About the second material using for the slab we have also some critical notes about the use of its properties in CFAST. The Thermal conductivity of concrete is not constant, as is assuming in CFAST $\lambda = 0.002$ see Figure 33 (left). The specific heat of concrete is also not constant as Figure 33 (right) shows.

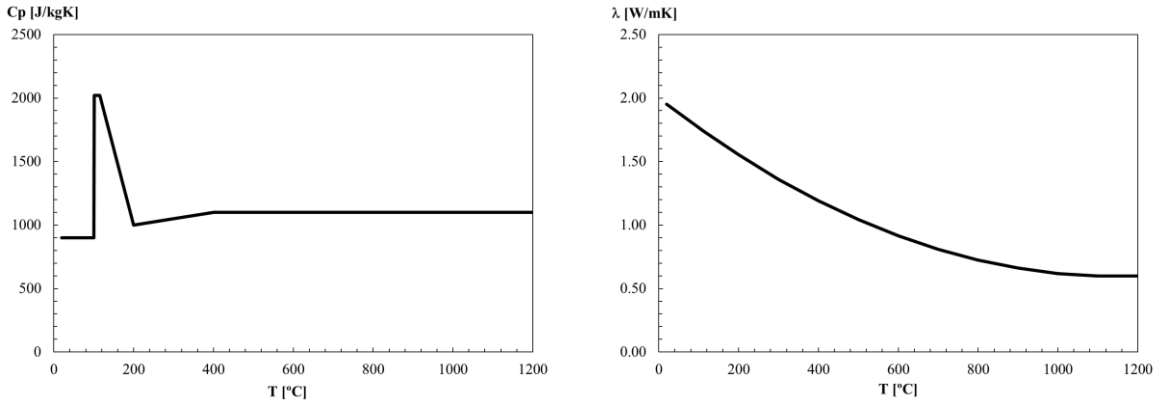

Figure 33. Specific heat of concrete (left) and Thermal conductivity of concrete (right) [55].

5.2.3- Compartments

The compartment name that we proposed is OPEN CAR PARKING, the geometry was assumed that the width (X) =10m with the origin position equal to 0m and the depth(Y)=10m with the origin position of the Y axis equal to 0m and the height (Z)= 3m with reference to the origin position of the coordinate system. Concrete was used for the ceiling, walls and floor. In this simulation, a two-zone model was considered), see Figure 34.

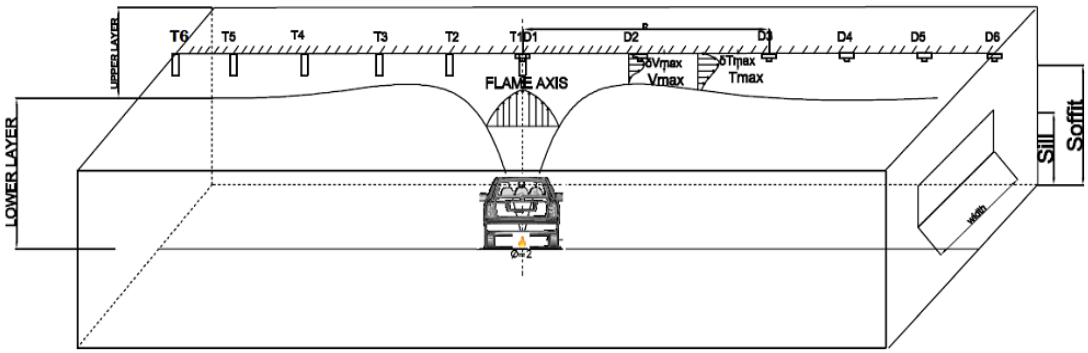

Figure 34. The geometry of our fire compartment.

5.2.4- Wall vents

The wall vents are defined using the definition of two more external compartments.

The geometry of the vents was defined to be coincident to the dimensions of the left and right surfaces of the main compartment, using a sill dimension equal to 0m, a soffit dimension equal to 3m and a width corresponding to 10m. The vents were considered fully open during the simulation.

5.2.5- Fires

The fire source of the event is located in the centre of the compartment, above the ground in 0.3m. The moment of ignition (ignition criterion) was considered equal to 0s, without ignition target. The total simulation time was set to 4200 s. HRR values were set for each car class.

5.2.6- Defining targets

Six targets were defined (OPEN CAR PARKING) for getting the local temperature of the hot gases in the plume zone and ceiling jet. These targets were made of steel, using thin plate shape (high section factor), with the normal vector corresponding to X direction. The position of six targets are defined in annex 2.

5.2.7- Defining the fire detectors

Six detectors were defined on the ceiling of the compartment, defined as heat alarms.

The activation temperature was defined to be 57,22 °C. The positionnof six heat alarms are defined in annex 2.

5.2.8- Output results

The compartment was divided into a grid. The size of the grid was tested before simulation to decide the number of divisions. This convergence test was done and the number of divisions was defined to be 50, see Figure 35.

The graphical results of the different CFAST simulations for the temperature and the velocity versus time are plotted in Figure 36 and Figure 37. The results for T and V depend on the ratio r/H and are represented by Figure 38 and Figure 40. The results of each car class are presented in the annex 2.

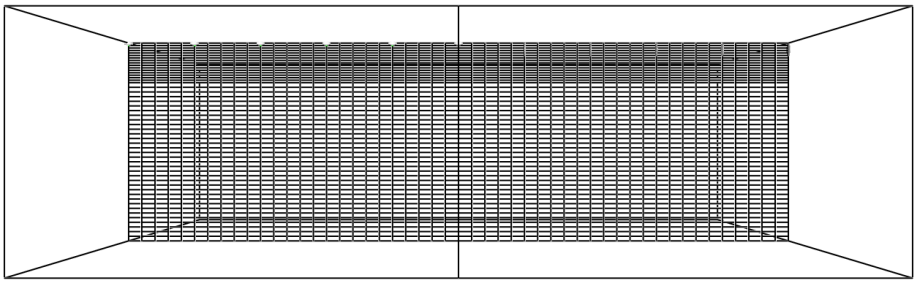

Figure 35. Grid size of the compartment.

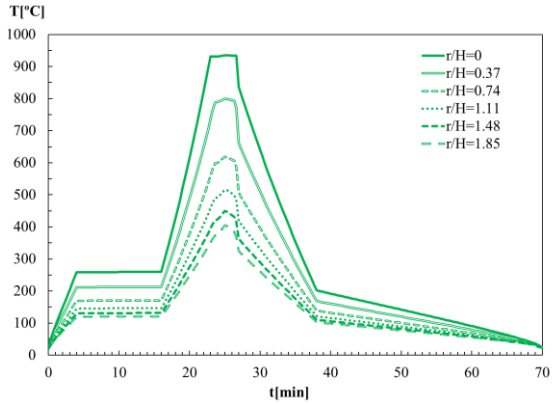

Class 1

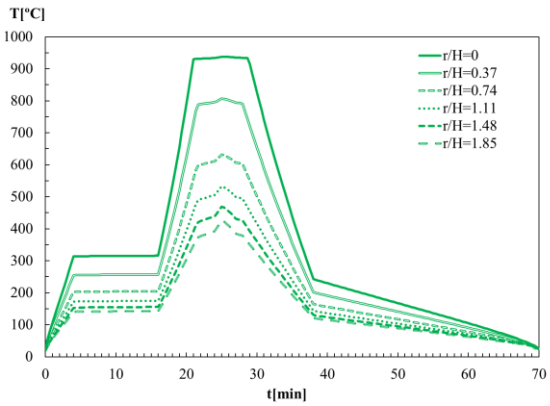

Class 2

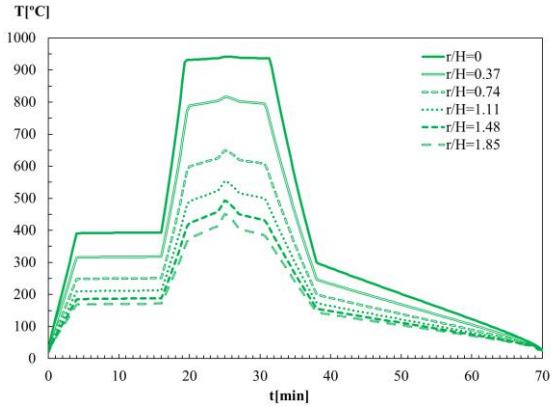

Class 3

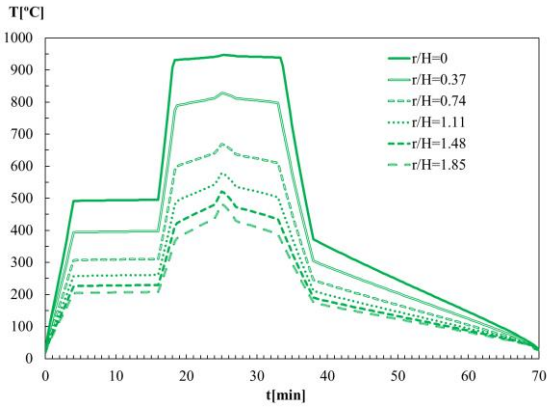

Class 4,5

Figure 36.Results of temperature from CFAST simulation.

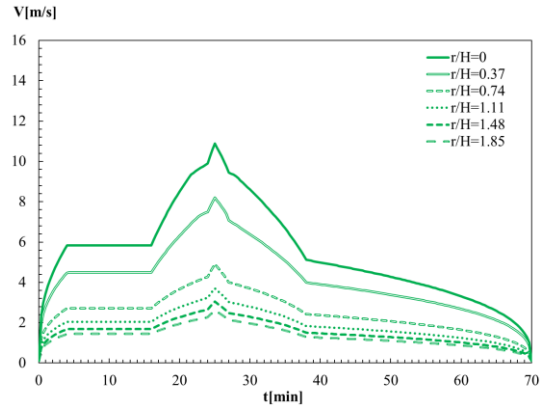

Class 1

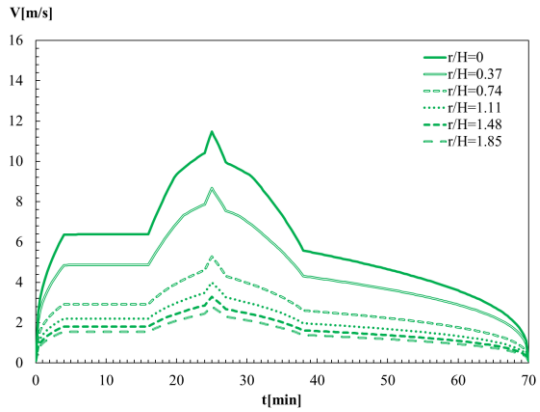

Class 2

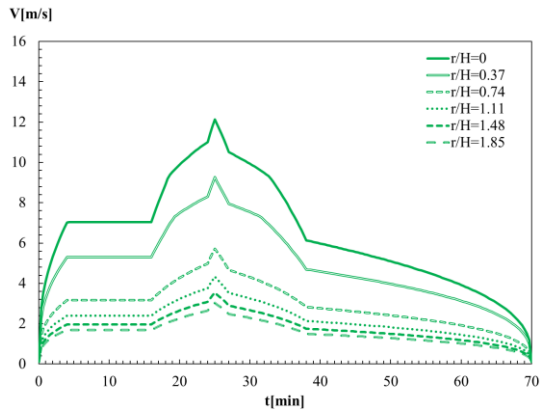

Class 3

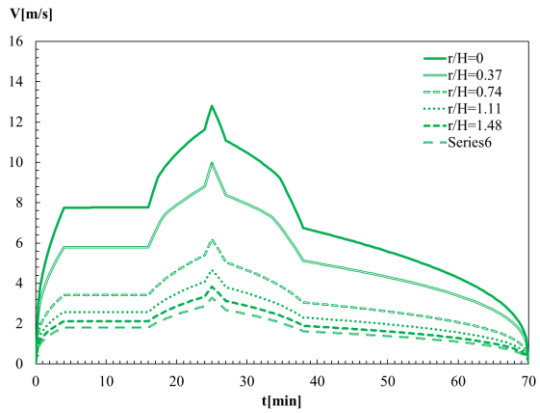

Class 4,5

Figure 37.Results of velocity from CFAST simulation.

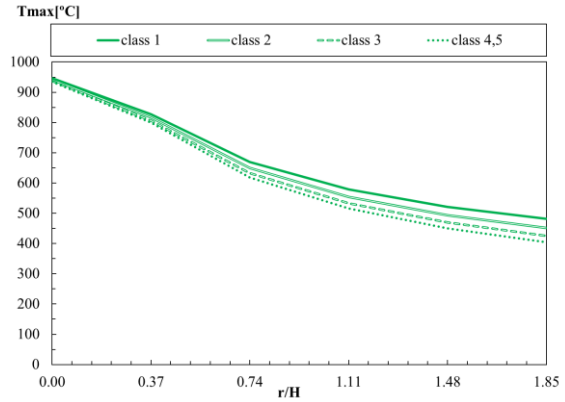

Figure 38.Results of T_{max} from CFAST simulation.

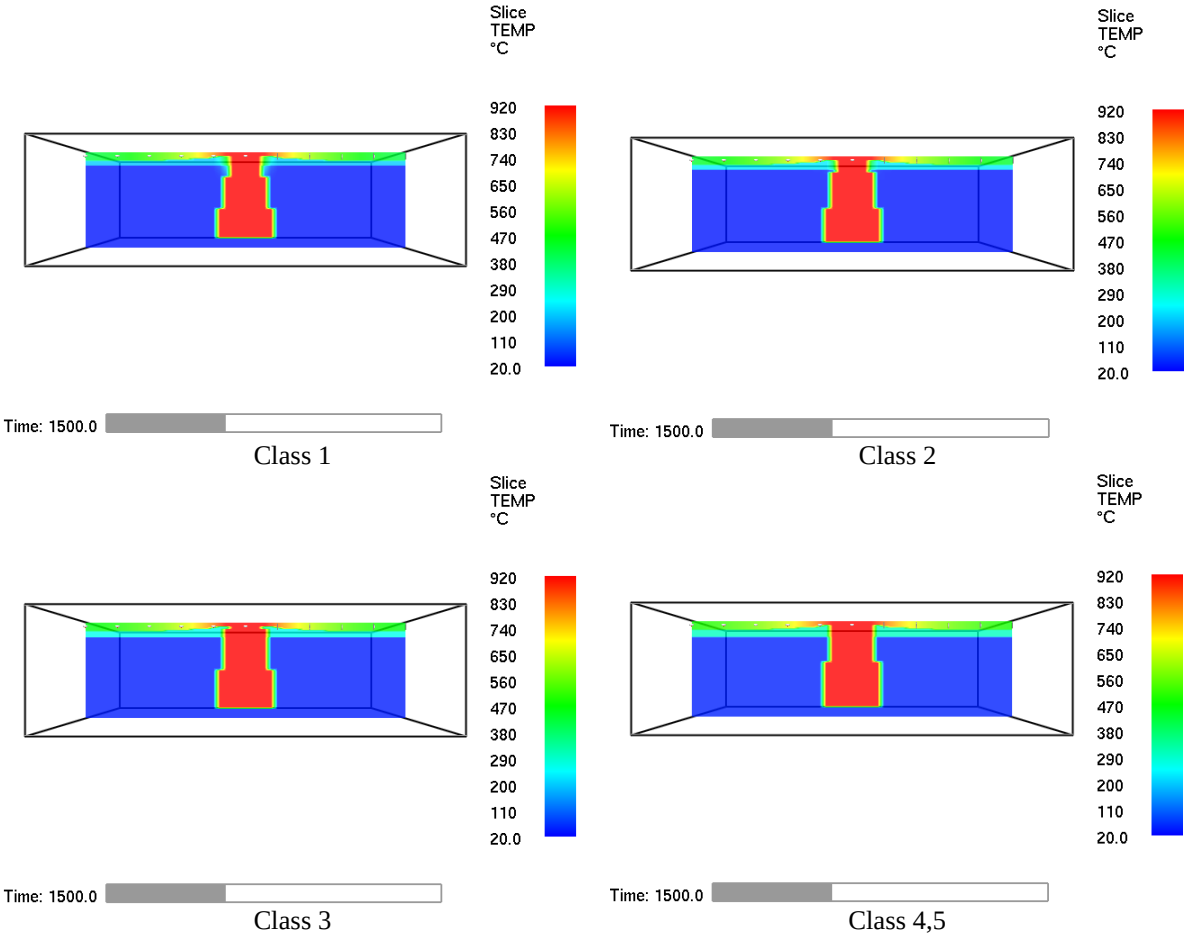

Figure 39.CFAST simulation for T_{max}.

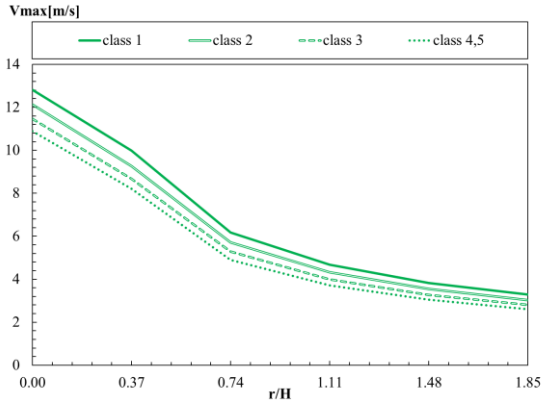

Figure 40.Results of V_{max} from CFAST simulation.

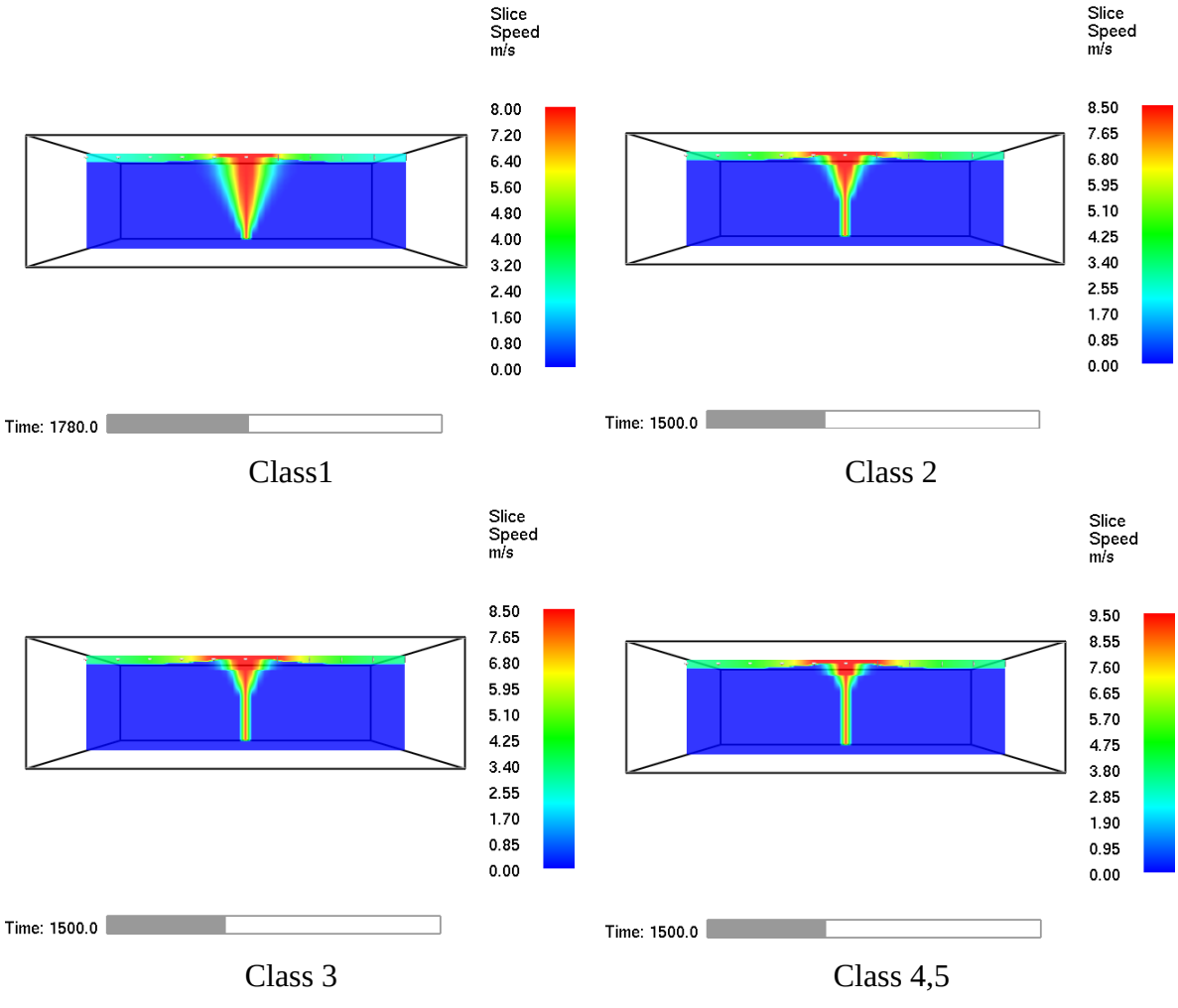

Figure 41.CFAST simulation for V_{max}.

5.3- Comparison of results

5.3.1- Maximum temperature comparison for all car classes

Figure 42 represents the comparison results for maximum temperature between correlative models and two zone models for all vehicle classes. The best region where all correlative models agree well with CFAST results is on the ratio r/H greater than 0.74.

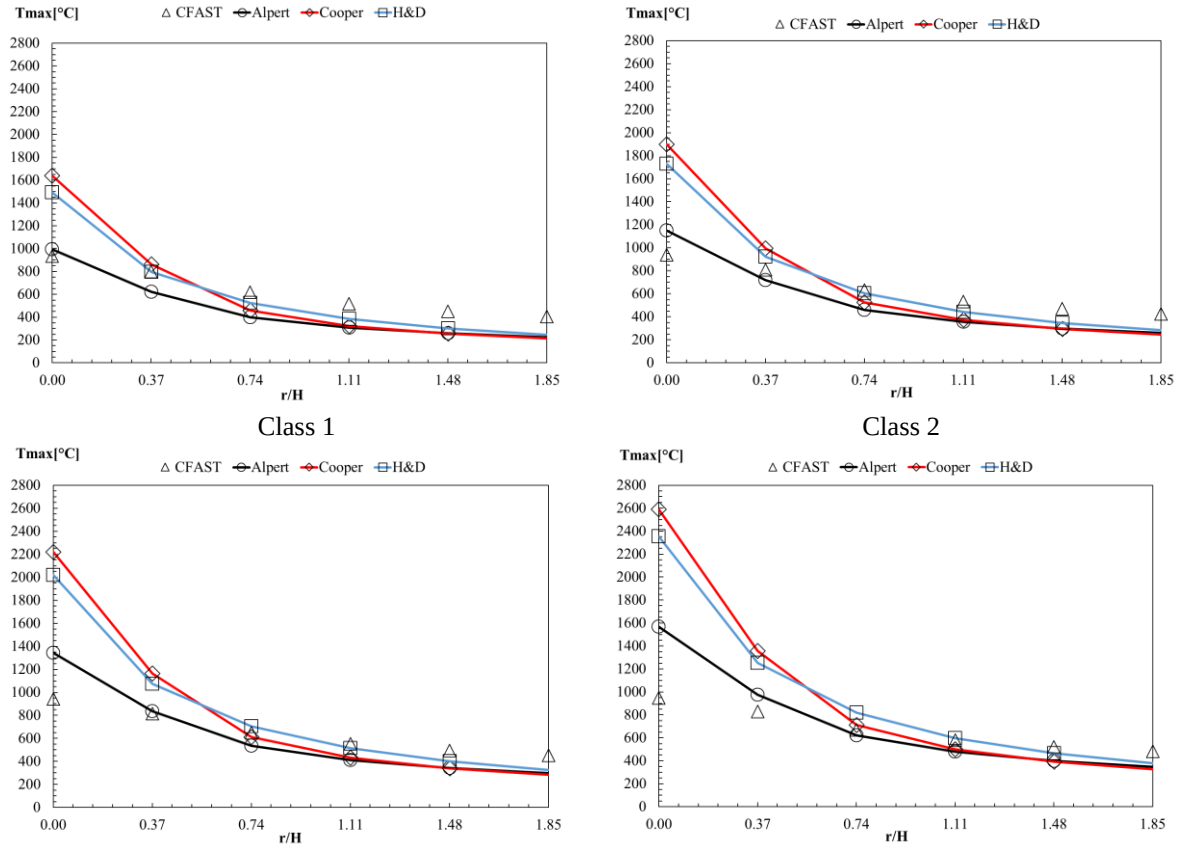

Figure 42.Comparison of Tmax for all car classes.

As general observation from the comparison between the results from the correlative models and CFAST results for the maximum temperature near the ceiling for all the car categories are that: when the ratio r/H is greater than 0.74 the correlations and CFAST results agree very well. The maximum temperature decreases with the ratio r/H, for both types of results (correlative and CFAST), there is a very big difference between the correlative models and CFAST on the plume zone.

5.3.2- Maximum velocity comparison for all car classes

Figure 43 represents the comparison results for maximum velocity between CFAST and the correlative models. The maximum velocity decreases with the ratio of r/H for both results.

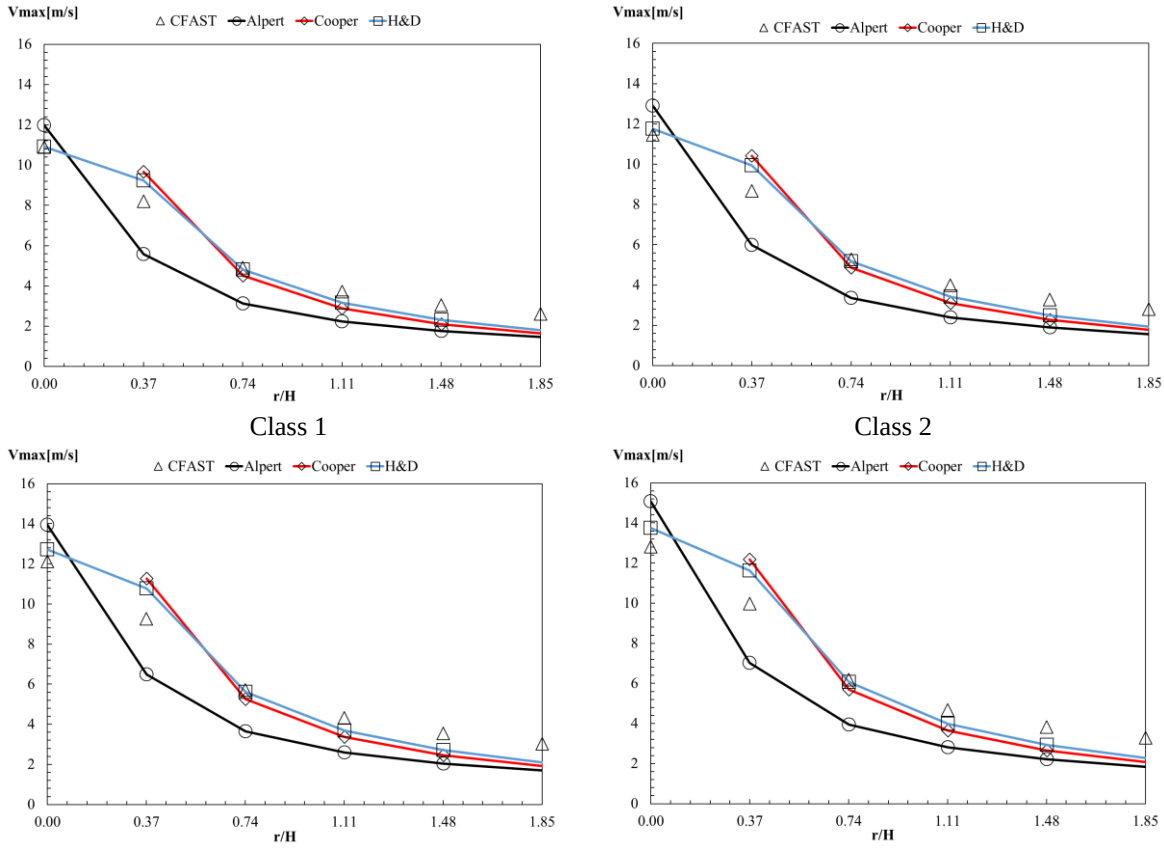

Class 1 Class 2

Class 3 Class 4,5

Figure 43.Comparison of Vmax for all car classes.

As general observation from the comparison between the results from the correlative models and CFAST results for the maximum velocity near the ceiling for all the car categories are that when the ratio of r/H is greater than 1.1.

There is a good agreement between the results from the correlative models and the numerical simulation of CFAST.

The difference between results of maximum temperature and maximum velocity are presented in annex 2.

6- FLUENT model

FLUENT's animate function was used to plot the results over a given time interval. The outputs of interest for most fire modelling applications are temperature, velocity, and pressure. Pressure was ignored in the majority of these simulations as a simplification. Three dimensional plots, along with graphs of temperature and velocity were used to view the results. The graphs showed the temperature and velocity at specific points in the compartment including the origin of the flame, the fire plume, the upper and lower portions of the vents, and the upper and lower layer in the compartment. In order for FLUENT to record data at specified points, each point was mapped with FLUENT's point generator.

FLUENT was primarily designed to run combustion models for furnaces, boilers, process heaters, gas turbines, and rocket engines in order to predict flow field and mixing characteristics, temperature fields, species concentrations, and particulates and pollutants. The energy equation is used to account for heat transfer in a FLUENT model. Heat transfer can occur by three main methods: conduction, convection, and radiation. The radiation model was used to show the compartments interaction with its surroundings. The k-epsilon model is a two-equation model that accounts for turbulent flows [56].

6.1- Presentation of FLUENT

FLUENT is a computational fluid dynamics (CFD) software. The first version of the FLUENT software was launched in October 1983 as collaboration between Sheffield University and a company called Creare Inc. FLUENT was written in the C computer language. The first version could involve both 2D and 3D structured grids using Cartesian or polar coordinates, steady-state flow, laminar or turbulent conditions, heat transfer, three-component combustion, a dispersed phase, and natural convection. FLUENT became very successful and in 1988 the FLUENT group at Creare broke away from the rest of the company establishing their own company, Fluent Inc. In August 1995, Fluent Inc. was acquired by Aavid Thermal Technologies Inc. FLUENT continued to improve and expand, buying Polyflow S.A. to gain POLYFLOW software code as well as improving their own code. In January 2000, Aavid Thermal Technologies was bought by Willis Stein & Partners. In May 2006, Fluent Inc. was bought by ANSYS Inc., the company that owns it today. The following sections discuss the models incorporated into FLUENT, particularly those related to modelling fire, as well as some documented examples in which FLUENT was used for fire related simulations [56].

6.2- Equations to be solved

The material presented in the previous section only applies to a system consisting of solid bodies in which there is no fluid ow. For systems in which there is fluid motion present, a different set of equations must be introduced that relate to the conservation principles that must be met by a system [57].

6.2.1- Continuity equation

Conservation of mass must be satisfied. Mass must not be created or destroyed. The equation governing this principle is known as the continuity equation [57] and is shown below in Eq 15.

$$\frac{\partial \rho}{\partial t} + \nabla(\rho V) = 0 \qquad \text{Eq 15}$$

where ρ id the density, t is the time and ∇ is Del operator $= \frac{\partial}{\partial x} i + \frac{\partial}{\partial y} j + \frac{\partial}{\partial z} k$, then V is the vector of velocity $= V_x i + V_y j + V_z k$. This equation can be expanded and becomes

$$\frac{\partial \rho}{\partial t} + \frac{\partial \rho V_x}{\partial x} + \frac{\partial \rho V_y}{\partial y} + \frac{\partial \rho V_Z}{\partial Z} = 0 \qquad \text{Eq 16}$$

6.2.2- Navier-stokes equation

The Navier-Stokes equations are a collection of the 3-dimensional momentum equations for any Newtonian fluid. In fluid dynamics, a Newtonian fluid is one in which the stresses at each point in the fluid are linearly proportional to the strain rate at that point. These equations ensure that in any system, the momentum is conserved. This means that the total force generated by the momentum transfer in each direction must be balanced by the rate of change of momentum in each direction. The Navier-Stokes equation is provided below [57] for the Z component. The other directions in space also apply.

$$\frac{\partial \rho V_z}{\partial t} + \frac{\partial (\rho V_x V_z)}{\partial x} + \frac{\partial (\rho V_y V_z)}{\partial y} + \frac{\partial (\rho V_z V_z)}{\partial z}$$
$$= \rho g_z - \frac{\partial p}{\partial z} + R_Z + \frac{\partial}{\partial x}(\mu_e \frac{\partial V_z}{\partial x}) + \frac{\partial}{\partial y}(\mu_e \frac{\partial V_z}{\partial y}) + \frac{\partial}{\partial z}(\mu_e \frac{\partial V_z}{\partial z}) + T_z \quad \text{Eq 17}$$

Where g_z is components of acceleration due to gravity that exists only in this direction, and R_z is distributed resistances, μ_e is the effective viscosity of the fluid, T_z refers to Viscous loss terms. These represent source terms that can be used to model things such as flow through screens or porous media. These terms are eliminated if no user-specified value is supplied.

The final form of the Navier-Stokes equations for an incompressible flow with gravity acting in the y direction and non-distributed resistances are given in Eq 18 [57].

$$\frac{\partial \rho V_z}{\partial t} + \frac{\partial (\rho V_x V_z)}{\partial x} + \frac{\partial (\rho V_y V_z)}{\partial y} + \frac{\partial (\rho V_z V_z)}{\partial z} \quad \text{Eq 18}$$
$$= -\frac{\partial p}{\partial z} + \frac{\partial}{\partial x}(\mu_e \frac{\partial V_z}{\partial x}) + \frac{\partial}{\partial y}(\mu_e \frac{\partial V_z}{\partial y}) + \frac{\partial}{\partial z}(\mu_e \frac{\partial V_z}{\partial z})$$

6.2.3- Energy equation

As stated before, the first law of thermodynamics requires that the energy of a system be conserved. The 3-dimensional energy equation for fluid flow is provided below [57].

$$\frac{\partial}{\partial t}(\rho C_p T) + \frac{\partial}{\partial x}(\rho V_x C_p T) + \frac{\partial}{\partial y}(\rho V_y C_p T) + \frac{\partial}{\partial z}(\rho V_z C_p T)$$
$$= \frac{\partial}{\partial x}(K_{xx} \frac{\partial T}{\partial x}) + \frac{\partial}{\partial y}(K_{yy} \frac{\partial T}{\partial y}) + \frac{\partial}{\partial z}(K_{zz} \frac{\partial T}{\partial z}) + Q_v \quad \text{Eq 19}$$

Where ρ is Density, Cp is specific heat, $V_{x;y;z}$ refers to the velocity in x, y, z directions and T represents the temperature, $K_{xx,yy,zz}$ is thermal conductivity in x, y, z directions, Q_V is the volumetric heat source.

6.2.4- Other equations

A symmetry limit condition in negative X and negative Y we have assumed that there is a steady stationary station condition, an opening with pressure P=101325[Pa] pressure out,

T∞=300 K and the turbulence kinetic energy, k, and its rate of dissipation, ε, are obtained from the following transport equations:

$$\frac{\partial}{\partial_t}(\rho k)+\frac{\partial}{\partial x_i}(\rho k u_i)=[(\mu+\frac{\mu_t}{\sigma_t})\frac{\partial k}{\partial X_j}]+G_k+G_b-\rho\varepsilon-Y_M+S_K \quad \text{Eq 20}$$

$$\frac{\partial}{\partial_t}(\rho\varepsilon)+\frac{\partial}{\partial X_i}(\rho\varepsilon u_i)=\frac{\partial}{\partial X_j}[(\mu+\frac{\mu_t}{\sigma_\varepsilon})\frac{\partial_\varepsilon}{\partial X_j}]+C_{1\varepsilon}\frac{\varepsilon}{K}(G_K+C_{3\varepsilon}G_b)-C_{2\varepsilon}\rho\frac{\varepsilon^2}{K}+S_\varepsilon \quad \text{Eq 21}$$

In these equations G_K represents the generation of turbulence kinetic energy due to the mean velocity gradients, G_b is the generation of turbulence kinetic energy due to buoyancy, Y_M represents the contribution of the fluctuating dilatation in compressible turbulence to the overall dissipation rate, $C_1\varepsilon$, $C_2\varepsilon$ and $C_3\varepsilon$ are constants. σ_K and σ_ε are the turbulent Prandtl numbers for K and ε, respectively. S_K and S ε are user-defined source terms.

6.3- The model

The model represents the fire compartment with 3m of height and 10m of width. The fire event is located in the middle of this compartment, considering a burning car with an equivalent pool fire with a diameter of 2m, the element size of edge sizing is hard behavior with 0.04 m value and the value of the element size of face sizing is 0.04 m with soft behavior. Figure 44 shows the mesh of a fire event with a class 1 car vehicle, burning in the centre of a fire compartment with the overall dimension of 10x3 m^2

This compartment uses the same boundary conditions in left side and right side which are opening, a concrete slab on the bottom and top floor and a concrete wall in the front and rear façade.

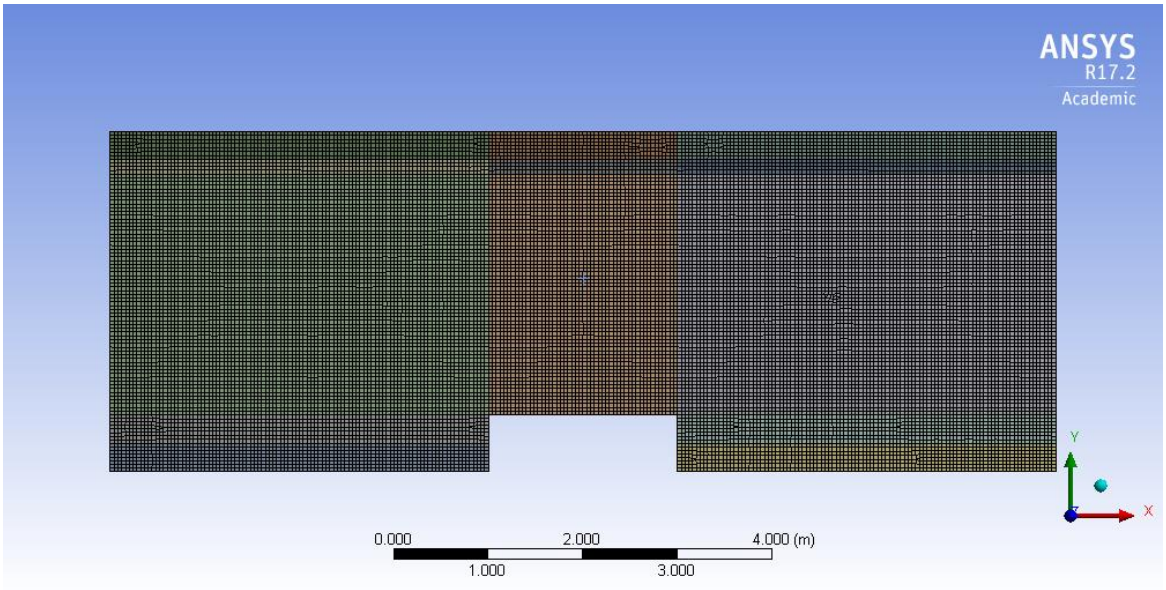

Figure 44.the Mesh of the model.

6.3.1- Material models

Two materials were defined which are the air for the fluid and concrete for the slabs. The air properties are presented in Figure 45.

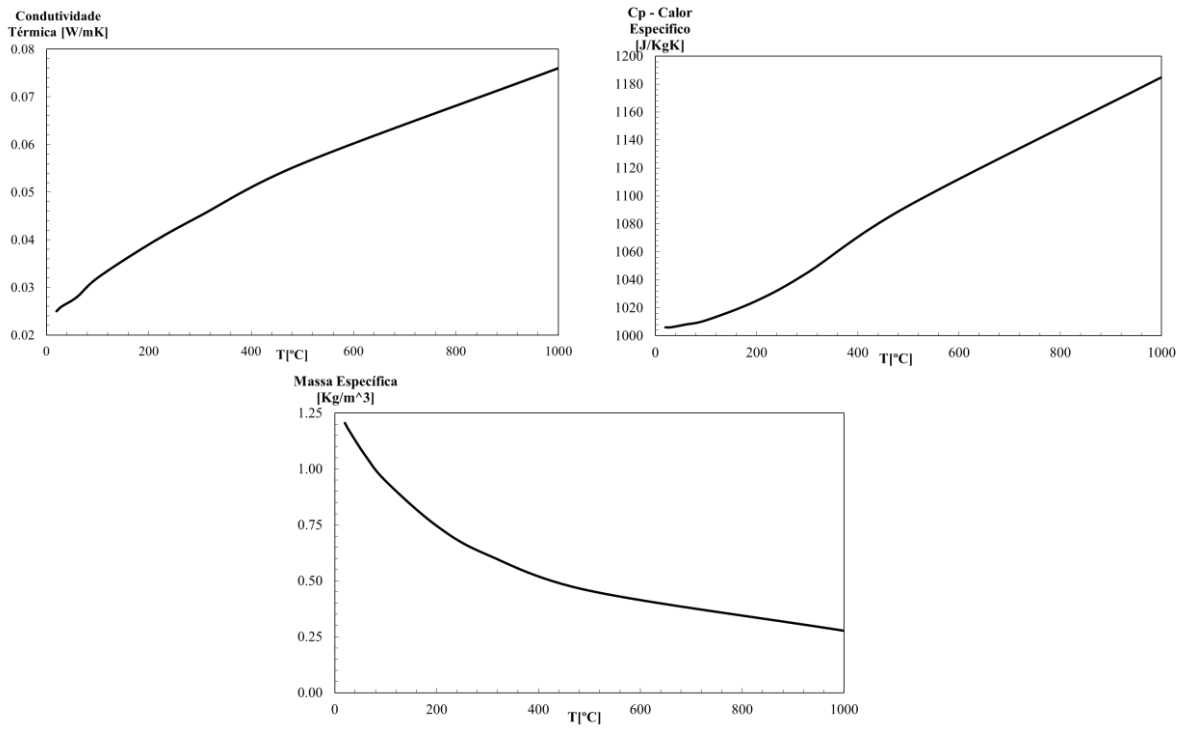

Figure 45.Properties of the air.

The properties of concrete presented are based on data points, and the graphical curves of the properties of concrete are shown in Figure 33.

6.3.2- Boundary conditions

We have assumed that there is a steady stationary station condition, an opening with pressure P=1[Pa] for the pressure out let boundary, T∞=300 K and radiation ε=1, wall fixed insulation heat flux=0 in fluid flow. Use of concrete material for a stationary wall (wall concrete insulation heat flux=0) and slabs with a thickness of 0.3 m. I add the equation source inlets T(t) and V(t) are based on CFAST previous analyses (for more explain look annex 3), as Figure 46 shows.

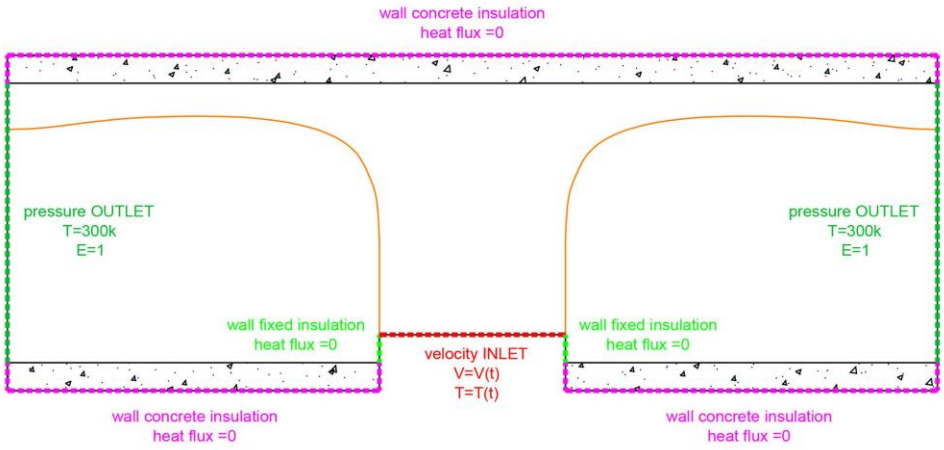

Figure 46.Boundary condition of the compartment.

Figure 47 and Figure 48 shows the graphical results of temperature and velocity for all car class depending of boundary conditions. Defined, the formulas of temperature and velocity for each class which are presented in annex 3.

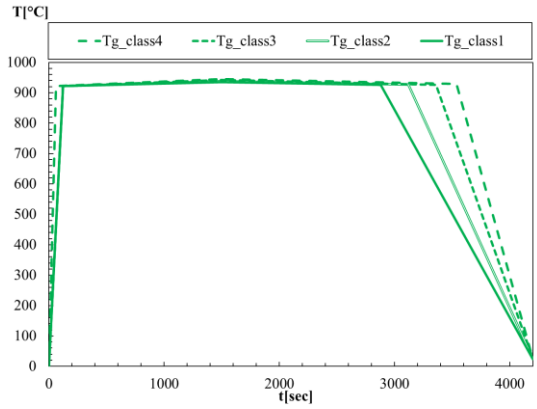

Figure 47. Results of Tg from CFAST of all car classes.

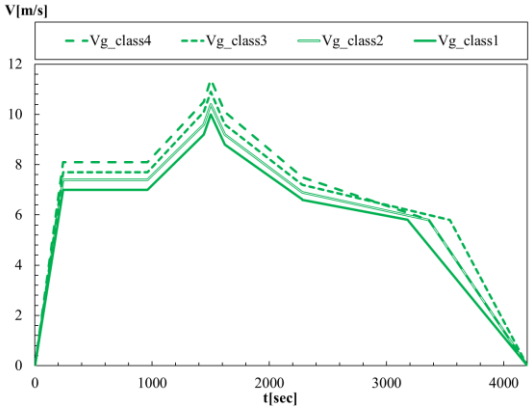

Figure 48. Results of Vg from CFAST of all car classes.

6.4- Comparison of results

6.4.1- Temperature results from ANSYS fluent simulation

Figure 49 shows the graphical results of temperature amplitude for all car classes depending of the targets positions.

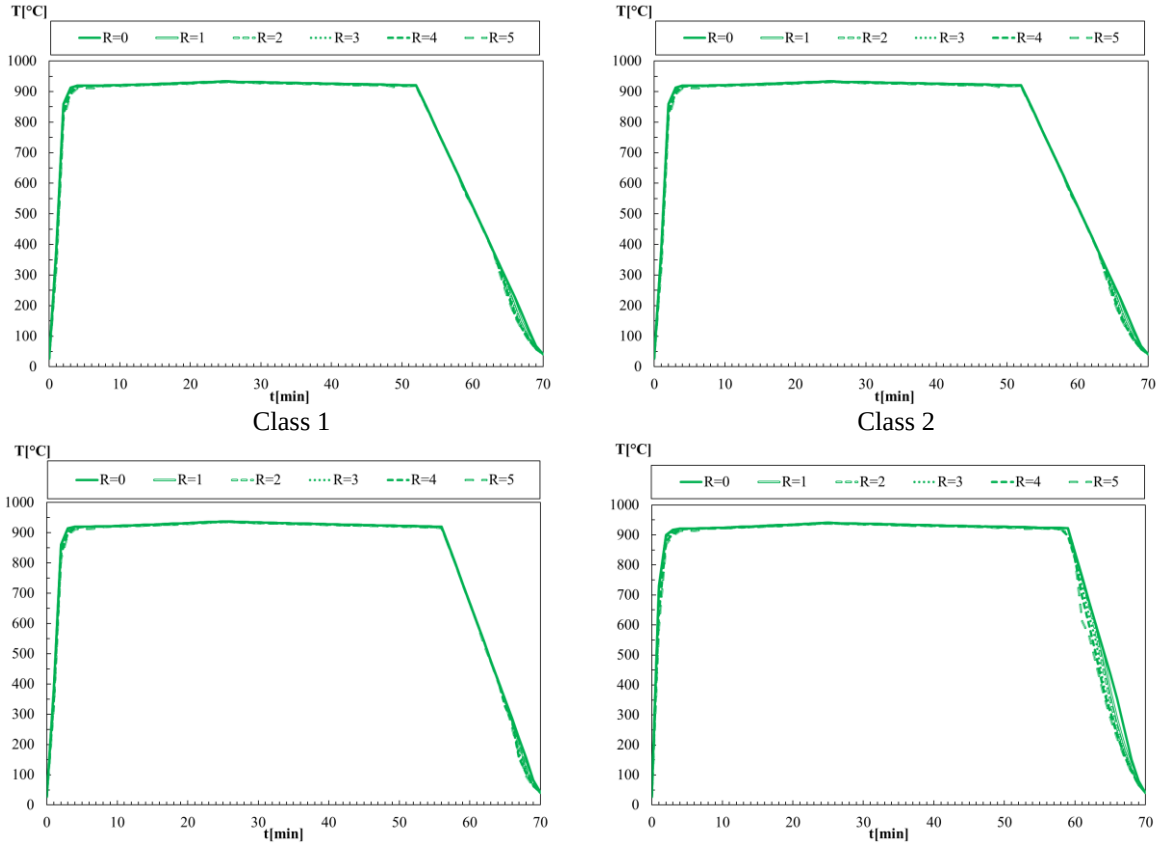

Class 1 Class 2

Class 3 Class 4,5

Figure 49.Results of temperature from ANSYS fluent simulation of all car classes.

The temperature increase after ignition at the monitor point 0.35 m above the floor and decrease when go down to the monitor point. The temperature rises on the ceiling jet level.

6.4.2- Velocity results from ANSYS fluent simulation

Figure 50 shows the graphical results of velocity amplitude for all car class, depending of the targets positions.

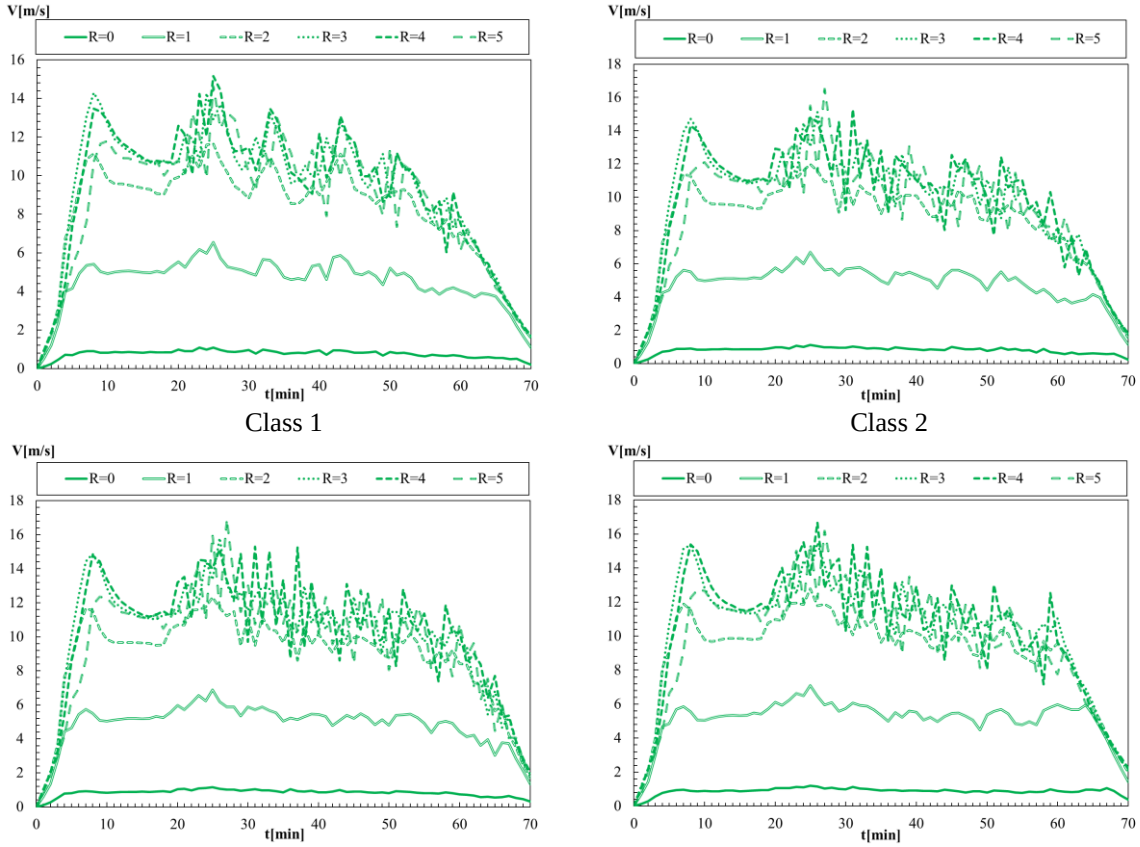

Figure 50.Results of velocity from ANSYS fluent simulation of all car classes.

The velocity results show that the highest values are when the R is 4 and 5 then in the second target the results are probably decreased because they are a transit area between two zones.

The results of Tmax and Vmax for all car classes are presented in annex 3.

6.4.3- Maximum temperature comparison for all car classes

Figure 51 represents the comparison results for maximum temperature between CFAST and the correlative models and ANSYS fluent for all vehicle classes.

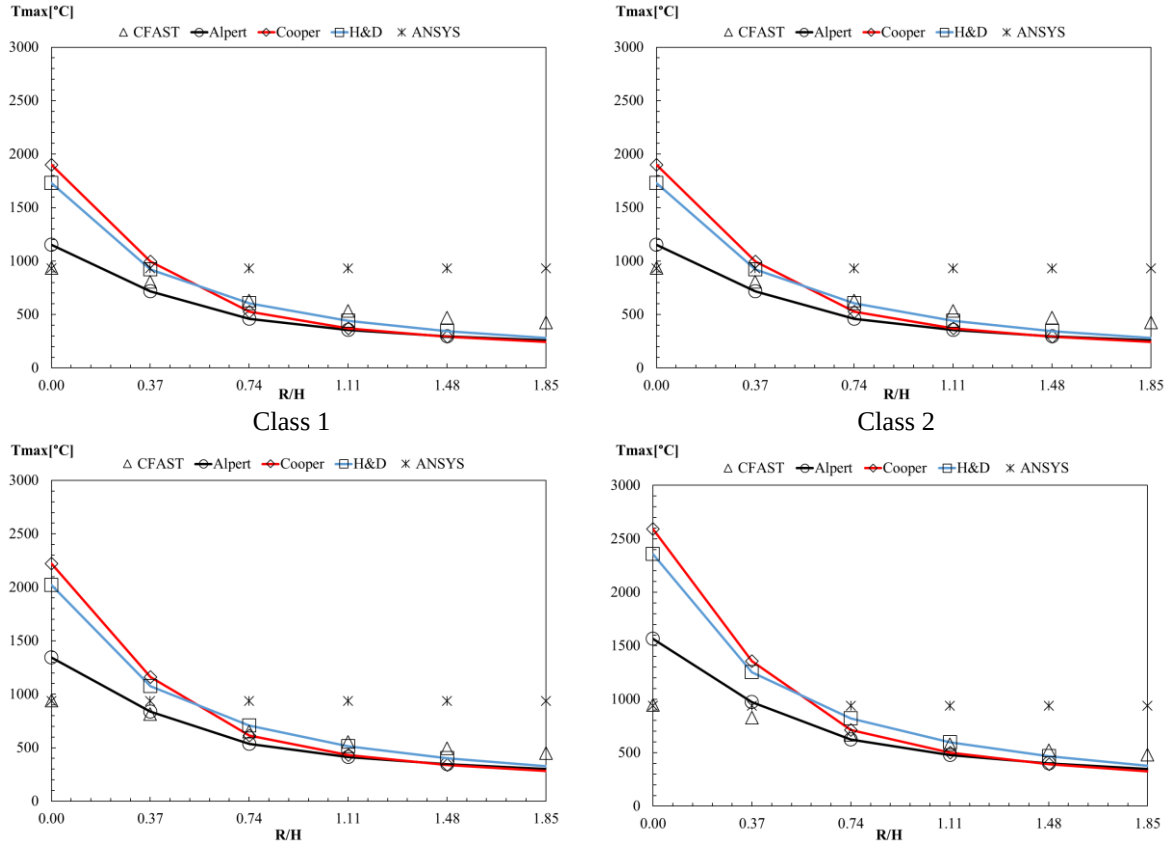

Class 1 Class 2

Class 3 Class 4,5

Figure 51.Results of Tmax from ANSYS fluent simulation of all car classes.

The best region where all correlative models agree well with CFAST and FLUENT results is on the ratio r/H greater than 0.37 less than0.74. the results are probably decreased because they are a transit area between two zones (upper layer and lower layer). CFD results over estimates the results for the maximum temperature.

6.4.4- Maximum velocity comparison for all car classes

Figure 52 represents the comparison results for maximum velocity between CFAST and the correlative models and ANSYS fluent.

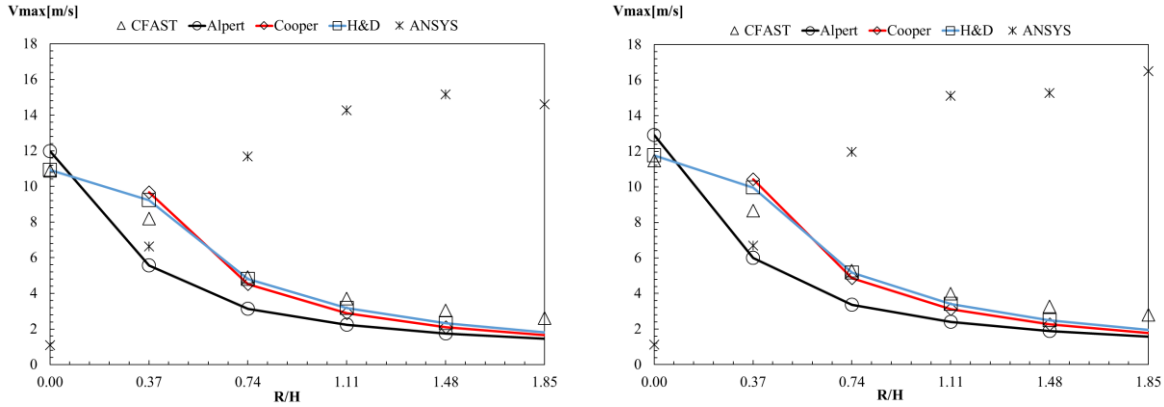

Class 1 Class 2

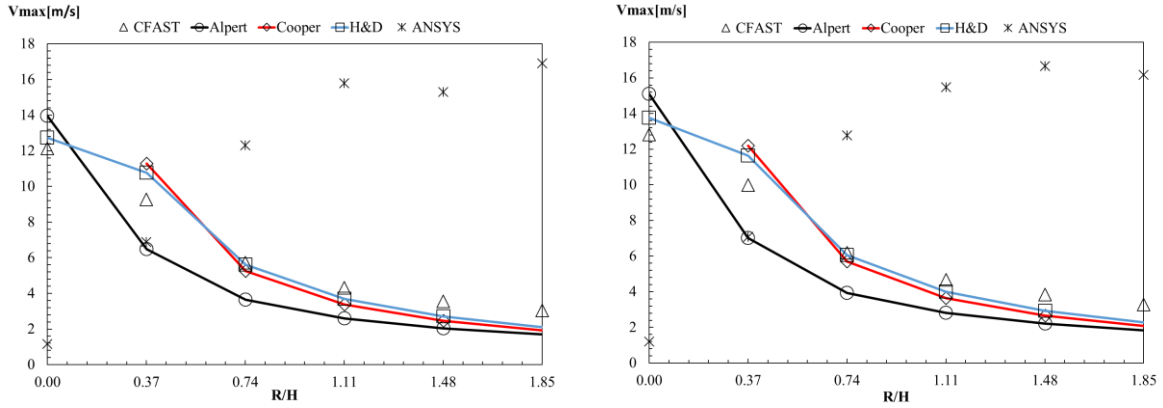

Class 3 Class 4,5

Figure 52.Results of Vmax from ANSYS fluent simulation of all car classes.

There is a good agreement between the results from the correlatives and two zone models and ANSYS when the ratio r/H=0.37, the results are probably decreased because they are a transit area between two zones (upper layer and lower layer). CFD results over estimates the results for the maximum velocity.

Figure 53 shows the model and the grid size.

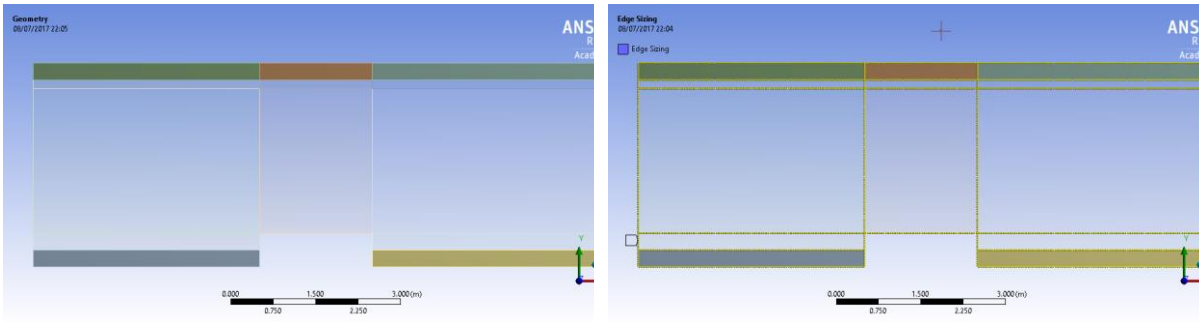

The model The grid size

Figure 53.Model and the grid size.

Figure 54 and Figure 55 shows the results of temperature and velocity of the CFD simulation when time equal to 1500s for all fire events.

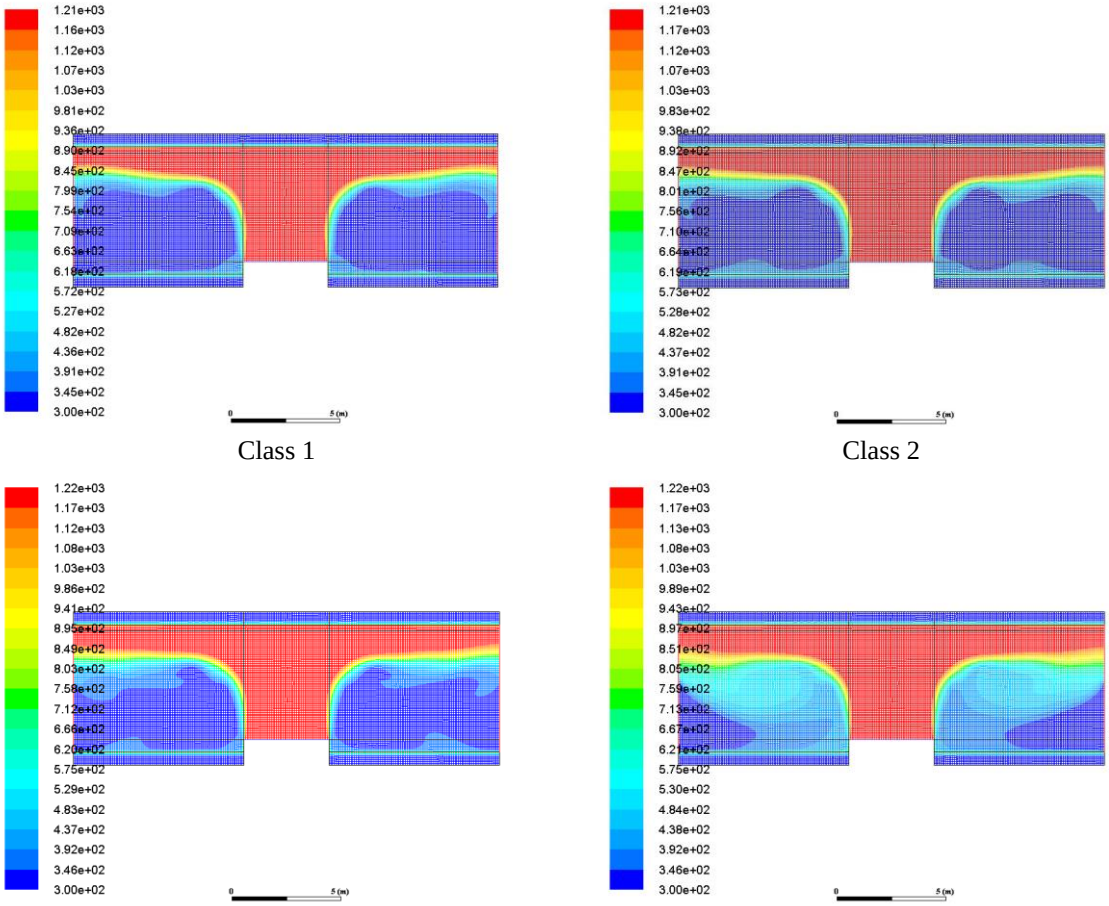

Class 1 Class 2

Class 3 Class 4,5

Figure 54.Results of Temperature when t=1500 s for all car classes.

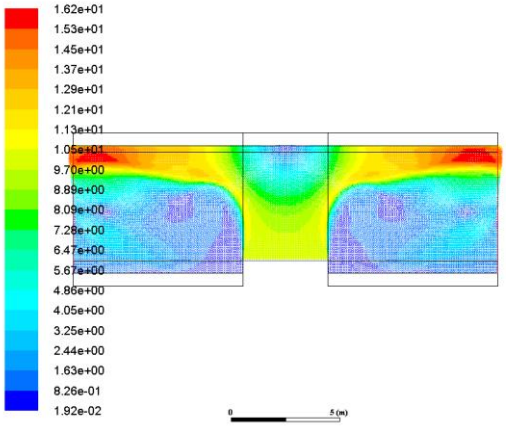

Class 1

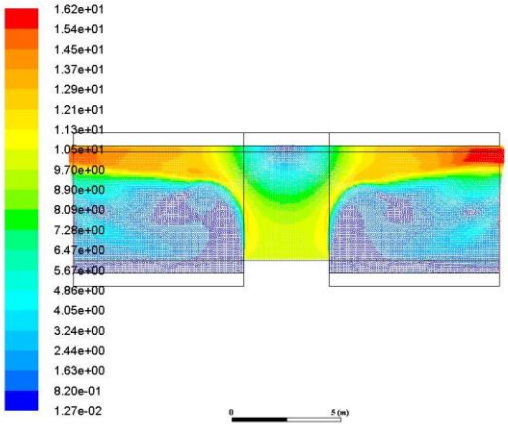

Class 2

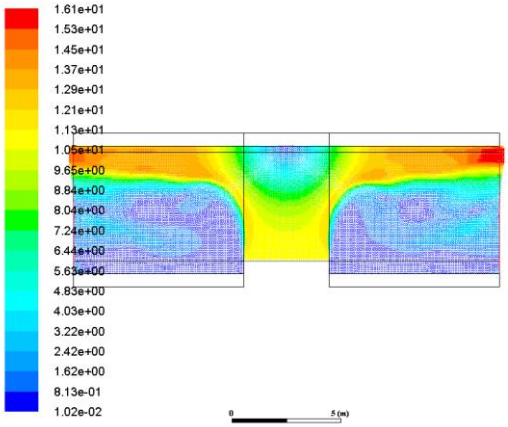

Class 3

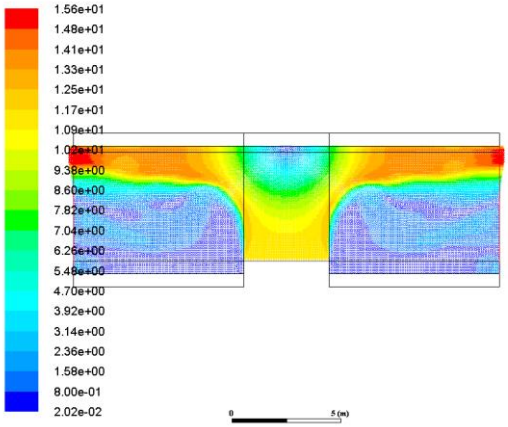

Class 4,5

Figure 55.Results of velocity when t=1500 s for all car classes.

From the results of maximum temperature and velocity near the ceiling, the area of fire is decreases with the increase of the ratio r/H.

7- Conclusions

The transient behaviour of a thermal induced fire plume and the associated ceiling jet is studied by the field modelling technique. Obviously, without a realistic simulation of combustion processes and an accurate prediction of thermal radiation effects, field model is not yet good enough for studying the building fire spread and the dynamics of the ceiling jet.

This study is related with the fire induced ceiling jet. The velocity and temperature of the hot gases due to fire in compartment are two major parameters to be calculated. These parameters were calculated by correlative models and numerical models (CFAST) and the software ANSYS fluent.

The comparison of the results between the correlative models, CFAST and ANSYS FLUENT showed an agreement between these results in specific radial positions, taking in consideration that each one of the software has a different way of doing calculations.

Our fire modelling capabilities are frequently used to support fire cause and origin investigations. In this capacity, Exponent uses the most widely used tools in fire modelling the (CFD) and the Consolidated Model of Fire and Smoke Transport (CFAST) which are developed and distributed by the National Institute of Standards and Technology.

In this study, there were overestimated for the maximum temperature, this issue need to be addressed in future studies. In future work set of small-scale experiments and numerical simulations with reducing the dimensions to measure dynamics in fire induced ceiling jet in open car parks for comparison between them.

References

[1] R. L. Alpert, «Calculation of Response Time of Ceiling-Mounted Fire Detectors,» *Fire Technology journal,* pp. 181-195, 1972.

[2] Gunnar Heskestad and Micheal. Delichatsios, "The Initial Convective Flow In Fire," *Fire Safety journal,* pp. 1113-1123, 1979.

[3] L. Y. C. a. A. Woodhouse, «The Buoyant Plume-Driven Adiabatic Ceiling Temperature Revisited,» chez *National Heat Transfer,* 1986.

[4] L. Y. Cooper and D. W. Stroup, «Thermal Response of Unconfined Ceilings Ahowe Growing Fires and the Importance of Convective Heat Transfer,» *Heat Transfer Journal,* vol. 109, pp. 172-178, 1987.

[5] Gunnar Heskestad, M&hael A. Delichatsios, «The Initial Convective Flow in Fire,» *Fire Safety Journal,* pp. 471-475, 1989.

[6] Stephen M. Olenick and Douglas J. Carpenter, «An Updated International Survey of Computer Models for Fire and Smoke,» *Fire Safety Journal,* 1992.

[7] Leonard Y. Cooper, «Fire-Plume-Generateo Ceiling Jet Characteristics and ConvectiveE Heat Transfer to Ceiling and Wall Surfaces in a Two-Layer Fire Environment : Uniform Temperature Ceiling and Walls,» *fire science technology,* vol. 13. No 1 & No 2, pp. 1-17, 1993.

[8] W. G. W. a. Y. Hasemi, "Heat transfer to an unconfined ceiling from an impinging buoyant diffusion flame," *Heat Mass Transfer,* vol. 42, p. 652–659, 2005.

[9] João Carlos Viegas, "The use of impulse ventilation for smoke control in underground car parks," *Tunnelling and Underground Space Technology,* vol. 25, pp. 42-53, 2009.

[10] Yasushi Oka , Osamu Imazeki , Osami Sugawa, «Temperature profile of ceiling jet flow along an inclined unconfined ceiling,» *Fire Safety Journal*, vol. 45, p. 221–227, 2010.

[11] Ronald L. Alpert, «The Fire-Induced Ceiling-Jet Revisited,» *Fire Safety Engineering,* pp. 1-20, 2011.

[12] Yasushi Oka , Masaki Ando, «Temperature and velocity properties of a ceiling jet impinging on a nunconfined inclined ceiling,» *FireSafety Journal,* vol. 55, p. 97–105, 2012.

[13] J. W. a. P. v. H. Nils Johansson, «Simple Ceiling Jet Correlation Derived From Numirical Experiments,» 2013.

[14] Tiannian Zhou , Yaping He , Xiao Lin , Xuehui Wanga, Jian Wanga, «Influence of constraint effect of sidewall on maximum smoke temperature distribution under a tunnel ceiling,» *Applied Thermal Engineering,* vol. 112, p. 932–941, 2016.

[15] Morton, B.R., Taylor, G.I. and Tuner, J.S.,, «Turbulent Gravitational Correction From Maintained and Instantaneous Sources.,» *Proc. R. Soc. Lond.A,* Vols. %1 sur %2234, No. 1196, pp. 1-23, 1956.

[16] A. RL, «Ceiling Jet Flows,» chez *Fire Protection Engineering, PJ DiNenno,* National Fire Protection Association: Quincy, MA, USA, SFPE Handbook of, 2002, pp. 2-18 -- 2-31..

[17] Heskestad G, Hamada T, «Ceiling Jets of Strong Fire Plumes,» *Fire Safety Journal,* vol. 21, pp. 69-82, 1993.

[18] H. PL, "The Flow of Hot Gases Along an Enclosed Shopping Mall - A Tentative Theory," 1970.

[19] Li S., Zong R., Zhao W., Yan Z., Liao G, «Theoretical and experimental analysis of ceiling-jet flow in corridor fires,» *Tunnelling and Underground Space Technology,* vol. 26, pp. 651-658, 2011.

[20] Li YZ, Lei B, Ingason H, «The maximum temperature of buoyancy-driven smoke flow beneath the ceiling in tunnel fires,» *Fire Safety Journal,* vol. 46(4), pp. 204-210, 2011.

[21] Li YZ, Ingason H,, "Position of maximum ceiling temperature in a tunnel Fire," *Fire Technology,* vol. 50, p. 889–905, 2014.

[22] Ingason H, Li YZ, «Model scale tunnel fire tests with longitudinal ventilation,» *Fire Safety Journal,* vol. 45, pp. 371-384, 2010.

[23] Ingason H, Li YZ, Lönnermark A, "Runehamar Tunnel Fire Tests," *Fire Safety Journal,* vol. 71, p. 134–149, 2015.

[24] Ingason H, Li YZ, "Model scale tunnel fire tests with point extraction ventilation.," *Journal of Fire Protection Engineering,* vol. 21(1), pp. 5-36, 2011.

[25] S. L. a. J. W. Wei Yao, «Numerical Prediction of Effects of Gravity on the Centerline Temperature and Velocity of Axi-symmetric Fire Plumes,» *Journal of Fire Sciences,* vol. 25, pp. 402-423, 2007.

[26] E. K. T. a. C. B. Zukosiki, "Entrainment in Fire Plumes," 1980/1981.

[27] Alpert, R.L, «Turbulent Ceiling-Jet Induced by Large-Scale Fires,» *Combustion Science and Technology,* vol. 11, pp. 197-213, 1971.

[28] Motevalli, V., and Mark, C.,, «Characterizing the Unconfined Ceiling Jet Under Steady-State Conditions: A Reassessment,» 1991.

[29] Veldman, C.C., Kubota, T., and Zukoski, E.E, «An Experimental Investigation Of The Heat Transfer From A Buoyant Gas Plume to A Horizontal Ceiling - Part 1. Unobstructed Ceiling,» National Institute of Standards and Technology Report NBS-GCR-77-97, 1975.

[30] You, H.Z., and Faeth, G.M, «An Investigation of Fire Impingement On a Horizontal Ceiling,» National Institute of Standards and Technology Report NBS-GCR-81-304, 1981.

[31] Cooper, L.Y, «Fire-Plume-Generated Ceiling Jet Characteristics And convective Heat Transfer To Ceiling And Wall Surfaces In a Two-Layer fire Environment: Uniform Temperature Fire Environment: Uniform Temperature Ceiling and Walls,» *Fire Science & Technology,* vol. 104, pp. 1-17, 1993.

[32] Cooper, L.Y, «Heat Transfer From a Buoyant Plume to an Unconfined Ceiling,» *Journal of Heat Transfer,* vol. 13, pp. 446-451, 1982.

[33] Cooper, L.Y., and Woodhouse, A., «The Buoyant Plume-Driven Adiabatic Ceiling Temperature Revised,» *Journal of Heat Transfer,* vol. 108, pp. 822-826, 1986.

[34] Poreh, M., Tsuei, Y.G., and Cermak, J.E, "Investigation of A Turbulent Radia Wall Jet," *ASME Journal of Applied Mechanics,* vol. 112, pp. 457-463, June 1967.

[35] Goldstein, R.J., Sobolik, K. A., Seol, W. S, "Effect of Entrainment on the Heat Transfer to a Heated Circular Air Jet Impinging on a Flat Surface.," *Transactions of the ASME,* vol. 112, pp. 608-611, 1990.

[36] R. G. Bill, «Numerical Simulation of Actual Delivered Density (ADD) Measurements.,» *Fire Safety Journal,* vol. Vol 20(3), pp. 227–240,, 1993.

[37] H.-Z. a. K. H.-C. You, «Strong Buoyant Plumes of Growing Rack Storage Fires,» *Symposium (International) on Combustion,* p. 1547–1554, 1984.

[38] Rew C, Deaves D, «Fire spread and flame length in ventilated tunnels - a model used in Channel tunnel assessments,» chez *in Proceedings of the International Conference on*

Tunnel Fires and Escape from Tunnels, Lyon, France:Independent Technical Conferences Ltd., 1999.

[39] Ying Zhen Li, Haukur Ingason, «Fire-induced ceiling jet characteristics in tunnels under different ventilation conditions,» SP Report, SP Technical Research Institute of Sweden, 2015.

[40] Lönnermark A, Ingason H, "Fire Spread and Flame Length in Large-Scale Tunnel Fires," *Fire Technology*, vol. Vol 21(1), pp. 283-302, 2006.

[41] T. A. Newman JS, «Flame Propagation in Ducts,» *Combustion and Flame,* vol. Vol 51, pp. 347-355, 1983.

[42] C. Haremza, A. Santiago and L. Simões da Silva,, «Design of Steel and Composite open car parks under fire,» *Advanced Steel Construction Vol. 9, No. 4,* Vols. %1 sur %29, No. 4, pp. 321-339, (2013).

[43] O.Vassart, B.Zhao, L.G.Cajot, F.Robert, U.Meyer,, "Background & Applications Structural Fire Design," M.Poljanšek, B.Nikolova, L.Sousa, S.Dimova, A.Pinto, Institute for the Protection and Security of the Citizen, 2014.

[44] Q. J. Karlsson B, "Chapter 4—fire plumes and flame heights," in *Enclosure fire dynamics*, 2000, pp. 60-93.

[45] E. 1991-1-2, Eurocode 1—basis of design and actions on structures—part 1–2:actions on structures exposed to fire, 2002.

[46] H. G, «Fire plumes, flame height, and air entrainment,» chez *DiNenno PJ (ed) Handbook of fire protection engineering, 3rd edn.*, 2002, p. 1–17.

[47] A. S. J. P. R. a. P. B. Gonc¸alo Ferraz, «Thermal Analysis of Hollow Steel Columns Exposed to Localised Fires,» *Fire Technology*, vol. Vol 52, p. 663–681, 2016.

[48] Björn Karlsson James G. Quintiere, Enclosure Fire Dynamics, Björn Karlsson, Ph.D.,James G. Quintiere, Ph.D.M.E.,, 1999.

[49] Mohamed Seddik Khetata, «Numerical Prediction Of Thermal And Dynamic Characteristics Of A Fire-Induced Ceiling-Jet,» School of Technology and Management Polytechnic Institute of Bragança, 2016.

[50] J. G. Quintiere, Fundamentals of Fire Phenomena, Chap 11, Compartment Fires,, ISBN: 978-0-470-09113-5,, March 2006..

[51] E. 1992-1-2, «EN 1991-1-2. Basic Design Methods and Worked Examples,» chez *Eurocodes: Background and Applications Structural Fire Design*, European committee for standardization, December 2004., pp. 1-60.

[52] W. K. Chow, “Numerical Studies on the Transient Behaviour of a Fire Plume and Ceiling,” Vols. Vol. 17, No 9, no. Comput. Modelling, pp. 71-79, MAY 1993.

[53] Johansson, Nils; Wahlqvist, Jonathan; Van Hees, Patrick, "Simple Ceiling Jet Correlation Derived from Numerical Experiments," Interscience, Proceedings of the 13th International Interflam Conference, 2013-01-01.

[54] David D. Evans, «CEILING JET FLOWS,» chez *Fire Protection Engineering*, DiNenno, P.J., et al.,, 2004, pp. 2/32-2/39 .

[55] E. 1993-1-2, Eurocode 3: Design of steel structures - Part 1-2: General rules -Structural fire design, Management Centre: rue de Stassart, 36 B-1050 Brussels , April 2005.

[56] R. Viall, «FIRE MODELING IN FLUENT,» April 24, 2008.

[57] N. M. Knop, «Thermal analysis of a fireplace using ANSYS, Graduate Theses and Dissertations,» Paper 10496, 2009.

Annex 1: Results from correlative models

The numerical values of the maximum temperature and velocity of the gases near the ceiling getting from the correlative models of burning car (all classes) are shown below.

1- Alpert's results

Table 4.Tmax and Vmax getting form Alpert's correlations.

	Class 1		Class 2		Class3		Class4		Class5	
r/H	$T_{max}[°c]$	$V_{max}[\frac{m}{s}]$	$T_{max}[°c]$	$V_{max}[\frac{m}{s}]$	$T_{max}[°c]$	$V_{max}[\frac{m}{s}]$	$T_{max}[°c]$	$V_{max}[\frac{m}{s}]$	$T_{max}[°c]$	$V_{max}[\frac{m}{s}]$
0.00	994	11.98	1150	12.90	1343	13.96	1566	15.09	1566	15.09
0.37	621	5.62	718	6.06	837	6.55	974	7.08	974	7.08
0.74	399	3.16	460	3.40	535	3.68	621	3.98	621	3.98
1.11	309	2.25	355	2.42	413	2.62	479	2.84	479	2.84
1.48	259	1.77	297	1.91	344	2.06	399	2.23	399	2.23
1.85	226	1.47	259	1.58	299	1.71	346	1.85	346	1.85

2- Cooper's results

Table 5.Tmax and Vmax getting form Cooper's correlations.

	Class 1		Class 2		Class3		Class4		Class5	
r/H	$T_{max}[°c]$	$V_{max}[\frac{m}{s}]$	$T_{max}[°c]$	$V_{max}[\frac{m}{s}]$	$T_{max}[°c]$	$V_{max}[\frac{m}{s}]$	$T_{max}[°c]$	$V_{max}[\frac{m}{s}]$	$T_{max}[°c]$	$V_{max}[\frac{m}{s}]$
0.00	1640	0.00	1900	0.00	2220	0.00	2591	0.00	2591	0.00
0.37	861	9.67	996	10.42	1162	11.27	1355	12.19	1355	12.19
0.74	457	4.51	527	4.86	613	5.26	713	5.69	713	5.69
1.11	323	2.89	372	3.11	432	3.37	501	3.64	501	3.64
1.48	255	2.11	293	2.27	340	2.45	394	2.65	394	2.65
1.85	213	1.65	244	1.77	283	1.92	327	2.07	327	2.07

3- Heskestad and Delichatsios's results

Table 6. Tmax and Vmax getting form Heskestad and Delichatsios correlations.

	Class 1		Class 2		Class3		Class4		Class5	
r/H	$T_{max}[°c]$	$V_{max}[\frac{m}{s}]$	$T_{max}[°c]$	$V_{max}[\frac{m}{s}]$	$T_{max}[°c]$	$V_{max}[\frac{m}{s}]$	$T_{max}[°c]$	$V_{max}[\frac{m}{s}]$	$T_{max}[°c]$	$V_{max}[\frac{m}{s}]$
0.00	1492	12.04	1728	13.47	2019	15.34	2356	17.71	2356	17.71
0.37	796	9.24	920	9.95	1074	10.76	1251	11.64	1251	11.64
0.74	524	5.97	605	6.43	705	6.96	820	7.52	820	7.52
1.11	384	4.62	443	4.98	515	5.39	598	5.82	598	5.82
1.48	301	3.86	346	4.15	401	4.49	465	4.86	465	4.86
1.85	246	3.35	282	3.61	326	3.91	378	4.22	378	4.22

4- Maximum temperature comparison between correlative models

A percentage of error between the results of the maximum temperature from the correlative models, taking the Alpert's results as reference are presented in Tables below:

Table 7.Comparison between correlative models for Tmax of class 1.

r/H	Alpert $T_{max}[°C]$	Cooper $T_{max}[°C]$	Error [%]	Heskestad $T_{max}[°C]$	Error [%]
0	994	1640	64.9	1492	50.1
0.37	621	861	38.6	796	28.1
0.74	399	457	14.5	524	31.4
1.11	309	323	4.6	384	24.3
1.48	259	255	-1.3	301	16.2
1.85	226	213	-5.4	246	8.8

Table 8.Comparison between correlative models for Tmax of class 2.

r/H	Alpert $T_{max}[°C]$	Cooper $T_{max}[°C]$	Error [%]	Heskestad $T_{max}[°C]$	Error [%]
0	1150	1900	65.1	1728	50.2
0.37	718	996	38.7	920	28.2
0.74	460	527	14.6	605	31.7
1.11	355	372	4.6	443	24.5
1.48	297	293	-1.3	346	16.4
1.85	259	244	-5.5	282	8.9

Table 9.Comparison between correlative models for Tmax of class 3.

r/H	Alpert $T_{max}[°C]$	Cooper $T_{max}[°C]$	Error [%]	Heskestad $T_{max}[°C]$	Error [%]
0	1343	2220	65.3	2019	50.3
0.37	837	1162	38.9	1074	28.3
0.74	535	613	14.7	705	31.9
1.11	413	432	4.6	515	24.8
1.48	344	340	-1.3	401	16.5
1.85	299	283	-5.6	326	9.0

Table 10.Comparison between correlative models for Tmax of class 4,5.

r/H	Alpert T_{max}[°C]	Cooper T_{max}[°C]	Error [%]	Heskestad T_{max}[°C]	Error [%]
0	1566	2591	65.4	2356	50.4
0.37	974	1355	39.0	1251	28.4
0.74	621	713	14.8	820	32.0
1.11	479	501	4.7	598	24.9
1.48	399	394	-1.3	465	16.7
1.85	346	327	-5.6	378	9.1

5- Maximum temperature comparison between correlative models

A percentages of error between the results of the maximum velocity from the correlative models, taking the Alpert's results as reference are presented in Tables below :

Table 11.Comparison between correlative models for Vmax of class 1.

r/H	Alpert $V_{max[\frac{m}{s}]}$	Cooper $V_{max[\frac{m}{s}]}$	Error [%]	Heskestad $V_{max[\frac{m}{s}]}$	Error [%]
0	11.98			12.04	0.5
0.37	5.62	9.67	72.0	9.24	64.2
0.74	3.16	4.51	43.0	5.97	89.1
1.11	2.25	2.89	28.3	4.62	105.4
1.48	1.77	2.11	18.8	3.86	117.7
1.85	1.47	1.65	12.0	3.35	127.8

Table 12.Comparison between correlative models for Vmax of class 2.

r/H	Alpert $V_{max[\frac{m}{s}]}$	Cooper $V_{max[\frac{m}{s}]}$	Error [%]	Heskestad $V_{max[\frac{m}{s}]}$	Error [%]
0	12.90			13.47	4.4
0.37	6.06	10.42	72.0	9.95	64.2
0.74	3.40	4.86	43.0	6.43	89.1
1.11	2.42	3.11	28.3	4.98	105.4
1.48	1.91	2.27	18.8	4.15	117.7
1.85	1.58	1.77	12.0	3.61	127.8

Table 13.Comparison between correlative models for Vmax of class 3.

r/H	Alpert $V_{max[\frac{m}{s}]}$	Cooper $V_{max[\frac{m}{s}]}$	Error [%]	Heskestad $V_{max[\frac{m}{s}]}$	Error [%]
0	13.96			15.34	9.9
0.37	6.55	11.27	72.0	10.76	64.2
0.74	3.68	5.26	43.0	6.96	89.1
1.11	2.62	3.37	28.3	5.39	105.4
1.48	2.06	2.45	18.8	4.49	117.7
1.85	1.71	1.92	12.0	3.91	127.8

Table 14.- Comparison between correlative models for Vmax of class 4,5

r/H	Alpert $V_{\max[\frac{m}{s}]}$	Cooper $V_{\max[\frac{m}{s}]}$	Error [%]	Heskestad $V_{\max[\frac{m}{s}]}$	Error [%]
0	15.09			17.71	17.4
0.37	7.08	12.19	72.0	11.64	64.2
0.74	3.98	5.69	43.0	7.52	89.1
1.11	2.84	3.64	28.3	5.82	105.4
1.48	2.23	2.65	18.8	4.86	117.7
1.85	1.85	2.07	12.0	4.22	127.8

Annex 2: Results from CFAST simulation

1- Positions of targets and heat alarm entering in CFAST simulation

The following tables show the position of each one of six targets and heat alarms which are situated on the ceiling, from these positions we aspect to have results of temperature and velocity with the respect of each radial position.

Table 15.Data of the six targets in the compartment.

Target Number	Compartment	X position[m]	Y position[m]	Z position[m]
Targ 1	OPEN_ CAR_ PARKING	5	5	2.9
Targ 2	OPEN_ CAR_ PARKING	6	5	2.9
Targ 3	OPEN_ CAR_ PARKING	7	5	2.9
Targ 4	OPEN_ CAR_ PARKING	8	5	2.9
Targ 5	OPEN_ CAR_ PARKING	9	5	2.9
Targ 6	OPEN_ CAR_ PARKING	10	5	2.9

Table 16.Data of the six heat alarms in compartment.

N° of heat alarm	Compartment	Position X [m]	Position Y [m]	Position Z [m]
Heat alarm 1	OPEN_ CAR_ PARKING	5	5	2.97
Heat alarm 2	OPEN_ CAR_ PARKING	4	5	2.97
Heat alarm 3	OPEN_ CAR_ PARKING	3	5	2.97
Heat alarm 4	OPEN_ CAR_ PARKING	2	5	2.97
Heat alarm 5	OPEN_ CAR_ PARKING	1	5	2.97
Heat alarm 6	OPEN_ CAR_ PARKING	0	5	2.97

2- Maximum temperature from CFAST numerical simulation

In the following table, the results of maximum temperature from CFAST simulation for all car classes are presented

Table 17.results of CFAST simulation for maximum temperature.

r/H	Class 1 T_{max} [°C]	Class 2 T_{max} [°C]	Class 3 T_{max} [°C]	Class 4 T_{max} [°C]	Class 5 T_{max} [°C]
0	935.87	939.16	953.85	949.30	949.30
0.37	802.67	810.67	834.15	833.29	833.29
0.74	625.18	639.45	674.65	678.69	678.69
1.11	523.83	541.68	583.57	590.42	590.42
1.48	459.24	479.37	525.52	534.16	534.16
1.85	414.92	436.63	485.70	495.56	495.56

3- Maximum velocity from CFAST numerical simulation

In the following table, the results of maximum velocity from CFAST simulation for all car classes are presented.

Table 18.results of CFAST simulation for maximum temperature.

r/H	Class 1 V_{max} [m/s]	Class 2 V_{max} [m/s]	Class 3 V_{max} [m/s]	Class 4 V_{max} [m/s]	Class 5 V_{max} [m/s]
0	10.93	11.52	12.13	12.85	12.85
0.37	8.01	8.55	9.23	9.97	9.97
0.74	4.91	5.29	5.72	6.18	6.18
1.11	3.71	4.00	4.32	4.67	4.67
1.48	3.04	3.28	3.55	3.83	3.83
1.85	2.61	2.81	3.04	3.29	3.29

4- Maximum temperature comparison between the correlations and CFAST

A relative deference between results of each one of the correlative models and CFAST simulation for the maximum temperature in each radial position containing all vehicles classes are shown in the tables below.

Table 19.Comparison of Tmax between correlative models and CFAST for class 1.

r/H	CFAST T_{max}[°C]	Alpert T_{max}[°C]	Error %	Cooper T_{max}[°C]	Error %	Heskestad T_{max}[°C]	Error %
0	935.87	994	-5.9%	1640	75.2%	1492	59.4%
0.37	802.67	621	29.2%	861	7.3%	796	-0.9%
0.74	625.18	399	56.8%	457	-27.0%	524	-16.2%
1.11	523.83	309	69.5%	323	-38.3%	384	-26.6%
1.48	459.24	259	77.6%	255	-44.4%	301	-34.6%
1.85	414.92	226	83.9%	213	-48.6%	246	-40.8%

Table 20.Comparison of Tmax between correlative models and CFAST for class 2.

r/H	CFAST T_{max}[°C]	Alpert T_{max}[°C]	Error %	Cooper T_{max}[°C]	Error %	Heskestad T_{max}[°C]	Error %
0	939.16	1150	-18.4%	1900	102.3%	1728	84.0%
0.37	810.67	718	12.9%	996	22.8%	920	13.5%
0.74	639.45	460	39.1%	527	-17.7%	605	-5.4%
1.11	541.68	355	52.4%	372	-31.4%	443	-18.3%
1.48	479.37	297	61.5%	293	-38.9%	346	-27.9%
1.85	436.63	259	68.8%	244	-44.0%	282	-35.5%

Table 21.Comparison of Tmax between correlative models and CFAST for class 3.

r/H	CFAST T_{max}[°C]	Alpert T_{max}[°C]	Error %	Cooper T_{max}[°C]	Error %	Heskestad T_{max}[°C]	Error %
0	953.85	1343	40.8%	2220	132.8%	2019	111.7%
0.37	834.15	837	0.3%	1162	39.3%	1074	28.7%
0.74	674.65	535	-20.8%	613	-9.1%	705	4.5%
1.11	583.57	413	-29.3%	432	-26.0%	515	-11.8%
1.48	525.52	344	-34.5%	340	-35.4%	401	-23.7%
1.85	485.70	299	-38.4%	283	-41.8%	326	-32.8%

Table 22.Comparison of Tmax between correlative models and CFAST for class 4,5.

r/H	CFAST $T_{max}[°C]$	Alpert $T_{max}[°C]$	Error %	Cooper $T_{max}[°C]$	Error %	Heskestad $T_{max}[°C]$	Error %
0	949.30	1566	-39.4%	2591	173.0%	2356	148.2%
0.37	833.29	974	-14.5%	1355	62.6%	1251	50.2%
0.74	678.69	621	9.2%	713	5.1%	820	20.9%
1.11	590.42	479	23.3%	501	-15.1%	598	1.3%
1.48	534.16	399	33.9%	394	-26.3%	465	-12.9%
1.85	495.56	346	43.0%	327	-34.0%	378	-23.7%

5- Maximum velocity comparison between the correlations and CFAST

A relative deference between results of each one of the correlative models and CFAST simulation for the maximum velocity in each radial position containing all vehicles classes are shown in the tables below:

Table 23.Comparison of Vmax between correlative models and CFAST for class 1.

r/H	CFAST $V_{max}[m/s]$	Alpert $V_{max}[m/s]$	Error %	Cooper $V_{max}[m/s]$	Error %	Heskestad $V_{max}[m/s]$	Error %
0	10.93	11.98	9.5%			12.04	10.1%
0.37	8.01	5.62	-29.8%	9.67	72.0%	9.24	15.3%
0.74	4.91	3.16	-35.7%	4.51	43.0%	5.97	21.6%
1.11	3.71	2.25	-39.3%	2.89	28.3%	4.62	24.6%
1.48	3.04	1.77	-41.8%	2.11	18.8%	3.86	26.8%
1.85	2.61	1.47	-43.6%	1.65	12.0%	3.35	28.5%

Table 24.Comparison of Vmax between correlative models and CFAST for class 2.

r/H	CFAST $V_{max}[m/s]$	Alpert $V_{max}[m/s]$	Error %	Cooper $V_{max}[m/s]$	Error %	Heskestad $V_{max}[m/s]$	Error %
0	11.52	12.90	12.0%			13.47	17.0%
0.37	8.55	6.06	-29.2%	10.42	21.8%	9.95	16.3%
0.74	5.29	3.40	-35.7%	4.86	-8.0%	6.43	21.6%
1.11	4.00	2.42	-39.3%	3.11	-22.1%	4.98	24.6%
1.48	3.28	1.91	-41.8%	2.27	-30.8%	4.15	26.8%
1.85	2.81	1.58	-43.6%	1.77	-36.8%	3.61	28.5%

Table 25.Comparison of Vmax between correlative models and CFAST for class 3.

r/H	CFAST $V_{max}[m/s]$	Alpert $V_{max}[m/s]$	Error %	Cooper $V_{max}[m/s]$	Error %	Heskestad $V_{max}[m/s]$	Error %
0	12.13	13.96	15.1%			15.34	26.5%
0.37	9.23	6.55	-29.0%	11.27	22.2%	10.76	16.7%
0.74	5.72	3.68	-35.7%	5.26	-8.0%	6.96	21.6%
1.11	4.32	2.62	-39.3%	3.37	-22.1%	5.39	24.6%
1.48	3.55	2.06	-41.8%	2.45	-30.8%	4.49	26.8%
1.85	3.04	1.71	-43.6%	1.92	-36.8%	3.91	28.5%

Table 26.Comparison of Vmax between correlative models and CFAST for class 4,5.

r/H	CFAST $V_{max}[m/s]$	Alpert $V_{max}[m/s]$	Error %	Cooper $V_{max}[m/s]$	Error %	Heskestad $V_{max}[m/s]$	Error %
0	12.85	15.09	17.4%			17.71	37.9%
0.37	9.97	7.08	-29.0%	12.19	22.2%	11.64	16.7%
0.74	6.18	3.98	-35.7%	5.69	-8.0%	7.52	21.6%
1.11	4.67	2.84	-39.3%	3.64	-22.1%	5.82	24.6%
1.48	3.83	2.23	-41.8%	2.65	-30.8%	4.86	26.8%
1.85	3.29	1.85	-43.6%	2.07	-36.8%	4.22	28.5%

Annex 3: Results from ANSYS fluent simulation

1- Material models

Table 27 represents the different properties of the concrete based on the date points, for each point the temperature is presented in [°C] and in [K].

Table 27.Properties of concrete based on data points.

Points	Temperature °C	Temperature K	C_p(dry,u=3.0%) J/kgK	Density kg/m3	Diffusivity $m2/s$
1	20	293	900	2300	9.4E-07
2	100	373	900	2300	8.5E-07
3	101	374	2020	2300	3.8E-07
4	115	388	2020	2300	3.7E-07
5	200	473	1000	2254	6.9E-07
6	300	573	1050	2220	5.8E-07
7	400	673	1100	2185	5.0E-07
8	500	773	1100	2165	4.4E-07
9	600	873	1100	2145	3.9E-07
10	700	973	1100	2125	3.5E-07
11	800	1073	1100	2105	3.1E-07
12	900	1173	1100	2084	2.9E-07
13	1000	1273	1100	2064	2.7E-07
14	1100	1373	1100	2044	2.7E-07
15	1200	1473	1100	2024	2.7E-07

The specific heat cp(θ) of dry concrete (u = 0%) [51].

2- Boundary condition

We create point in CFAST for every fire event (measure temperature and velocity) the data is presented in Tables below:

Table 28..Data of the target 7 in the compartment.

Target Number	Compartment	X position[m]	Y position[m]	Z position[m]
Targ 7	OPEN_ CAR_ PARKING	5	5	0.35

Table 29.Data of the heat alarm7 in the compartment.

N° of heat alarm	Compartment	Position X [m]	Position Y [m]	Position Z [m]
Heat alarm 7	OPEN_ CAR_ PARKING	5	5	0.35

When we got the results, we defined the formulas of temperature and velocity. First law of thermos dynamics, uses to convert fire output:

$$Q - W = (\Delta h + \Delta KE + \Delta PE)\dot{m} \quad \text{Eq 22}$$

$$\Delta h = C_p \Delta T \quad \text{Eq 23}$$

$$\dot{m} = AV\rho \quad \text{Eq 24}$$

Defined the formulas of temperature and velocity for each class which are presented below:

$$\Delta y = m\Delta x \quad \text{Eq 25}$$

Where y represents values of temperature (should be in kelvin) or velocity and x represents values of times (should be in second).

Class 1

0≤tim≤120	$T = 273{,}15 + (7{,}5166 \times tim)$	Eq 26
120<tim≤1500	$T = 273{,}15 + (922 + 0{,}00942 \times (tim - 120))$	Eq 27
1500<tim≤2880	$T = 273{,}15 + (935 - 0{,}00652 \times (tim - 1500))$	Eq 28
2880<tim≤4200	$T = 273{,}15 + (926 - 0{,}6833 \times (tim - 2880))$	Eq 29
0≤tim≤240	$V = 0{,}02916 \times tim$	Eq 30
240<tim≤960	$V = 7$	Eq 31
960<tim≤1440	$V = 7 + 0{,}00458 \times (tim - 960)$	Eq 32
1440<tim≤1500	$V = 9{,}2 + 0{,}0133 \times (tim - 1440)$	Eq 33
1500<tim≤1620	$V = 10 - 0.01 \times (tim - 1500)$	Eq 34
1620≤tim≤2280	$V = 8{,}8 - 0{,}0033 \times (tim - 1620)$	Eq 35
2280<tim≤3180	$V = 6{,}6 - 0{,}0008 \times (tim - 2280)$	Eq 36
3180<tim≤4200	$V = 5{,}8 –, 00568 \times (tim - 3180)$	Eq 37

Class 2

0<tim≤120	$T = 273{,}15 + (7{,}516 \times tim)$	Eq 38
120<tim≤1500	$T = 273{,}15 + (922 + 0{,}001159 \times (tim - 12))$	Eq 39
1500<tim≤3120	$T = 273{,}15 + (938 - 0{,}00679 \times (tim - 1500))$	Eq 40
3120<tim≤4200	$T = 273{,}15 + (927 - 0{,}83518 \times (tim - 3120))$	Eq 41
0≤tim≤240	$V = 0{,}03083 \times tim$	Eq 42

240<tim≤960	$V = 7{,}4$	Eq 43
960<tim≤1440	$V = 7{,}4 + 0{,}00458 \times (tim - 960)$	Eq 44
1440<tim≤1500	$V = 9{,}6 + 0{,}01333 \times (tim - 1440)$	Eq 45
1500<tim≤1620	$V = 10{,}4 - 0{,}01 \times (tim - 1500)$	Eq 46
1620<tim≤2280	$V = 9{,}2 - 0{,}00348 \times (tim - 1620)$	Eq 47
2280<tim≤3360	$V = 6{,}9 - 0{,}001018 \times (tim - 2280)$	Eq 48
3360<tim≤4200	$V = 5{,}8 - 0{,}0069 \times (tim - 3360)$	Eq 49

Class 3

0≤tim≤120	$T = 273{,}15 + (7{,}5166 \times tim)$	Eq 50
120<tim≤1500	$T = 273{,}15 + (922 + 0{,}01449 \times (tim - 120))$	Eq 51
1500<tim≤3360	$T = 273{,}15 + (94 - 0{,}0086 \times (tim - 1500))$	Eq 52
3360<tim≤4200	$T = 273{,}15 + (926 - 1{,}071 \times (tim - 3360))$	Eq 53
0<tim≤240	$V = 0{,}0320 \times tim$	Eq 54
240<tim≤960	$V = 7{,}7$	Eq 55
960<tim≤1440	$V = 7{,}7 + 0{,}005 \times (tim - 960)$	Eq 56
1440<tim≤1500	$V = 10{,}1 + 0{,}01333 \times (tim - 1440)$	Eq 57
1500≤tim≤1620	$V = 10{,}9 - 0{,}01083 \times (tim - 1500)$	Eq 58
1620<tim≤2280	$V = 9{,}6 - 0{,}00363 \times (tim - 1620)$	Eq 59
2280<tim≤3540	$V = 7{,}2 - 0{,}001111 \times (tim - 2280)$	Eq 60
3540<tim≤4200	$V = 5{,}8 - 0{,}00878 \times (tim - 3540)$	Eq 61

Class 4,5

0≤tim≤60	$T = 273{,}15 + (15{,}03 \times tim)$	Eq 62
60<tim≤1500	$T = 273{,}15 + (922 + 0{,}01597 \times (tim - 60))$	Eq 63
1500<tim≤3540	$T = 273{,}15 + (945 - 0{,}0078 \times (tim - 1500))$	Eq 64
3540<tim≤4200	$T = 273{,}15 + (926 - 1{,}366 \times (tim - 3540))$	Eq 65
0<tim≤240	$V = 0{,}03375 \times tim$	Eq 66
240<tim≤960	$V = 8{,}1$	Eq 67

960<tim≤1440	$V = 8{,}1 + 0{,}005 \times (tim - 960)$	Eq 68
1440<tim≤1500	$V = 10{,}5 + 0{,}015 \times (tim - 1440)$	Eq 69
1500<tim≤1620	$V = 11{,}4 - 0{,}01083 \times (tim - 1500)$	Eq 70
1620<tim≤2280	$V = 10{,}1 - 0{,}00393 \times (tim - 1620)$	Eq 71
2280<tim≤3360	$V = 7{,}5 - 0{,}001574 \times (tim - 2280)$	Eq 72
3360<tim≤4200	$V = 5{,}8 - 0{,}0069 \times (tim - 3360)$	Eq 73

After that we put the formulas in velocity inlet like boundary condition we got the results simulation ANSYS fluent.

The results simulation of maximum temperature and velocity from ANSYS fluent are presented in Tables below:

Table 30.Maximum velocity and temperature from ANSYS fluent.

	Class 1		Class 2		Class3		Class 4,5	
r/H	$T_{max}[°c]$	$V_{max}[\frac{m}{s}]$	$T_{max}[°c]$	$V_{max}[\frac{m}{s}]$	$T_{max}[°c]$	$V_{max}[\frac{m}{s}]$	$T_{max}[°c]$	$V_{max}[\frac{m}{s}]$
0.00	934	1.09	933	1.12	938	1.17	941	1.21
0.37	934	6.63	934	6.70	938	6.88	941	7.09
0.74	933	11.69	933	11.98	937	12.32	941	12.78
1.11	934	14.27	933	15.12	937	15.80	940	15.48
1.48	933	15.17	932	15.28	936	15.31	939	16.66
1.85	932	14.62	932	16.51	936	16.90	939	16.18